이학박사 학위논문

p-type doping for transparent perovskite semiconductor of alkali-earth stannate and its pn-junctions

투명 페로브스카이트 반도체 알칼리토 주석 산화물의 p 형 도핑과 그 pn 접합 연구

2014 년 2 월

서울대학교 대학원

물리천문학부

김 훈 민

p-type doping for transparent perovskite semiconductor of alkali-earth stannate and its pn-junctions

투명 페로브스카이트 반도체 알칼리토 주석 산화물의 p 형 도핑과 그 pn 접합 연구

지도 교수 차 국 린

이 논문을 이학박사 학위논문으로 제출함.
2014년 2 월

이 논문을 이학박사 학위논문으로 제출함

서울대학교 대학원
물리천문학부
김 훈 민

김훈민의 이학박사 학위 논문을 인준함
2014 년 2 월

위 원 장 _____ 국 양

부위원장 _____ 차 국 린

위 원 _____ 김 기 훈

위 원 _____ 박 제 근

위 원 _____ 방 윤 규

p-type doping for transparent perovskite semiconductor of alkali-earth stannate and its pn-junctions

by

Hoon Min Kim

Supervised by

Professor Kookrin Char

A dissertation submitted to the Faculty of
Seoul National University
in Partial Fulfillment of the Requirements
for the Degree of
Doctor of Philosophy

February 2014

Department of Physics and Astronomy
Graduate School
Seoul National University

Abstract

Transparent oxide semiconductors (TOSs) are widely used as transparent electrodes because they are optically transparent in the visible light and UV regions and their electrical conductivity can be manipulated. However, applications of TOSs are limited to transparent electrodes and panel displays because of a lack of p-type conducting transparent oxide materials. The discovering and developing Cu-based p-type TOSs has allowed the fabrication of fundamental semiconductor devices such as pn junctions and field effect transistors; however, there are few reports of TOS materials that can be injected with dopants to from both p- and n-type materials.

Recently, it was reported that La-doped $BaSnO_3$ (BLSO) has high oxygen stability and good electrical conductivity. However, even though BSO thin films exhibit a high epitaxiality, the films contains many grain boundaries and dislocations that act as charge traps and scattering centers. We are attempting to find a substrate more suitable than $SrTiO_3$ (STO) for improving the electrical properties of BLSO thin films; however, BLSO thin films on alternative substrates show a poorer mobility than those on STO. In addition, the low doped BLSO thin film acts like a p-type semiconductor due to the effects of threading dislocations even though the dopant is an n-type carrier.

Because the d-orbital does not participate in the bonding between Sn and O in $BaSnO_3$ (BSO), this bond can be stronger than that in other perovskite materials, and allows for the possible doping with a p-type carrier. We have been successfully in doping BSO with K using pulsed laser deposition. Although K-doped BSO exhibits a rather high resistivity at room temperature, its conductivity increased dramatically at higher temperatures. The activation

energy of the K-dopant was estimated to be about 0.5 eV. Furthermore, the conductivity decreased when a small amount of oxygen was removed from the film, consistent with the behavior of p-type doped oxides. The results of doping BSO with other elements such as Ga and Cu are presented.

We have fabricated pn junctions using K-doped BSO (BKSO) and BLSO as the p- and n-type semiconductors, respectively. I-V characteristics of these devices showed the typical rectifying behavior of pn junctions in room temperature. In addition, I-V characteristics of these devices exhibit an ideal diode behavior with the ideality factor between 1 and 2 in high temperature, implying high integrity of the BSO materials. Moreover, the junction properties were found to be very stable after repeated high-bias, high-temperature thermal cycling. Our demonstration of pn junctions based on a single perovskite BSO further enhances the potential of a transparent perovskite semiconductor BSO system, whose high mobility and stability have previously been shown.

We investigated $SrSnO_3$ (SSO), which has a 4 eV direct band gap. SSO thin films were deposited on $KTaO_3$ (KTO) to minimize the lattice mismatch with SSO. Images obtained with TEM and AFM showed that the SSO thin films on KTO exhibit almost no threading dislocations. In measuring the electrical properties of the SSO thin films with various dopants such as Sb, La and Ru, we found that the mobility was generally lower than that of BLSO thin films due to tilting of the SnO_6 octahedral. Ru-doped SSO showed p-type behavior even at room temperature. We fabricated a pn junction using Sb-doped SSO and Ru-doped as the n- and p-type semiconductors, respectively. We found that the current of the SSO based pn junction was higher than that based on BSO system; there were several problems with the pn junction, such as large leakage current and large parasitic resistance. If we combine the BSO and SSO system, however,

it will be possible to fabricate LED devices because of the direct band gap, low leakage current pn junction and low resistivity conduction.

Keywords: Transparent oxide semiconductor, $BaSnO_3$, p-type oxide with potassium doping, pn homojunction with single perovskite oxide, $SrSnO_3$, p-type oxide with ruthenium doping

Student number: 2007-20416

Contents

List of Tables

List of Figures

1. Introduction

1.1 p-doping on oxides and their pn junctions

Oxide materials have been intensively investigated because they exhibit insulating, semiconducting, or metallic behavior and novel phenomena such as colossal magneto-resistance and high temperature superconductivity. Among them, perovskite oxides possess great potential for advancing science and technology because of their various unique functionalities, including superconductivity [1], magnetism [2], ferroelectricity [3], and multiferrocity [4]. For example, $SrTiO_3$ (STO) has been extensively studied for these characteristics as well as its high-mobility 2DEG behavior [5, 6] at the interface with $LaAlO_3$. Recently, transparent conducting oxides (TCOs) such as Sn-doped indium oxide (ITO) [7, 8] and In-Ga-Zn-O (IGZO) [9] are widely used as transparent electrodes for display applications and solar cells because they are optically transparent in the visible and UV regions and modulate the electrical conductivity [10, 11]. However, the large electronegativity of oxygen and charge compensation by oxygen vacancies makes it difficult to dope oxide materials with a p-type dopant. Therefore, we reviewed the progress of p-type oxide research and investigated the mechanisms of various p-type oxides and their applications.

Although TCOs have a good conductivity and wide controllable range, their application is limited to transparent electrodes and panel displays because of a lack of p-type conducting transparent oxide materials [12]. In 1997, there was a report of fabrication of p-type transparent conducting oxide films of $CuAlO_2$ [13] and the discovery of p-type TCOs has led to a class of materials known as transparent oxide semiconductors (TOSs) [10, 13]. Since then, a series of p-type

TCOs based on Cu^{+}-bearing oxides, such as $CuGaO_2$ [14], $CuInO_2$ [15, 16], $SrCu_2O_2$ [17] and LnCuOCh (where Ln = lanthanide and Ch = S or Se) [18-21] have been fabricated as the result of material exploration efforts. In general, because of the large electronegativity of oxygen, the valence band edge of oxides is strongly localized to the oxygen ions in the oxide materials. However, in Cu-based TOSs, the $3d^{10}$ closed shell orbital of the Cu^{+} ion is hybridized with the oxygen 2p state, which pushes a more dispersive band up to an energy above the non-bonding O 2p or Cu 3d states. The electronic structures of $CuAlO_2$ which probed by normal/inverse photoemission spectroscopy show that the hybridized orbitals are distinctly nearer to the Fermi level than the typical oxygen 2p state [22]. In a similar manner to the Cu^{+} ion, Rh^{3+} metal ions with a $4d^6$ shell hybridize with oxygen because of the quasi-closed shell configuration [23].

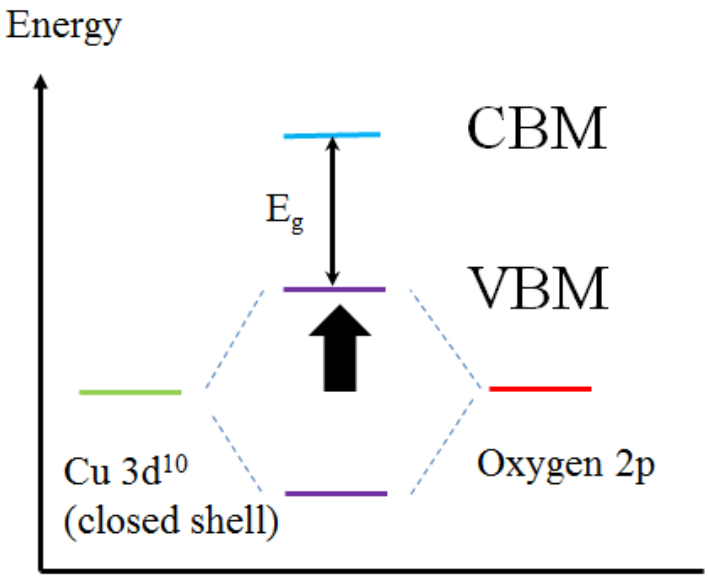

Figure 1.1. Schematic of the chemical bond between an oxide ion and a cations that has a closed shell electronic configuration.

As p-type TOSs have been developed, fundamental semiconductor devices such as light emitting diodes (LEDs) and UV detectors using pn junctions can be fabricated. Near-UV-LEDs are composed of pn heterojunctions of TOSs: p-type $SrCu_2O_2$ and n-type ZnO. Efficient electroluminescence centered at 382 nm was observed when a forward current was injected into the pn-heterojunction diode [24, 25]. A transparent UV light detector was also fabricated using a high-quality pn heterojunction diode composed of TOSs, p-type NiO and n-type ZnO, and its UV-light response was characterized at room temperature [26]. However, there are few reports of TOS materials that can be injected with dopants to fabricate p- and n-type materials [16].

Perovskite oxides are important functional materials that exhibit the various physical properties noted above. An investigation of p-doping perovskite has mainly focused on manganite materials [27-30] because of the relative lack of p-type perovskite oxide materials. The 3d band of Mn splits into the t_{2g} and e_g bands under a crystalline field, and the e_g band is split further into the e_{g1} and e_{g2} bands because of the Jahn-Teller effect. The e_{g1} band is fully occupied while the e_{g2} band is completely empty. Mn^{3+} ions can be oxidized into Mn^{4+} ions by doping divalent ions such as Sr at the La^{3+} sites, which is equivalent to introducing holes into the e_{g1} band [27, 28]. Manganese materials have been intensively researched because of their colossal magneto-resistance effect. A pn junction fabricated using such materials, as shown in Figure 1.4, has a large leakage current and stability problems even at room temperature, although it does exhibit photo-response [28, 29], because the p-doping mechanism is different to the conventional doping mechanism. As shown in Figure 1.5, pn junctions composed of Nb-doped $SrTiO_3$ (STO) (n-type) and In-doped STO (p-type) are demonstrated [31, 32]. However, the use of a STO substrate (not a

film) for the n-type semiconductor limits device fabrication. Therefore, it will be very useful for scientific research and engineering applications if both the thermal and electrical stability and n- and p- type doping mechanism can be shown to similar to those of a conventional semiconductor.

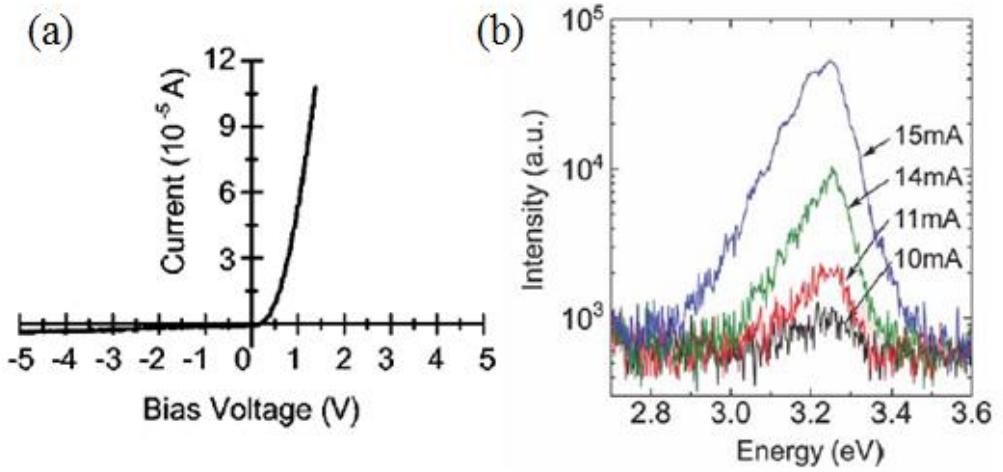

Figure 1.2. (a) A typical I-V characteristic of the transparent pn heterojunction p-$SrCu_2O_2$/n-ZnO. (b) UV emission spectra of the pn junction LED for tens of currents [24].

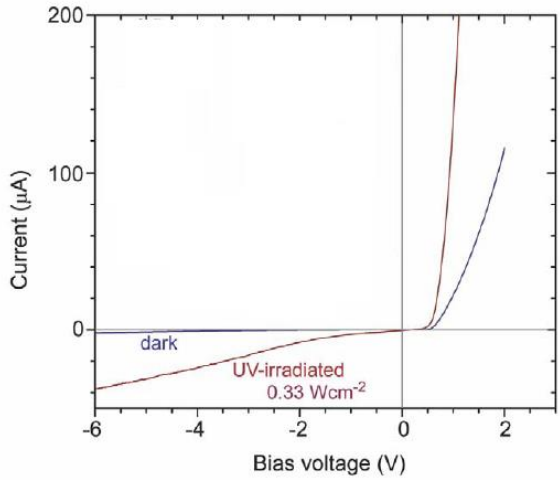

Figure 1.3. Typical I-V characteristics of a pn-heterojunction p-NiO/n-ZnO diode in the dark and under UV illumination; total power density is 0.33 W·cm^{-2} at room temperature [25].

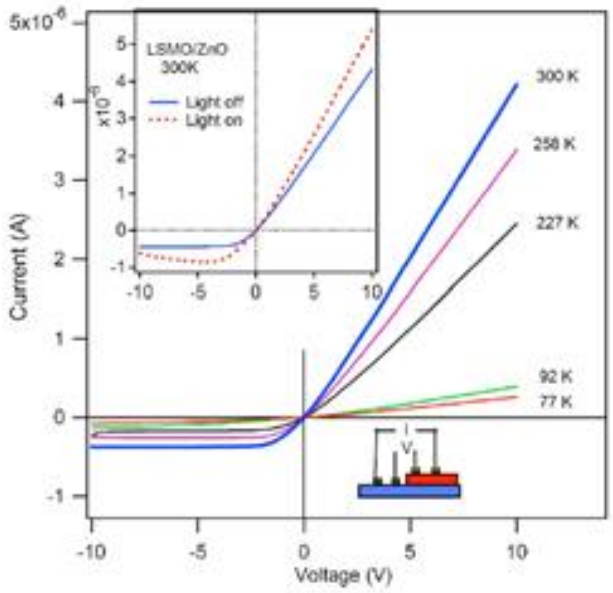

Figure 1.4. I-V characteristics of p-LSMO/n-ZnO junction of various temperatures. The inset shows the current-voltage curves at 300 K with irradiance of 80 mW/cm^2 and without light irradiation [28].

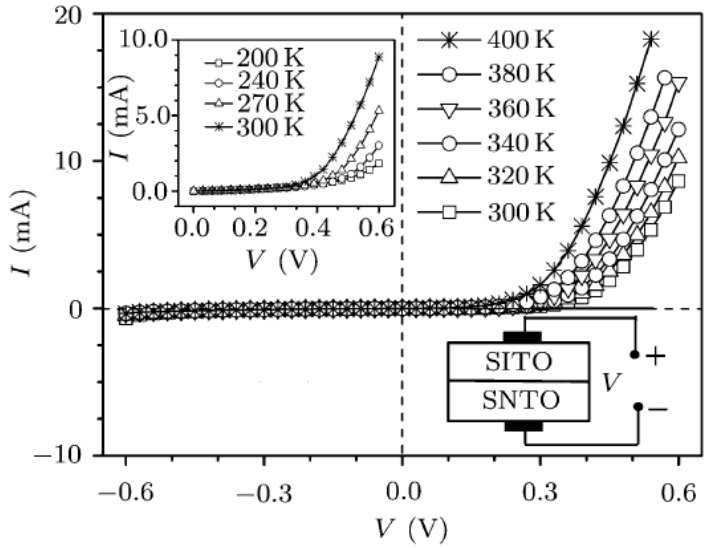

Figure 1.5. I-V curves of the SITO/SNTO pn junction at 300–400K. The upper inset shows the forward-bias I-V curves at 200–300 K and the lower inset is the schematic circuit of the measurement [32].

1.2 $BaSnO_3$: transparent perovskite semiconductor

Wider application of perovskite oxides is limited mainly because of the instability of oxygen, which results in uncertainty in the oxygen stoichiometry and movement at interfaces. This oxygen instability has made thermally stable p- and n-doping in a single perovskite system elusive in spite of its enormous significance in optoelectronic applications. Recently, we reported that $BaSnO_3$ (BSO) exhibits a high oxygen stability and good electrical conductivity in La-doped BSO (BLSO) for an n-type degenerate semiconductor [33]. In contrast to conventional transition metal perovskite oxides, the 5s-orbital of the Sn^{4+} ion is directly bonded to the 2p-orbital of the O_2 ions in BSO system [34]. As the d-orbital does not participate in this bonding between Sn and O, the bond can be stronger than that in other perovskite materials, and it becomes possible to dope the system with a p-type carrier.

La-doped $BaSnO_3$ (BLSO) is reported to have a high oxygen stability and good electrical conductivity [33]. The oxygen diffusion constant measured at 530 ^oC is approximately 10^{-15} cm^2/s^{-1}, which is lower than other perovskite oxides such as titanates (10^{-8}) [35], cuprates (10^{-11}) [36] and manganites (10^{-13}) [37]. In single crystals, the mobility reached 320 $cm^2/V{\cdot}s$ at a doping level of 8 $\times$ 10^{19} cm^{-3}, constituting the highest value among wide-band-gap semiconductors [38-41] (see Figure 1.6). Also, BLSO thin films have a good electrical conductivity of 0.2 $m\Omega{\cdot}cm$ and avery high mobility of 70 $cm^2/V{\cdot}s$. Therefore, BSO has the potential to open the way for the development of transparent perovskite semiconductors (TPSs) because it can be applied to strongly correlated perovskite systems combined with the TOS regime.

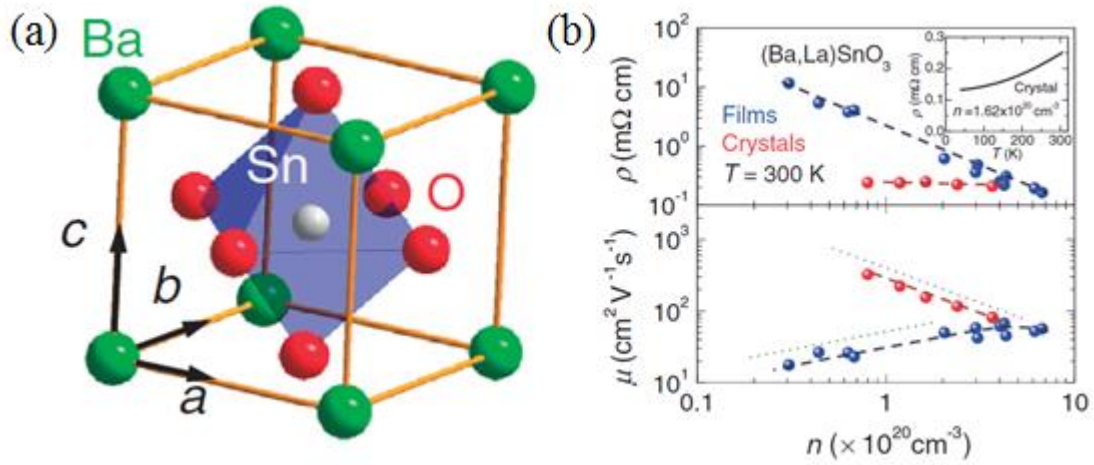

Figure 1.6. (a) Cubic perovskite $BaSnO_3$ which lattice is constant is 4.116 Å. (b) Resistivity and mobility of the BLSO thin films and single crystals are plotted as functions of carrier density at 300 K [32].

Reference

[1] R. J. Cava, B. Batlogg, J. J. Krajewski, R. Farrow, L. W. Rupp Jr, A. E. White, K. Short, W. F. Peck, & T. Kometani, Nature **332,** 814-816 (1988).

[2] Y. Tokura & Y. J. Tomioka, Magn. Magn. Mater. **200**, 1 (1999).

[3] G. H. Haertling, J. Am. Ceram. Soc. **82**, 797 (1999).

[4] T. Kimura, T. Goto, H. Shintani, K. Ishizaka, T. Arima & Y. Tokura, Nature **426**, 55 (2003).

[5] A. Ohtomo & H. Y. Hwang , Nature **427**, 423 (2004).

[6] S. Thiel, G. Hammerl, A. Schmehl, C. W. Schneider, & J. Mannhart, Science **313**, 1942 (2006).

[7] T. Minami, Semicond. Sci. Technol. **20 S35** (2005).

[8] A. L. Dawar, J. C. Joshi. J. Mater. Sci. **19**, 1 (1984).

[9] T. Kamiya, K. Nomura & H. Hosono, Sci. Technol. Adv. Mater. **11**, 044305 (2010).

[10] H. Ohta & H. Hosono., materials today **7**, 42 (2004).

[11] D. S. Ginley & C. Bright, Mater. Res. Soc. Bull. **25**, 8 (2000).

[12] S. Sheng, G. Fang, C. Li, S. Xu, & X. Zhao1, phys. stat. sol. **8**, 1891 (2006).

[13] H. Kawazoe, M. Yasukawa, H. Hyodo, M. Kurita, H. Yanagi & H. Hosono, Nature **389**, 939 (1997).

[14] K. Ueda, T. Hase, H. Yanagi, H. Kawazoe, H. Hosono, H. Ohta, M.

Orita & M. Hirano J. Appl. Phys. **89**, 1790 (2001).

[15] C. N. R. Rao, A. Govindaraj, F. Leonard Deepak, N. A. Gunari & Manashi Nath , Appl. Phys. Lett. **78**, 1583 (2001).

[16] H. Yanagi, K. Ueda, H. Ohta, M. Orita, M. Hirano & H. Hosono, Solid State Commun. **121**, 15 (2001).

[17] A. Kudo, H. Yanagi, H. Hosono & H. Kawazoe., Appl. Phys. Lett. **73**, 220 (1998).

[18] K. Ueda, S. Inoue, S. Hirose, H. Kawazoe & H. Hosono, Appl. Phys. Lett. **77**, 2701 (2000).

[19] K. Ueda, S. Inoue, H. Hosono, N. Sarukura & M. Hirano, Appl. Phys. Lett. **78**, 2333 (2001).

[20] K. Ueda & H. Hosono, J. Appl. Phys. **91**, 4768 (2002).

[21] K. Ueda, K. Takafuji, H. Hiramatsu, H. Ohta, T. Kamiya, M. Hirano, & H. Hosono , Chem. Mater. **15**, 3692 (2003).

[22] H. Yanagi, H. Kawazoe, A. Kudo, M. Yasukawa & H. Hosono, J. Electroceram. **4**, 407 (2000).

[23] H. Mizoguchi, M. Hirano, S. Fujitsu, T. Takeuchi, K. Ueda & H. Hosono, Appl. Phys. Lett. **80** 1207 (2002).

[24] H. Ohta, K. Kawamura, M. Orita, M. Hirano, N. Sarukura & H. Hosono., Appl. Phys. Lett. **77**, 475 (2000).

[25] H. Hosono, H. Ohta, K. Hayashia, M. Oritaa & M. Hiranoa, J. Cryst. Growth **237**, 496 (2002).

[26] H. Ohta, M. Hirano, K. Nakahara, H. Maruta, T. Tanabe, M. Kamiya, T. Kamiya & H. Hosono Appl. Phys. Lett. **83**, 1029 (2003).

[27] K. Lord, D. Hunter, T. M. Williams, & A. K. Pradhan, Appl. Phys. Lett. **89**, 052116 (2006).

[28] D. J. Wang, Y. W. Xie, C. M. Xiong, B. G. Shen & J. R. Sun, Europhys. Lett. **73**, 401 (2006).

[29] J. R. Sun, S. Y. Zhang, B. G. Shen & H. K. Wong, Appl. Phys. Lett. **86**, 053503 (2005).

[30] J. Zhang, H. Tanaka & T. Kawai, Appl. Phys. Lett. **80**, 4378 (2002).

[31] Q. Zhou, K. Jin, H. Lu, P. Han, Z.Chen, K. Zhao, Y. Zhou & G. Yang, Europhys. Lett. **71**, 283 (2005).

[32] G. Liu, K. Jin, M. He, J. Qiu, J. Xing, H. Lu & G. Yang, Chin. Phys. Lett. **25,** 2209 (2008).

[33] H. J Kim, U. Kim, H. M. Kim, T. H. Kim, H. Mun, B. G. Jeon, K. T. Hong, W. J. Lee, C. Ju, K. H. Kim & Kookrin Char, Appl. Phys. Exp. **5**, 061102 (2012).

[34] H. Mizoguchi, H. W. Eng and P. M. Woodward, Inorg. Chem. **43**, 1667 (2004).

[35] C. Schaffrin, Phys. Status Solidi **35,** 79 (1976).

[36] K. N. Tu, N. C. Yeh, S. I. Park & C. C. Tsuei, Phys. Rev. B **39,** 304 (1989).

[37] L. Malavasi & G. Flor., J. Phys. Chem. B **107**, 13880 (2003).

[38] D. K. Gaskill, A. E. Wickenden, K. Doverspike, B. Tadayon, & L. B. Rowland, J. Electron. Mater. **24**, 1525 (1995)..

[39] R. L. Weiher, J. Appl. Phys. **33**, 2834 (1962)..

[40] H. Toyosaki, M. Kawasaki, and Y. Tokura, Appl. Phys. Lett. **93**, 132109 (2008).

[41] A. Ohtomo, K. Tamura, K. Saikusa, K. Takahashi, T. Makino, Y. Segawa, H. Koinuma, & M. Kawasaki, Appl. Phys. Lett. **75**, 2635 (1999).

2. Properties of n-type BSO thin films

As mentioned in Chapter 1, BLSO thin films exhibit an excellent electrical mobility and high oxygen stability. However, there are some significant differences between BSO single crystals and thin films: the mobility of a BLSO single crystal is about 320 $cm^2/V{\cdot}s$ and that of BLSO thin film is about 70 $cm^2/V{\cdot}s$ for a high doping concentration [1]. Furthermore, there are distinct differences in the behavior of the electron mobility of single crystals and thin films in response to changes in the carrier concentration. Unlike a single crystal, the mobility of a thin film decrease as the carrier concentration decreased. Even though our films have a high epitaxiality, there will be a large number of grain boundaries and dislocations that act as charge traps and scattering centers for the carriers, as shown in Figure 2.1 [2]. Moreover, there is suggestion that the effect of dislocations on the electrical transport properties in BLSO films is much larger than that in other materials such as GaN [2]. That means that more carriers are trapped in dislocation traps and that a higher carrier density is required to shield the scattering by the dislocation. Therefore, the conductivity of a BLSO thin film is very low when the doping concentration is relatively low. The structure and defect content of the interface between a substrate and the epitaxially grown thin film is of considerable importance, particularly in the technology of solid state electronic devices [3]. In this section, we describe the efforts made in finding a more suitable substrate for resolving the dislocation problems and the comment on measurements of the conductivity of BLSO thin films at high temperature in different background atmospheres to determine the type of carrier in the BLSO thin films.

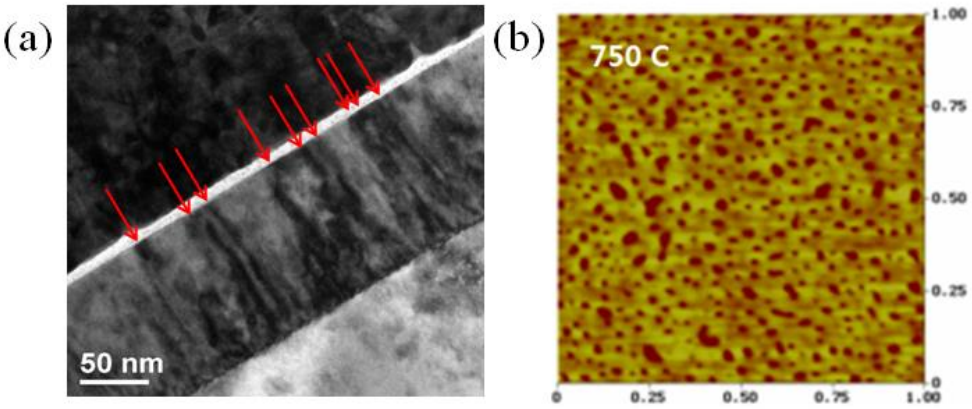

Figure 2.1. (a) The cross-sectional TEM image of BLSO thin film obtained by using two beam condition, showing threading dislocations by arrows. (b) Images of surface morphologies after etching with 0.4 % HNO_3 for 10 s [2].

	Cell plane(Å^2)	Lattice mismatch (%)
$BaSnO_3$	16.941	0
$SrTiO_3$	15.249	-5.12
r-Al_2O_3 (1/4)	18.297	3.92
$BaTiO_3$	15.952	-2.96
$MgAl_2O_4$ (1/4)	16.322	1.84
MgO	17.74	2.33

Table 2.1. The area of cell planes and their lattice mismatch with $BaSnO_3$. (1/4) in r-Al_2O_3 and $MgAl_2O_4$ indicate that value is ¼ of the cell plane.

2.1 Properties of BLSO thin films at various substrates

2.1.1 BLSO thin film deposition

We deposited various doped BLSO thin films (deposited at 750 ^{o}C) on various buffer layers and substrates which described below using BLSO and BSO targets by pulsed laser deposition system with a KrF excimer laser (λ = 248 nm) under 100 mTorr oxygen pressure with 1 ~ 1.5 J/cm^2 energy intensity. To specifically doped lanthanum ions, we used a sequential deposition method which deposits thin films by sequentially alternating targets for each determined pulse shots [4]. The plume of the BLSO and BSO targets are shown in Figure 2.2 when laser is ablaze at target. As you can see, the size of the plume of BLSO and BSO are almost identical. Therefore, we concluded that the deposition rate matched to the nominal shot ratio of the BLSO and BSO targets assuming that La is not volatile at high temperature.

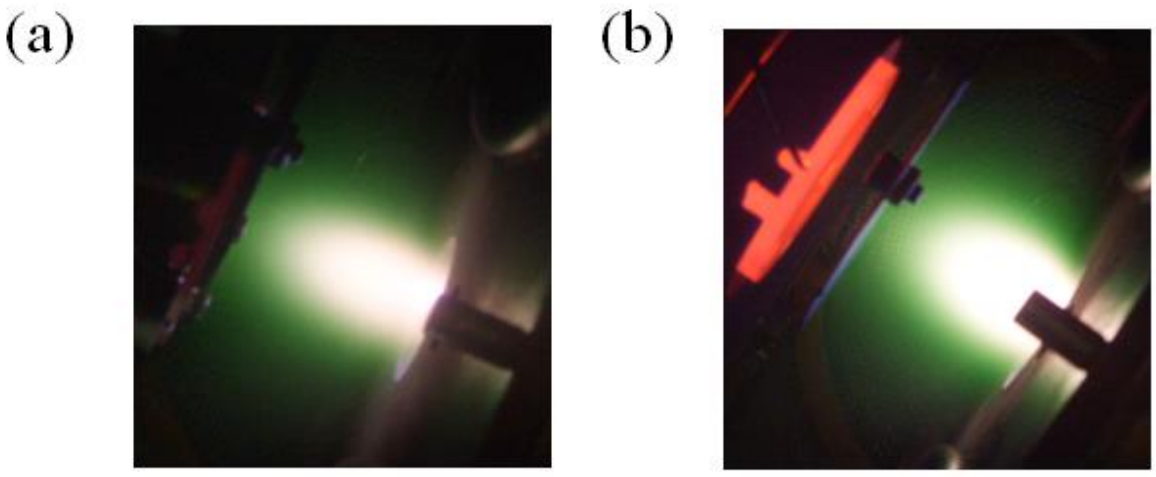

Figure 2.2. Shapes of the plume for laser ablation. (a) plume of BSO (b) plume of BLSO.

2.1.1 r-cut sapphire

As shown in Figure 2.3 (a), the structure sapphire crystal is a hexagonal system, where an axis C for forming a central axis, a plane C (0001) vertical to it [5]. And the plane R (1102) inclined at a constant angle to the axis C, and an axis R is vertical to it when the major axis and plane of the crystal system are expressed with hexagonal indices. As shown at Table 2.1, the lattice mismatch between r-cut sapphire (1/4 plane) and BSO is about 3.92 %. However, because the BLSO thin film is not grown epitaxially on r-cut sapphire directly, we used MgO thin film as a buffer layer. There were many reports to using the MgO buffer layer for obtaining higher crystalline thin films [6-8]. The gonio scan result of BLSO/MgO/r-cut sapphire is indicated in Figure 2.3 (b). There are clearly shown that peaks of MgO buffer layer and BLSO thin films matching to the sapphire substrate are observed and no other peaks are existed. It means that the BLSO thin film on MgO/r-cut sapphire have epitaxial structure and their full width half maximum (FWHM) of rocking curve for omega scan is about 0.25^{o}, which indicate it has highly crystalline. Its electrical properties are shown in Table 2.2. However, it exhibit that the mobility of the BLSO thin film on MgO/r-cut sapphire is 7.96 $cm^2/V{\cdot}s$ which about ten times low compare with that of BLSO on STO (about 70 $cm^2/V{\cdot}s$). Because the structure of r-cut sapphire and BSO is different and the difficulty of MgO growth, the electrical properties of BLSO on MgO/r-cut sapphire is not good as BLSO on STO although it have relatively low lattice mismatch with BSO.

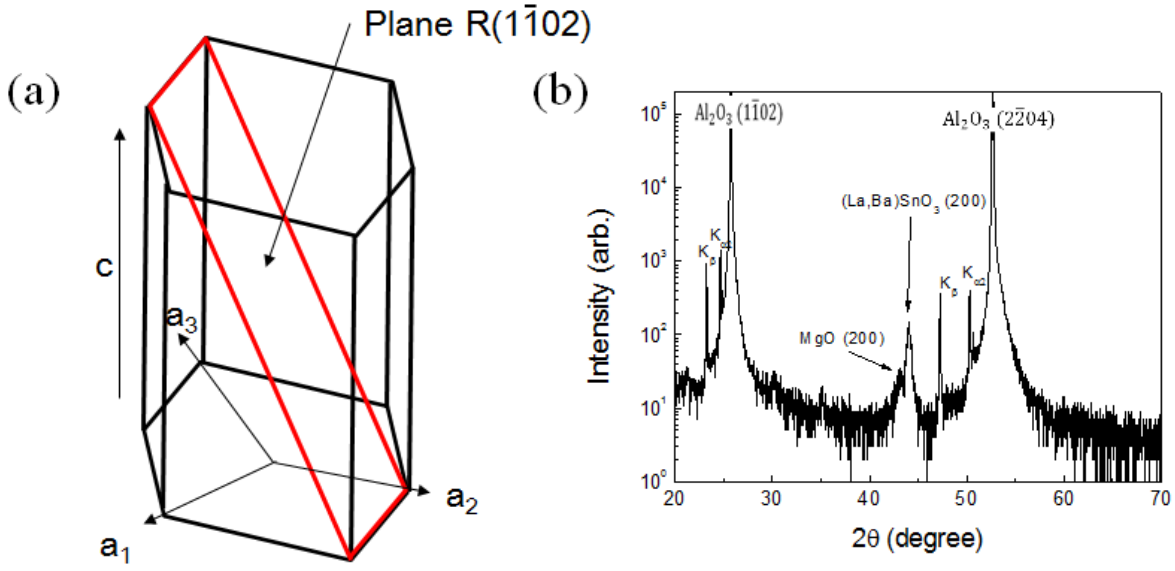

Figure 2.3. (a) The structure of r-cut sapphire in hexagonal sapphire structure (b) θ-2θ scan of BLSO /MgO /r-Al_2O_3 by X-ray diffraction method.

2.1.2 $MgAl_2O_4$

$MgAl_2O_4$ (100) substrate, which generally used for depositing GaN system [9-11], have spinel structure that means the oxygen packs face-centered cubic (FCC) and cations put partial occupancy of tetrahedral and octahedral sites i.e. 1/8 of tetrahedral and 1/2 of the octahedral sites are occupied. A spinel unit-cell is made up of eight FCC cells made by 2 × 2 × 2 oxygen ions configuration, so it is a big structure which consisting of 32 oxygen atoms, 8 A atoms and 16 B atoms. As shown at Table 2.1., the lattice mismatch between $MgAl_2O_4$ (1/4 plane) and BSO is about only 1.84 %. We deposit BLSO on many buffer layers on $MgAl_2O_4$ substrate; no buffer layer, $BaTiO_3$ (BTO), and STO on various temperature. The gonio scan results of various BLSO thin films on buffer layers/$MgAl_2O_4$ are indicated in Figure 2.4. Only using STO which grown at

600 ^{o}C as buffer layer show truly epitaxial structure. Surprisingly, using BTO buffer layer thin film is worse crystalline structure than using STO buffer layer even though BTO have only 2.96 % lattice mismatch which is clearly lower than that of STO (5.12 %). It may originate from the non-stoichiometry of the BTO thin film and its oxygen and Ba vacancies [12-13]. Its mobility of BLSO thin film on STO (grown at 600 ^{o}C) on $MgAl_2O_4$ shows about up to half of that of BLSO/STO (31.5 $cm^2/V{\cdot}s$) as shown at Table 2.3. We conclude that qualities of thin films using STO buffer layer is not exceed of that using STO single crystal substrate and other buffer layer is not work very well.

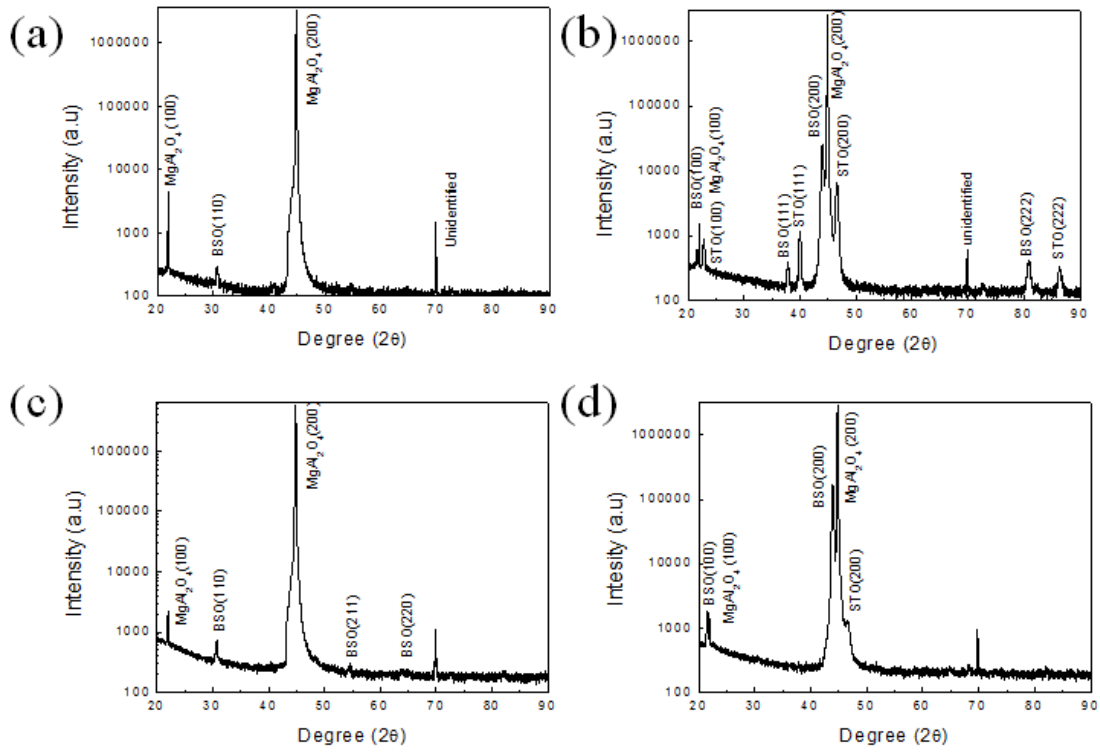

Figure 2.4. θ-2θ scan of (a) BLSO/$MgAl_2O_4$ (b) BLSO/STO(750 ^{o}C) $MgAl_2O_4$ (c) BLSO/BTO(700 ^{o}C)/$MgAl_2O_4$ (d) BLSO/STO(600 ^{o}C) /$MgAl_2O_4$ by X-ray diffraction method.

2.1.3 MgO

MgO (100) substrate has simple rock-salt structure for usually depositing superconducting system such as YBCO [14-16]. The lattice mismatch between r-cut sapphire (1/4 plane) and BSO is about 2.33 %. The gonio scan results BLSO thin film on MgO are indicated at Figure 2.5. The FWHM of rocking curve for BLSO (200) peak is 0.24^{o}, which shows highly crystalline structure. The highest mobility of BLSO thin film is up to 15.7 cm^2/V·s when we use BSO grown at 700 ^{o}C as buffer layer as shown at Table 2.4. From the electrical properties of BLSO /MgO system, we suggest that BLSO grown at 700 ^{o}C is more matched to MgO substrate than BLSO grown at 750 ^{o}C. We think that there are many parameters for matching between substrate and thin film besides lattice mismatch. In conclusion, the suitable substrate which has good lattice match and same perovskite structure must be found to obtaining BLSO thin film with better performance.

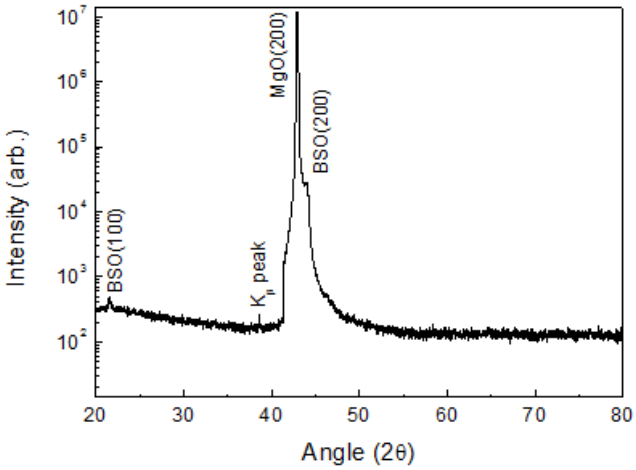

Figure 2.5. (b) θ-2θ scan of BLSO(750 ^{o}C) /BSO(700 ^{o}C)/MgO by X-ray diffraction method.

Sample	LBSO/MgO/r-Al_2O_3
Resistivity (Ω·cm)	0.00252
Mobility (cm^2/V·s)	7.96
Carrier concentration (/cm^3)	-3.11E+20

Table 2.2. The resistivity, mobility and carrier concentration on BLSO thin films on r-Al_2O_3 substrate.

Sample	BLSO on MgAl2O4	BLSO/STO (750 °C) on $MgAl_2O_4$
Resistivity (Ω·cm)	0.75	0.00111
Mobility (cm^2/V·s)	-	13.4
Carrier concentration (/cm^3)	-	4.22 x 10^{20}

Sample	BLSO/BTO on MgAl2O4	BLSO/STO (600 °C) on $MgAl_2O_4$
Resistivity (Ω·cm)	32	0.000653
Mobility (cm^2/V·s)	-	31.5
Carrier concentration (/cm^3)	-	3.03 x 10^{20}

Table 2.3. The resistivity, mobility and carrier concentration on BLSO thin films on $MgAl_2O_4$ substrate.

Sample	BLSO4%(50nm)/ MgO(100)	BLSO4%(40nm at 750°C)/BLSO 4%(10nm at 700°C)/MgO(100)
Resistivity (Ω·cm)	0.00443	0.00212
Mobility (cm^2/V·s)	11.5	15.7
Carrier concentration (/cm^3)	-1.23 x 10^{20}	-1.87 x 10^{20}

Table 2.4. The resistivity, mobility and carrier concentration on BLSO thin films on MgO substrate.

2.2 High temperature experiment of BLSO thin films

As we described above, the conductivity is significantly diminished by threading dislocations or grain boundaries for charge trapping and inelastic scattering. We measure the resistance at high temperature because it confirmed the type of the carrier by changing background atmosphere at high temperature although its resistance is too high to measure at room temperature. We recorded the resistance as increasing temperature in oxygen atmosphere to decide that sample has metallic or semiconducting behavior. And we change atmosphere oxygen to argon and oxygen again when temperature maintains constant. The oxygen vacancies act as electron donor in oxide materials. It means that vacancies generally induce the n-type carrier. Therefore, resistance of the p-type material should be increased if we change background atmosphere from oxygen to argon and that of n-type material should be decreased in same condition.

Surprisingly, the electrical behavior of 2 % BLSO thin film and 0.6 % BLSO at high temperature thin film is completely different. The resistance of 2 % BLSO thin film increased constantly when temperature is raised; however, the resistance of 2 % BLSO thin film decreased constantly. It indicates that 2 % BLSO thin film is degenerate semiconductor which shows almost metallic behavior and 0.6 % BLSO thin film exhibits conventional semiconducting behavior. And the resistance change of BLSO thin films by alternating background atmosphere is shown in Figure 2.6. As you can see, the resistance of 2 % BLSO thin film changes from 130 Ω in oxygen atmosphere to 125 Ω in argon atmosphere. On the contrary, the resistance of 0.6 % BLSO thin film changes from about 1000 Ω in oxygen atmosphere to 3500 Ω in argon atmosphere. The abrupt changes of resistance occur when we change background atmosphere. This phenomenon might come from the effect of

surface bonding such as dangling bond which hold the oxygen ions. In conclusion, the small amount of La-doped BSO thin film acts like p-type semiconductor even though n-type carriers are doped because of the effect of threading dislocations. Therefore we only fabricate BLSO thin film which has high carrier concentration about 10^{19} /cm^3 for n-type system.

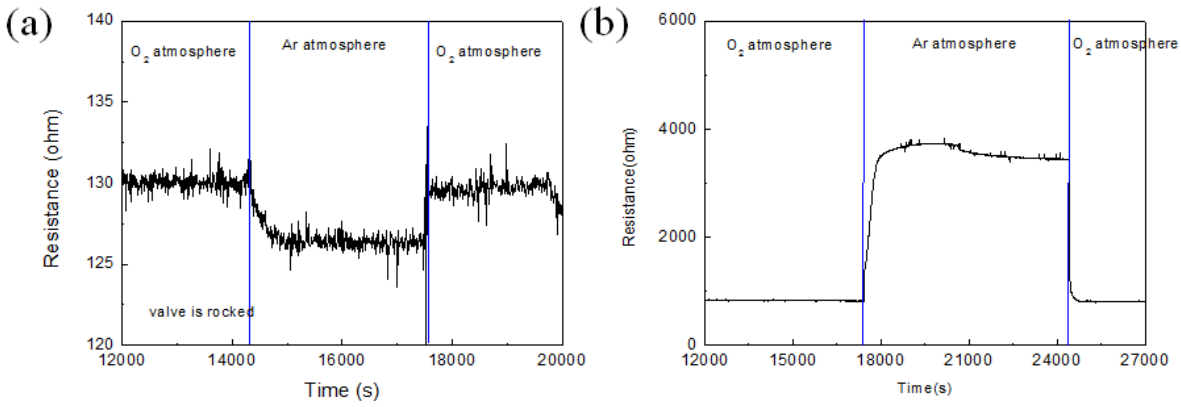

Figure 2.6. High temperature experiment results of (a) 2 % BLSO thin film measured at 500 ^{o}C (b) 0.6 % BLSO thin film at 700 ^{o}C.

Reference

[1] H. J Kim, U. Kim, H. M. Kim, T. H. Kim, H. Mun, B. G. Jeon, K. T. Hong, W. J. Lee, C. Ju, K. H. Kim & Kookrin Char, Appl. Phys. Exp. **5**, 061102 (2012).

[2] H. Mun, U. Kim, H. M. Kim, C. Park, T. H. Kim, K. H. Kim & K. Char, Appl. Phys. Lett. **102,** 252105 (2013).

[3] D. Hull & D. J. Bacon., Introduction to dislocations. (Elsevier, 2011) Chapter 9.6.

[4] L. Mieville, T. H. Gaballe, L. Antagnazza, and K. Char, Appl. Phys. Lett. **70**, 126 (1997).

[5] Kinoshita & M. Umehara, US patent, US 2004/0109486 A1 (2004).

[6] J. G. Lisoni, M. Siegert, C.H Lei, W. Biegel, J. Schubert, W. Zander & C. Buchal., Thin Solid films, **389**, 219 (2001).

[7] C. H. Lei, C. L. Jia, J. G. Lisoni, M. Siegert, J. Schubert, C. Buchal & K Urban., J. Crys. Growth **219**, 397 (2000).

[8] P. A. Stampe, M. Bullock, W. P. Tucker & R. J. Kennedy, J. Phys D **32**, 1778 (1999).

[9] S. Nakamura, M.i Senoh, S. Nagahama, N. Iwasa, T. Yamada, T. Matsushita, H. Kiyoku & Y. Sugimoto Appl. Phys. Lett. **68**, 2105 (1996).

[10] A. Kuramata, K. Horino, K. Domen, K. Shinohara & T. Tanahashi, Appl. Phys. Lett. **67**, 2521 (1995).

[11] A. N. Efimov, A. O. Lebedev, V. V. Lundin & A. S. Usikov, Cryst.

Reports **45**, 312 (2000).

[12] G.V Lewis & C.R.A Catlow, J. Phys. Chem. Solids **47**, 89 (1986).

[13] N. H. Chan, R. K. Sharma & D. M. Smyth, J . Am. Ceram. Soc. **64**, 556 (1981).

[14] B. H. Moeckly, S. E. Russek, D. K. Lathrop, R. A. Buhrman, J. Li & J. W. Mayer, Appl. Phys. Lett. **57**, 1687 (1990).

[15] D. M. Hwang, T. S. Ravi, R. Ramesh, S. W. Chan, C. Y. Chen, L. Nazar, X. D. Wu, A. Inam and T. Venkatesan, Appl. Phys. Lett. **57**, 1690 (1990).

[16] S. Miki, M. Fujiwara, M. Sasaki, B. Baek, A. J. Miller, R. H. Hadfield, S. W. Nam & Z. Wang, Appl. Phys. Lett. **92**, 061116 (2008).

3. Properties of p-type BSO thin films

3.1 K-doped BSO (BKSO) thin films

3.1.1 BKSO thin film deposition

We deposited 100 nm think BKSO thin film (deposited at 700 ^{o}C) on 5 nm thick BSO buffer layer (deposited at 750 ^{o}C) on the STO (001) substrate using BSO and K_2SnO_3 (KSO) targets by pulsed laser deposition system with a KrF excimer laser (λ = 248 nm) under 100 mTorr oxygen pressure with 1 ~ 1.5 J/cm^2 energy intensity. To partially dope potassium ions, we used a sequential deposition method which deposits thin films by sequentially alternating targets for each determined pulse shots [1]. The plume of the BSO and KSO targets are shown at Figure 3.1 when laser is ablaze at target. As you can see, the size of the plume of BSO and KSO are very different. Therefore, the deposition rate is not exactly matched to the shot ratio of the BSO and KSO targets. Also, we consider that doping rate is not precisely determined by nominal shot ratios because potassium is quite volatile at high temperature.

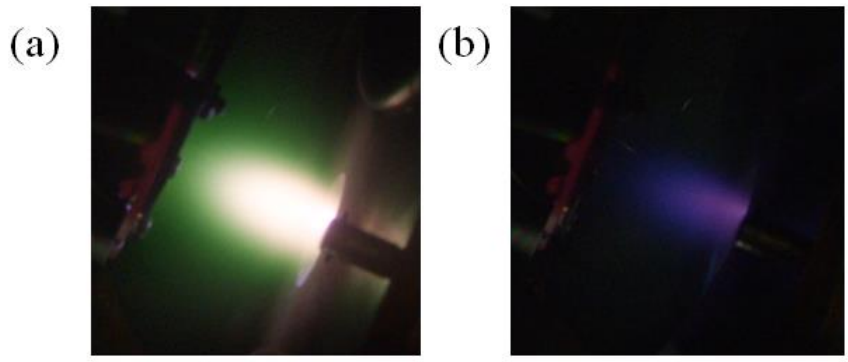

Figure 3.1. Plumes for laser ablation in pulsed laser deposition method. (a) Plume of BSO and (b) KSO.

3.1.2 Electron spectroscopy for chemical analysis

In order to quantify the concentration of potassium at BKSO thin film, electron spectroscopy for chemical analysis (ESCA) method was used. The equation of the relative density between the dopant and host atoms derived by measured intensity ratio is as follows:

$$\frac{\eta_d}{\eta_h} = \frac{I_d \sigma_d \lambda(\varepsilon_d) D(\varepsilon_d)}{I_h \sigma_h \lambda(\varepsilon_h) D(\varepsilon_h)} \quad (3.1)$$

where I is the intensity of the X-ray peak, σ is the photo-excitation probability, λ is the mean free path of an excited electron with energy ε, D is the fraction of electrons detected by the analyzer, and the lower subscripts d and h are used for dopants and host atoms in equation (3.1) [2]. We assumed that detection efficiencies for Ba and K elements are same, and the mean free path and photo-excitation probability (denoted in parenthesis) of Ba and K are 25.8 (0.473) and 17.2 (0.248) [2, 3]. Using above formula and X-ray intensity obtained by ESCA shown in Figure 3.2, we can estimate doping ratio of potassium at the several different BKSO thin films, which are shown in Figure 3.3. Using this peaks and equation (3.1), we concluded that the estimated doping rate of K is generally proportional to the shot ratio of BSO and KSO targets as you can see at Figure 3.3. Therefore, we derive the exact doping ratio of K in BKSO thin films from ESCA.

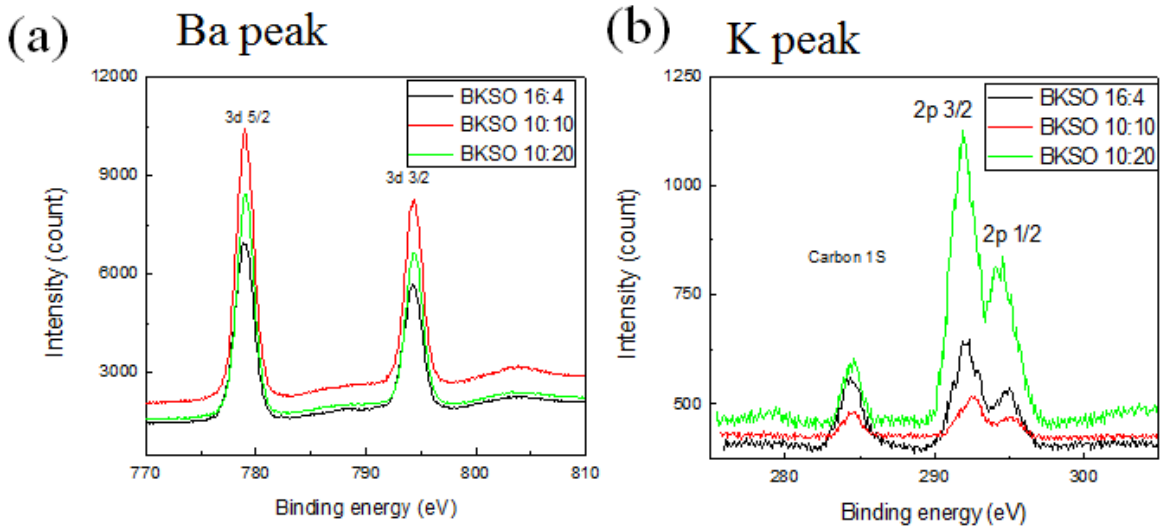

Figure 3.2. XPS peaks for (a) Ba and (b) K by ESCA method. We calculated the concentration of K about Ba by 3d 5/2 peak for Ba and 2p 3/2 for K.

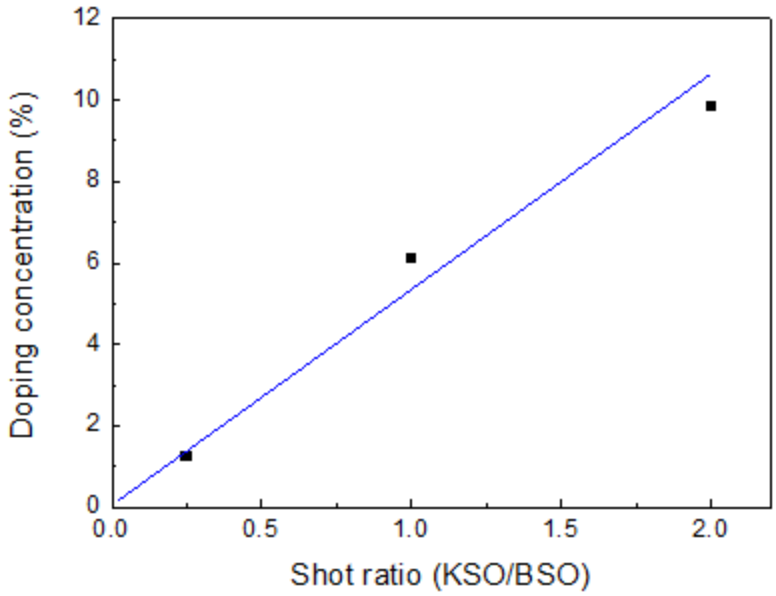

Figure 3.3. Doping centration vs. shot ratio graph plotted by ESCA method. Blue line is linear estimation for fitting. The shot ratio indicates for proportion to the number of laser shots for KSO and BSO target.

3.1.3 Structural and Surface properties of BKSO thin films

For proof of the epitaxiality of the BKSO thin film, as already shown at BSO and BLSO thin film [4], we obtained the structural information of BKSO thin film by the X-ray diffraction method, represented in Figure 3.4. The θ-2θ scan confirms that the epitaxial film was deposited along the direction of STO substrate. Compared with the peak of the BSO film buffer layer, definitely higher X-ray peak intensities as we deposit thicker BKSO films strongly supports that BKSO thin films on BSO buffer layer are grown to highly epitaxial structure. The values of full width at half maximum (FWHM) of the ω-scan at the BKSO (002) peak position for BSO buffer, BKSO 1.5 %, 6 % and 11 % are 0.11^{o}, 0.13^{o}, 0.40^{o} and 0.42^{o}, as indicated in Figure 3.5 which shows that BKSO film have highly crystalline and well oriented structure. Also, to confirm the surface homogeneity of the BKSO film, we use the AFM image as shown in Figure 3.6 and the SEM picture as shown in Figure 3.7. Through the AFM image, we found the surface of the 6 % BKSO films to be almost atomically flat and have a very low roughness value which is 0.738 nm. The roughness of the BLSO thin film is 0.223 nm. Though the roughness of the BKSO is larger than BLSO thin film, it has excellent surface to fabricating device and consisting their interface. By the SEM image, the 6 % BKSO films exhibit highly flat surface morphology and no potassium segregation was observed contrary to the image of KSO thin film with segregations.

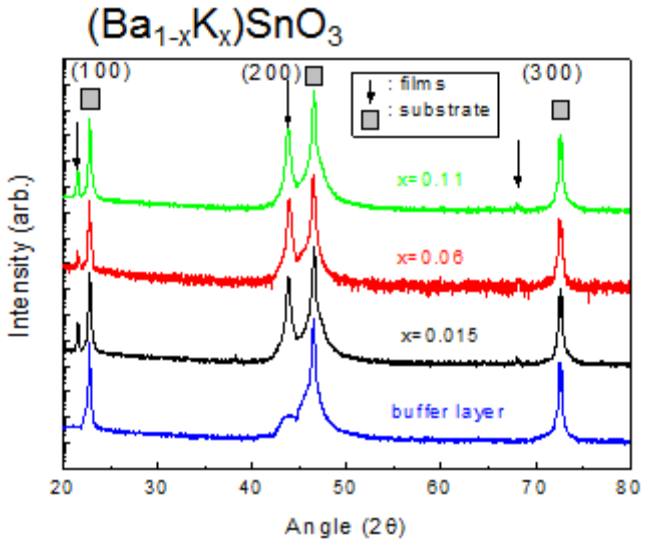

Figure 3.4. A θ-2θ scan of various BKSO thin films on STO substrate with BSO buffer layer (BSO/STO) and BSO buffer film.

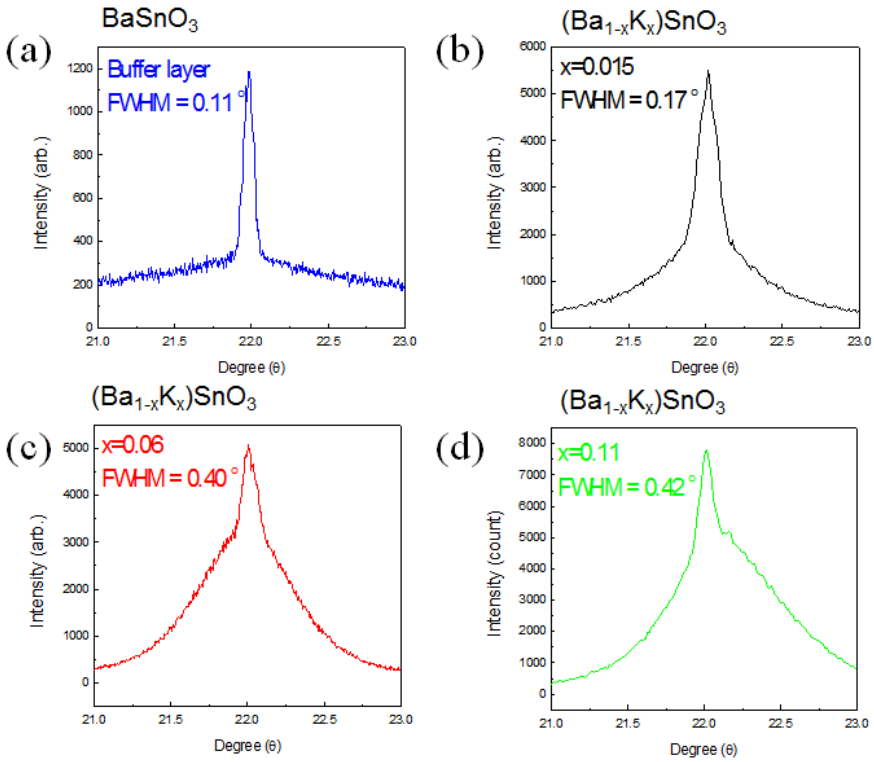

Figure 3.5. A rocking curve for BSO and BKSO (200) peak of various BKSO thin films on STO substrate. (a) BSO buffer film (b) 1.5 % BKSO film (c) 6 % BKSO film (d) 11 % BKSO film.

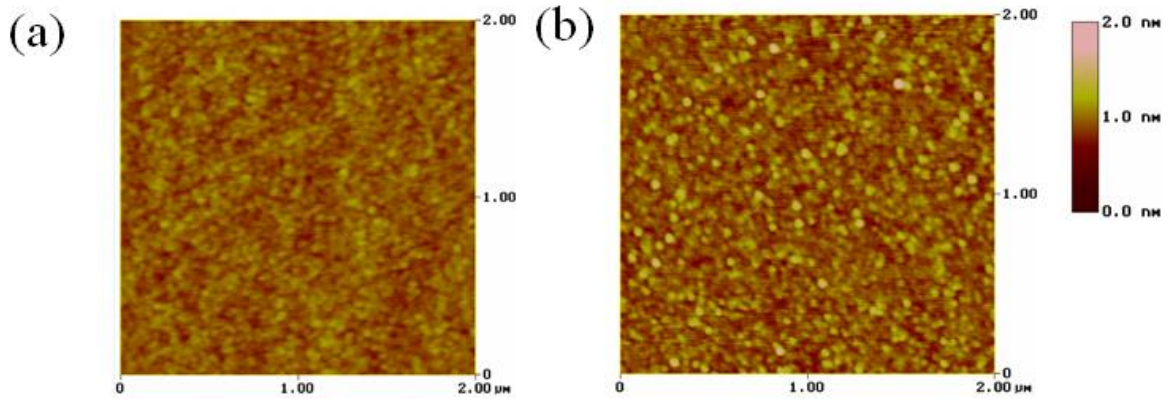

Figure 3.6. (a) AFM image of BLSO thin film on STO with roughness value 0.223 nm (b) AFM image of the 6 % BKSO thin film on BSO/STO with roughness value 0.738 nm.

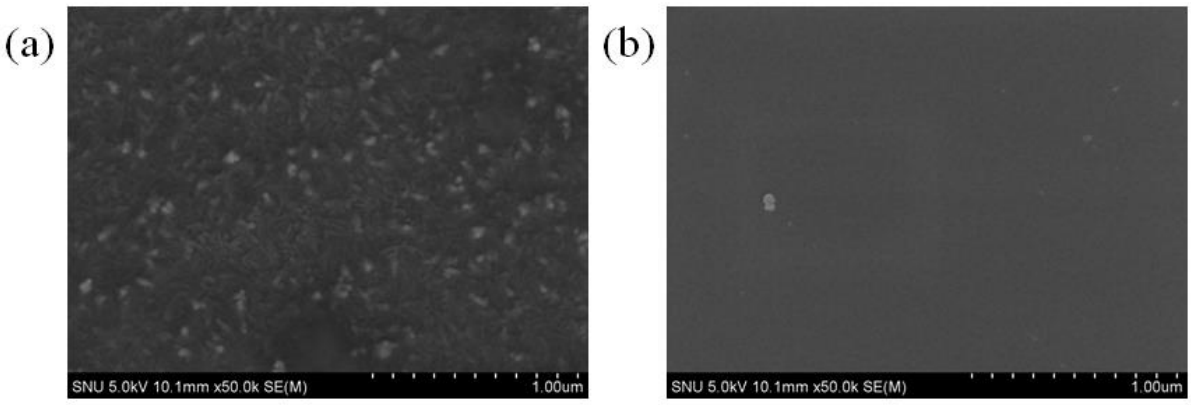

Figure 3.7. (a) SEM image of KSO thin film on STO with many congregations (b) SEM image of the 6 % BKSO thin film on BSO/STO with no K congregation.

3.1.4 High temperature measurement of BKSO thin film

To investigate the electrical properties of BKSO thin film, we execute measurement of the resistance of the 1.5 %, 6 % and 11 % BKSO thin films at high temperature because resistance was too high to measure at room temperature. We used for measuring resistances by the voltage-driven 2-probe method which is able to detect much higher resistance. Because of very high resistance even at high temperature, we suppose that contact resistance is not significantly affected for high temperature measurement. To evaluate the activation energy of K in BKSO thin film, we plot the graph for resistance versus reciprocal temperature [5-9], as shown in Figure 3.8. As you can see, resistance is almost exponentially decayed for rising temperature. We calculate the activation energy for the low temperature region by extrapolation method denoted by dash line, because the resistance is too high to measure at low temperature and low temperature region is important for pn junction operation. We estimate the activation energy which value is 0.49 eV using the conventional Arrhenius formula [10]. From this activation energy, we obtained the carrier concentration of holes in this 6 % and 11 % BKSO thin film to be about 5.67×10^{12} and 1.03×10^{13} /cm^3 at room temperature, assuming a full activation of intrinsic K doping concentration at given activation energy. The corresponding mobility from the measured conductivity is about 0.0556 and 0.303 cm^2/V·s for 6 % and 11 % BKSO films at room temperature. The lower mobility for the lowest doping indicates that charge trapping mechanism is enhanced by grain boundaries/dislocations [4, 11].

To confirm that the BKSO thin films are indeed p-type, we measured changing resistance by switching the background atmosphere from O_2 to Ar and O_2 again at 750 ^{o}C in a tube furnace system. In oxide thin film, the oxygen

vacancies are existed which regarded as act for n-type carrier. In general, oxygen vacancies are reduced at O_2 and induced at Ar background, especially at very high temperature. Therefore, we determine the carrier type by observing the change of resistances when changing the background gas. As shown in Figure 3.9, the all resistances of BKSO films increased when the background gas atmosphere was changed from O_2 to Ar. This finding indicates that the BKSO thin film is indeed a p-type doped semiconductor. The resistance ratios between O_2 and Ar gas of 1.5 %, 6 %, 11 % BKSO thin films are 7.6, 9.6 and 11.7, respectively. It means that the amounts of K are clearly affected to the resistance ratios, indicating that K in BKSO thin film acts as p-type dopants. When the background gas atmosphere was switched back to the oxygen, the resistance abruptly switched to the original value in the oxygen atmosphere although the resistance increase in Ar atmosphere was rather gradual. This sudden change of resistance might be originated from the oxygen ions trapping at the surface by forming a kind of dangling bonds Ar background atmosphere because of the strong oxygen bonding of at BKSO thin films.

3.1.5 Summary

We deposited an epitaxial K-doped BSO thin film on BSO buffer layer and confirmed its crystallinity and K incorporation by X-ray diffraction and ESCA. Although BKSO exhibited rather high resistivity at room temperature, its conductivity increased dramatically at high temperature, yielding high activation energy of 0.49 eV. The conductivity decreased when a small amount of oxygen was removed from the films consistent with the behavior of p-type doped oxides in contrast to that of n-type BLSO. We need to increase the p-doping level for better performance by finding a more suitable dopant.

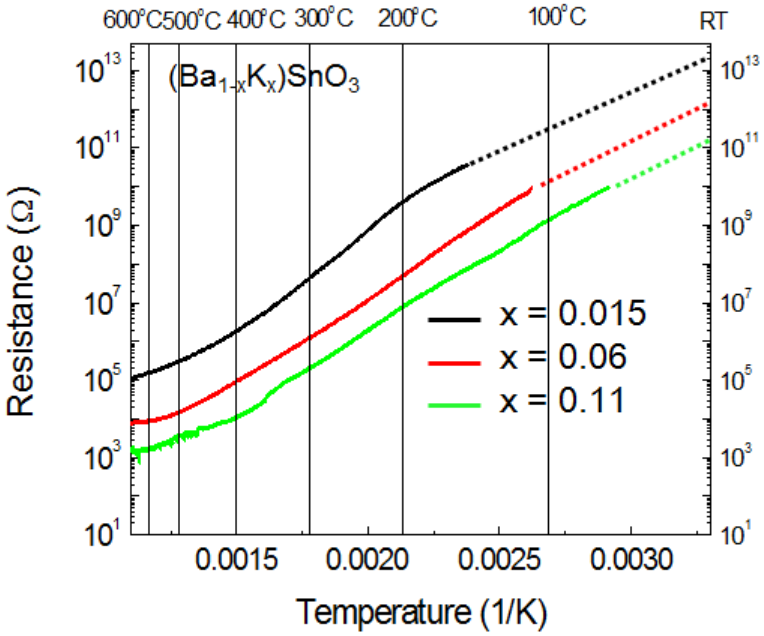

Figure 3.8. High temperature measurement result for BKSO thin films. The graph indicates that resistance versus inverse temperature graph of the BKSO thin films. Each line is two probe measurement results and each dash line is estimation line for extrapolation.

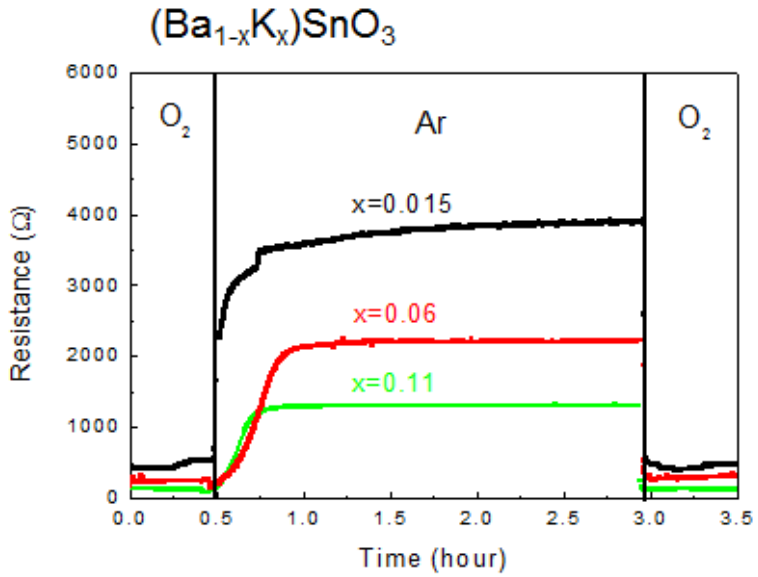

Figure 3.9. High temperature measurement result for BKSO thin films by resistance versus time graph of the BKSO thin films for changing background atmosphere.

3.2 Other p-type doping BSO thin film

3.2.1 Ga-doped BSO (BSGO) thin film

Gallium was used as conventional p-type carrier dopant for ZnO [12] and coping technique with N for ZnO [13, 14]. We deposited 100 nm think BSGO thin film (deposited at 700 ^{o}C) on the STO (001) substrate using BSO and Ga_2O_3 targets by pulsed laser deposition system using sequential deposition method. For proof of the epitaxiality of the BSGO thin film, we obtained the structural information of BSGO thin film by the X-ray diffraction method, represented in Figure 3.10. The θ-2θ scan confirms that the film was deposited epitaxially along the direction of STO substrate. The values of FWHM of the ω-scan, as indicated at Figure 3.10 (b), at the BSGO (002) peak position is 1.38 ^{o} which indicate relatively bad crystalline orientation mainly due to the absence of the BSO buffer layer. To investigate the electrical properties of BSGO thin film, we execute measurement of the resistance BSGO thin films at high temperature using 4 probe methods. We estimate the activation energy which value is 0.81 eV using the conventional Arrhenius formula using reciprocal temperature vs. resistance graph as indicated in Figure 3.11 (a). Also, to confirm that the BSGO thin films are indeed p-type, we measured changing resistance by switching the background atmosphere from O_2 to Ar and O_2 again at 700 ^{o}C in a tube furnace system. The resistance ratios of BSGO thin films between O_2 and Ar gas is 4.33 as shown at Figure 3.11 (b). In conclusion, the activation energy of Ga in BSGO thin film is too high, we regarded that Ga is not suitable dopant for p-type of BSO thin film.

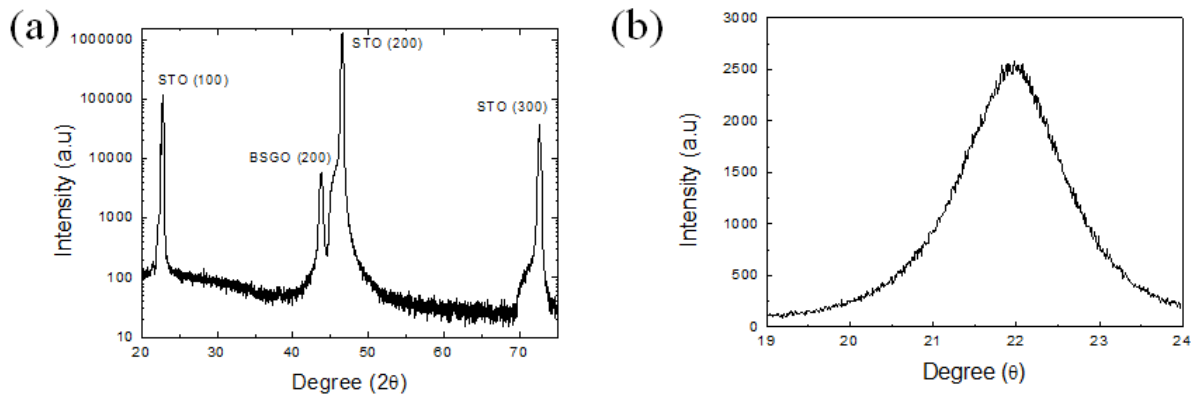

Figure 3.10. (a) A θ-2θ scan of BSGO thin films on STO substrate without BSO buffer layer. (b) A rocking curve for BSO and BSGO (200) peak which FWHM is 1.38^{o}.

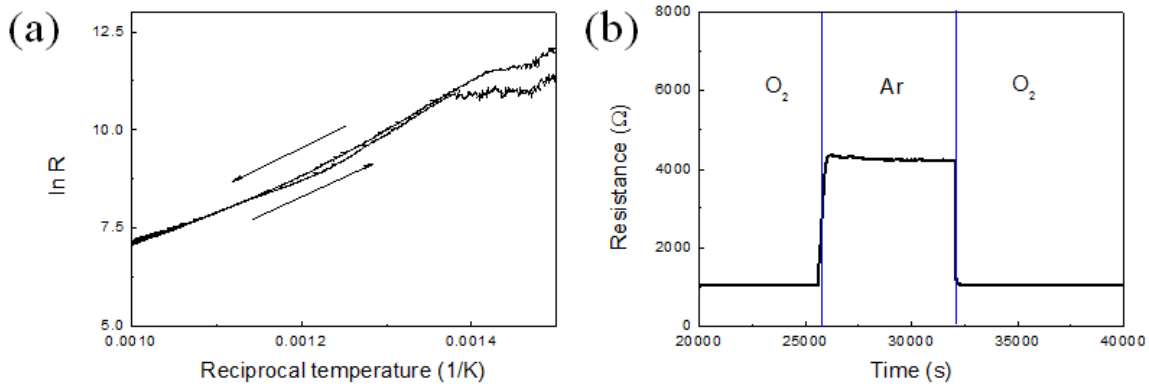

Figure 3.11. High temperature measurement result for BSGO thin films. (a) Resistance versus inverse temperature graph of the BSGO thin films. (b) Resistance versus time graph of the BKSO thin films for changing background atmosphere.

3.2.2 Cu-doped BSO (BSCO) thin film

Cu have great attention when Cu^{+} bearing oxide show p-type in TCO regime such as $CuGaO_2$ [15] and $SrCu_2O_2$ [16]. We deposited 100 nm think BSCO thin film (deposited at 700 ^{o}C) on the STO (001) substrate using BSO and CuO targets by pulsed laser deposition system using sequential deposition method, almost same as BKSO and BSGO case. For proof of the epitaxiality of the BSCO thin film. We obtained the structural information of BSGO thin film by the X-ray diffraction method, represented in Figure 3.12. The θ-2θ scan confirms that the film only have epitaxial phase along the direction of STO substrate. The values of FWHM of the rocking scan, as indicated in Figure 3.12 (b), at the BSCO (002) peak position is 0.18 ^{o} which shows that BSCO film has highly crystalline and well oriented structure. To investigate the electrical properties of BSCO thin film, we executed measurement of the resistance BSCO thin films at high temperature using 4 probe methods. We estimate the activation energy which value is 0.64 eV using the conventional Arrhenius formula using reciprocal temperature vs. resistance graph as indicated in Figure 3.13. Also, to confirm that the BSCO thin films are indeed p-type, we measured changing resistance by switching the background atmosphere from O_2 to Ar and O_2 again at 700 ^{o}C in a tube furnace system. The resistance ratios of BSCO thin films between O_2 and Ar gas is 8.60 as shown at Figure 3.13 (b). The reason that activation energy of Cu is too high is that Cu ion doped as 2^{+} ions, not 1^{+} ion, as we confirmed by the XPS result.

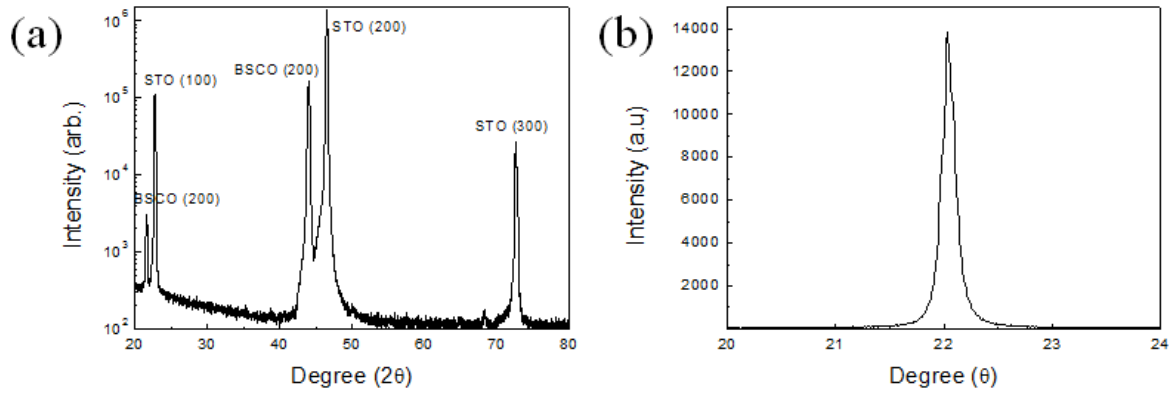

Figure 3.12. (a) A θ-2θ scan of BSCO thin films on STO substrate on BSO buffer layer. (b) A rocking curve for BSO and BSCO (200) peak which FWHM is 0.18°.

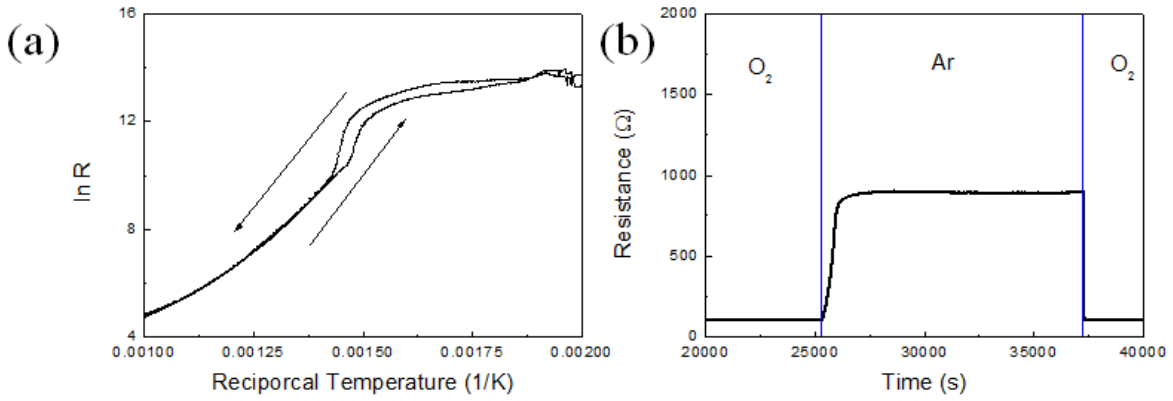

Figure 3.13. High temperature measurement result for BSCO thin films. (a) Resistance versus inverse temperature graph of the BSCO thin films. (b) Resistance versus time graph of the BSCO thin films for changing background atmosphere.

Reference

[1] L. Mieville, T. H. Gaballe, L. Antagnazza, and K. Char, Appl. Phys. Lett. **70**, 126 (1997).

[2] D. R. Chen, Journal of Electron Spectroscopy and Related Phenomena **9**, 29 (1976).

[3] J. H. Scofield, Lawerence Livermore Laboratory, Report No. UCRL-51326 (1973).

[4] H. J Kim, U. Kim, H. M. Kim, T. H. Kim, H. Mun, B. G. Jeon, K. T. Hong, W. J. Lee, C. Ju, K. H. Kim & Kookrin Char, Appl. Phys. Exp. **5**, 061102 (2012).

[5] O. Lopatiuk-Tirpak, W. V. Schoenfeld, L. Chernyak, F. X. Xiu, J. L. Liu, S. Jang, F. Ren, S. J. Pearton, A. Osinsky & P. Chow, Appl. Phys. Lett. **88**, 202110 (2006).

[6] Y. Pei, A. D. LaLonde, H. Wang & G. Jeffrey Snyder, Energy Environ Sci. **5**, 7963 (2012).

[7] P. Huang & A. Petric J. Electrochem. Soc. **143**, 1644 (1996).

[8] V. Thangadurai &W. Weppner, J. Electrochem. Soc. **148**, 1294 (2001).

[9] H. He, X. Huang & L. Chen, Electrochimica Acta **46**, 2871 (2001).

[10] D. B. Rogers, J. M. Honig & J. B. Goodenough, Mat. Res. Bull. **2**, 223 (1967).

[11] H. Mun, U. Kim, H. M. Kim, C. Park, T. H. Kim, K. H. Kim & K. Char, Appl. Phys. Lett. **102,** 252105 (2013).

[12] M. Joseph, H. Tabata& T. Kawai Jpn. J. Appl. Phys. **38**, 1205 (1999).

[13] Y. Yan & S. B. Zhang, Phys. Rev. Lett. **86**, 5723 (2001).

[14] M Joseph, H. Tabata, H. Saeki, K. Ueda & T. Kawai Physica B **302**, 140 (2001).

[15] K. Ueda, T. Hase, H. Yanagi, H. Kawazoe, H. Hosono, H. Ohta, M. Orita & M. Hirano, J. Appl. Phys. **89**, 1790 (1999).

[16] A. Kudo, H. Yanagi, H. Hosono & H. Kawazoe., Appl. Phys. Lett. **73**, 220 (1998).

4. pn junction fabricated with BLSO and BKSO

4.1 Theory

In semiconductor, the Fermi level E_F is near the valence band edge in the p-type material and near the conduction band edge in the n-type material. When the p- and n-type semiconductors are jointed together, the large carrier concentration gradients at the junction due to carrier diffusion; Holes from the p-side diffuse into the n-side, and electrons from the n-side diffuse into the p-side [1]. Diffusion will continue until basic criterion for thermal equilibrium is attained, i.e. the Fermi energy is constant throughout the system. During this process, the uncompensated charged ions are referred as space charge and the region in which they are located is the depletion region [2]. The voltage drops across the junction under equilibrium conditions and the appearance of charge near the metallurgical boundary. This voltage drop across the depletion region under equilibrium conditions is known as built-in potential [3]. The most important characteristic of pn junction is that they have rectifying behavior [1]. The current increases rapidly as the voltage increases, when we apply forward bias (positively voltage on the p-side). However, there are virtually no current flows when we apply a reverse bias.

4.1.1 Electrostatic analysis of pn junction

We assumed an abrupt junction the concentration of doping atoms changes discontinuously from a uniform value N_A on the p-side to another uniform value N_D on the n-side [3]. In thermal equilibrium condition, we will show that how to use the Poisson equation and current density equations to calculate the built-in electric, the potential and the width of the depletion layer. We assumed abrupt

pn junction which charge densities are abruptly changed. And there are the space charge regions adjacent to the junction interface only uncompensated donor and acceptor ions existed. The space charge region is a so-called depletion layer.

From the fact that charge density passing through pn junction is zero, the charge density of p side is

$$j_p = q\mu_p \left(pE - \frac{kT}{q}\frac{\partial p}{\partial x} \right) = 0 \qquad (4.1)$$

From equation (4.1), we find electric field

$$E_x = \frac{kT}{q}\frac{1}{p}\frac{\partial p}{\partial x} = -\frac{\partial \varphi}{\partial x} \qquad (4.2)$$

φ is the electrostatic potential. Because the intrinsic charge density$n_i = \sqrt{n_p N_D} = \sqrt{N_A p_n}$ and equation (4.2), we know the relation of the built-in potential in the junction

$$V_b = \frac{E_q}{q} + \frac{kT}{q}\ln\left[\frac{N_A N_D}{n_i^2}\right] \qquad (4.3)$$

If we only consider 1 dimensional junction, we find the charge density at depletion region by depletion approximation at junction interface,

$$\begin{aligned} \rho\,(x) &= -qN_A \left(-x_p \le x \le 0\right) \\ &= qN_D \ (0 \le x \le x_n) \qquad (4.4) \\ &= 0 \ (x \le x_p \ and \ x \ge x_n) \end{aligned}$$

Because the distribution of charges formed the step junction under equilibrium condition from (4.4) , the continuity of the electric field is found to

require [2]

$$N_A x_p = N_D x_n \qquad (4.5)$$

Put equation (4.4) to Poisson equation we get the formula

$$\frac{d^2\varphi}{dx^2} = qN_A/(\varepsilon\varepsilon_0)\ (-x_p \le x \le 0)$$

$$= -\mathrm{q}N_D/(\varepsilon\varepsilon_0)\ (0 \le x \le x_n \qquad (4.6)$$

$$= 0\ (x \le x_p\ and\ x \ge x_n)$$

Hence the electric field of the depletion region is

$$\mathrm{E(x)} = -\frac{qN_A}{\varepsilon\varepsilon_0}(x_p + x)\ (-x_p \le x \le 0) \qquad (4.7)$$

$$= -\frac{qN_D}{\varepsilon\varepsilon_0}(x_n - x)\ (0 \le x \le x_n)$$

Also, the electrostatic potential is obtained from the equation (4.6),

$$\varphi(\mathrm{x}) = \frac{qN_A}{2\varepsilon\varepsilon_0}(x_p + x)^2\ (-x_p \le x \le 0) \quad (4.8)$$

$$= V_b - \frac{qN_D}{2\varepsilon\varepsilon_0}(x_n - x)^2\ (0 \le x \le x_n)$$

The results of the electric field and electrostatic potential as a function of position for an abrupt p-n junction (equation (4.4) to (4.8)) are shown in Figure. 4.1.

Lastly, Solving about x_p and x_n combining equation (4.7)

$$x_n = \left[\frac{2K_s\varepsilon_o}{q}\frac{N_A}{N_D(N_A+N_D)}V_{bi}\right]^{1/2} \qquad (4.9)$$

$$x_p = \left[\frac{2K_s\varepsilon_o}{q}\frac{N_D}{N_A(N_A+N_D)}V_{bi}\right]^{1/2} \quad (4.10)$$

And the total width of the depletion region is $W \equiv x_p + x_n = W_p + W_n$.

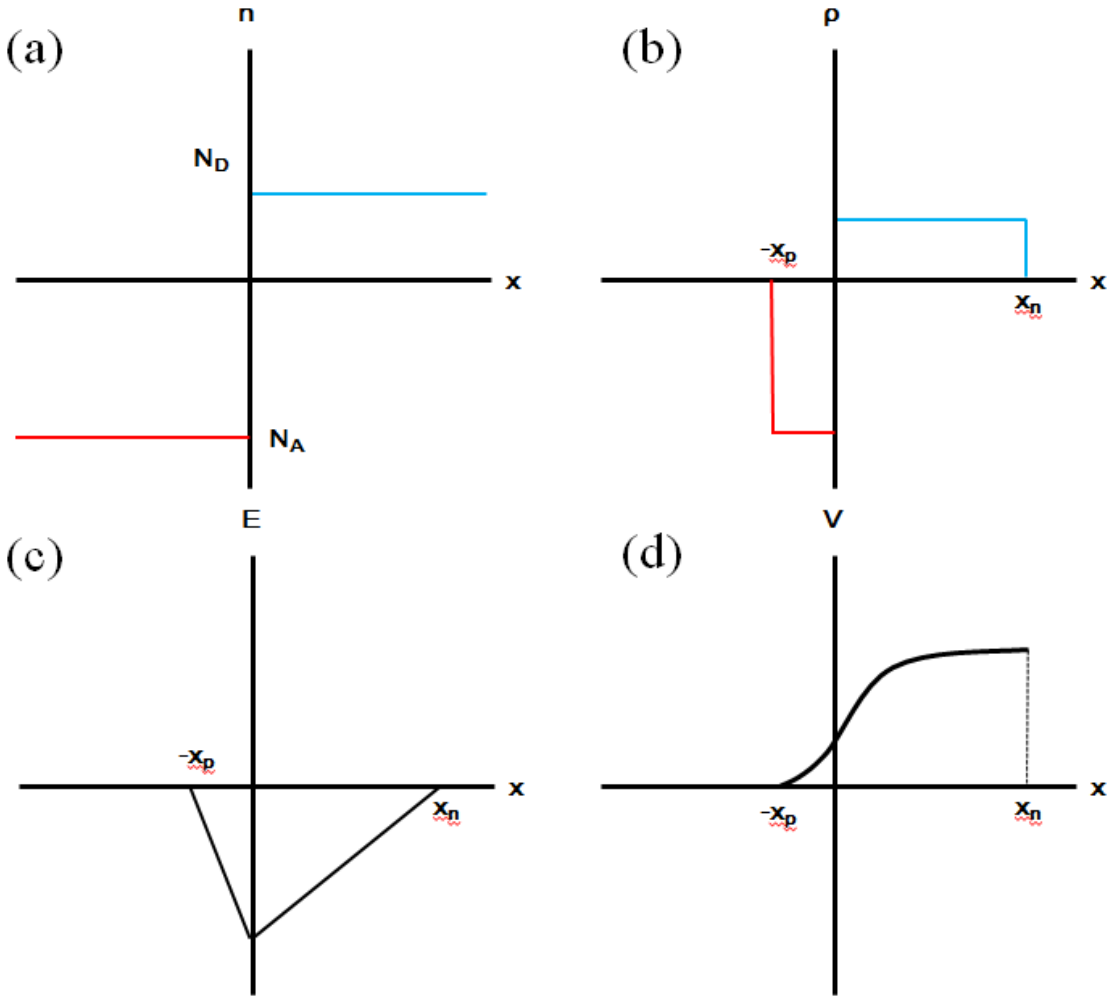

Figure 4.1. Depletion approximation based qualitative solution for the electrostatic variables in a pn step junction under equilibrium conditions. (a) Step junction profile (b) charge density (c) electric field and (d) electrostatic potential as a function of position.

4.1.2 The ideal I-V characteristics

We use the subscript n and p to denote the semiconductor type and the subscript o to specify the condition of thermal equilibrium. Using built-in potential and the mass action low $p_{p0}n_{n0} = n_i^2$, we obtain the electron density at the boundary of the depletion region [1]:

$$n_p - n_{p0} = n_{p0}\left[\exp\left(\frac{qV}{kT}\right) - 1\right] \quad (4.11)$$

$$p_n - p_{n0} = p_{n0}\left[\exp\left(\frac{qV}{kT}\right) - 1\right] \quad (4.12)$$

Since the neutral region is small, there is no reason for any substantial minority carrier drift current to flow. Therefore, the current is originated due almost entirely to diffusion [4]. From (4.11) and (4.12) the current density of each side is as below:

$$J_p = -qD_p[p_n - p_{n0}]/L_p \quad (4.13)$$

$$J_n = -qD_n[n_p - n_{p0}]/L_n \quad (4.14)$$

The D means that the diffusion constant and L is the diffusion length which is equal to$\sqrt{D\tau}$. Therefore, the ideal current through pn junction at forward bias is described by following equations:

$$\mathrm{I} = I_0\left[\exp\left(\frac{qV}{kT}\right) - 1\right] \quad (4.15)$$

$$I_0 = \frac{qAD_p p_{n0}}{L_p} + \frac{qAD_n n_{p0}}{L_n} \quad (4.16)$$

The barrier thus produced can be modulated by and applied voltage, thereby causing the currents through the junction to be modulated [3].

4.1.3 The asymmetry pn junction

We called the asymmetry pn junction when the one side is doped much heavily than the other side [4]. In the asymmetry pn junction, the depletion layer thickness and the potential on the heavily doped side is neglected in calculation. For example, for the n^+-p junction, $I = I_0[\exp(qV/kT) - 1]$ with $I_0 = qAD_n n_{p0}/L_n$. In the highly asymmetrical junction, carriers coming from the highly doped region create a layer of mobile charge in the depletion region of the less-doped zone [5]. Since acceptor doping is much lower than donor doping, electrons are not neglected in the n-region or in the p-region without imposing the depletion approximation [5], may not obeying conventional ideal pn junction formula.

For asymmetrical abrupt p-n junctions, due to accumulation of free carriers there is an inversion layer at the junction interface close to the lowly doped side. To solve the problem, the free carrier, p and n, must be taken into account during calculations. In a case of n^+-p junction, a larger number of electrons will be accumulated at the p-side of the junction to form an n-type inversion layer. Such a charge accumulation is able to change the value of the built-in voltage and width of the depletion region.

4.2 Fabrication of pn junction

We fabricate the BKSO/BLSO pn junction which consists of 1 % BLSO for the n-type and 6 % or 11 % BKSO for the p-type. Firstly, 4 % BLSO layer was deposited on the STO (100) substrate which has highly conductive and sustains good epitaxiality. The resistivity of 4 % BLSO layer is about 0.2 mΩ·cm, the resistance through this conducting layer is less than 100 Ω including contact resistances. Then we deposited 1 % BLSO film with 100 nm thickness using Si stencil mask. The resistivity, mobility and carrier concentration of 1 % BLSO film which is used for n-type were 0.0274 Ω·cm, 23.4 $cm^2/V \cdot s$ and 9.76×10^{19} $/cm^3$, respectively. As discussed in Chapter 2, n-type films which have less carrier concentration is able to deposit due to the effect of threading dislocation [7, 8]. And BKSO film was deposited at 0.7×0.7 mm^2 patterned cell by using another Si stencil mask. The picture of the cell is shown in Figure 4.2 (a). We deposit BKSO thin films with changing parameters such as film thickness (100 nm, 500 nm) and concentration of dopant (6 %, 11 %). And then, about 2 nm thick metallic $SrRuO_3$ (SRO) layer was deposited on BKSO film to improve the contact between junction and probe. We used SRO as p-type contact because its work function is larger than 5 eV [8]. The whole schematic of pn junction structure is illustrated at Figure 4.2 (b).

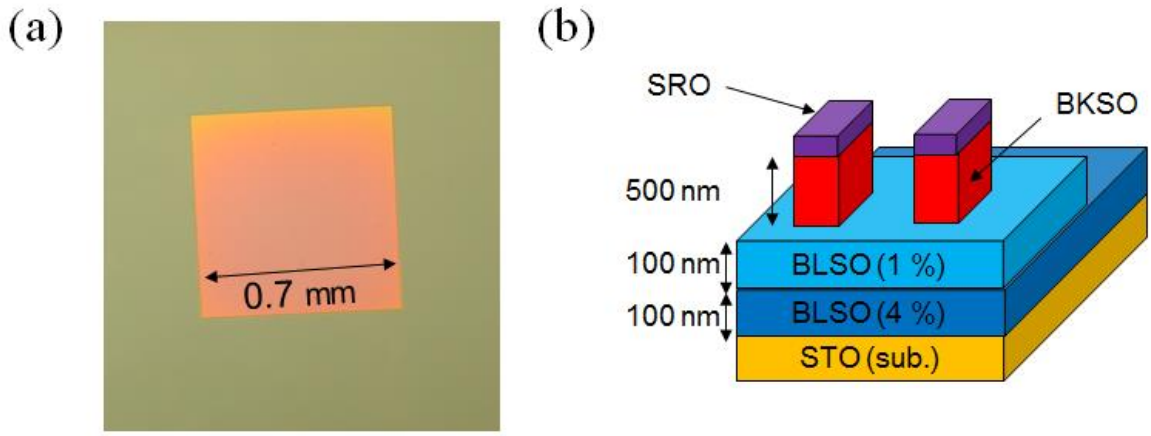

Figure 4.2. (a) The picture of cell for pn junction fabricated by using stencil mask. The area of the cell is 0.7 × 0.7 mm^2 (b) Schematics of the BKSO/BLSO pn junction. Each pn junction contains 2 cells.

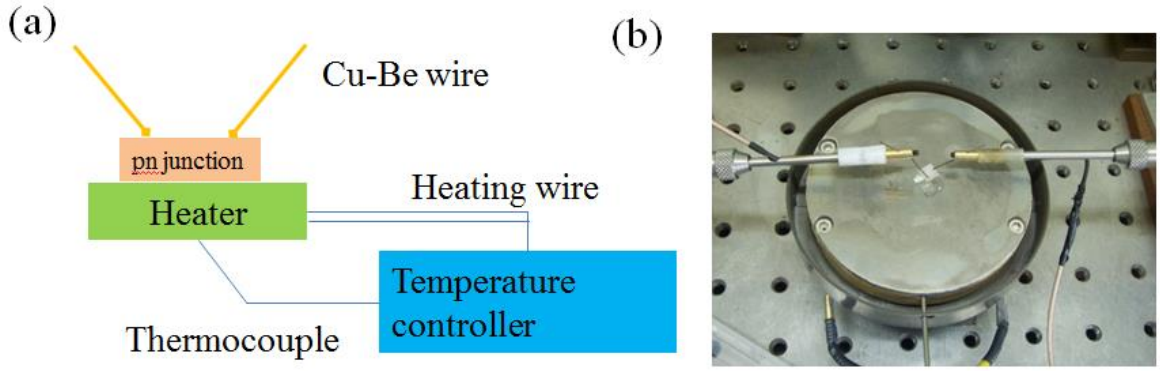

Figure 4.3. (a) The schematics of pn junction measurement system with temperature variation and (b) The picture of the pn junction measurement system.

We measure the I-V characteristics of pn junction considering the temperature change. For temperature variation measurement, we set up the temperature control system consisting of heater, thermocouple and control system. A diameter of heater is 3 inch and there exist a heating element which flow the current from the control system to raise temperature below the heating plate. The heater temperature is measured by thermocouple which put in the heating plate transferred to the control system which enable to negative feedback at a fixed temperature. Figure 4.3 (a) describe this schematics and Figure 4.3 (b) shows the picture of the heater and wire. Also, to improve contact and enlarge contact area, we use resilient 0.5 mm diameter Cu-Be wire as probe tips.

4.3 I-V characteristics of pn junction

4.3.1 The confirmation of ohmic contact

Firstly, the contact properties between the electrode and thin film and between thin films were investigated. The contact of the pn junction is very important because its rectifying behavior may originate from the Schottky-like contact between semiconductor and metal. The contact between 4 % BLSO layer and Cu-Be probe is definitely ohmic contact which resistance value is about 100 Ω because 4 % BLSO layer is degenerate semiconductor [6, 7]. Also, SRO is p-type metal [9] and 4 % BLSO and 1 % BLSO is originated from same material, between SRO-probe and 4 % BLSO-1 % BLSO is naturally ohmic contact. Therefore the most important thing to consider is the existence of the Schottky barrier at interface between SRO as p-type electrode and BKSO which carrier concentration is very low as p-type materials when we consider the contact in device.

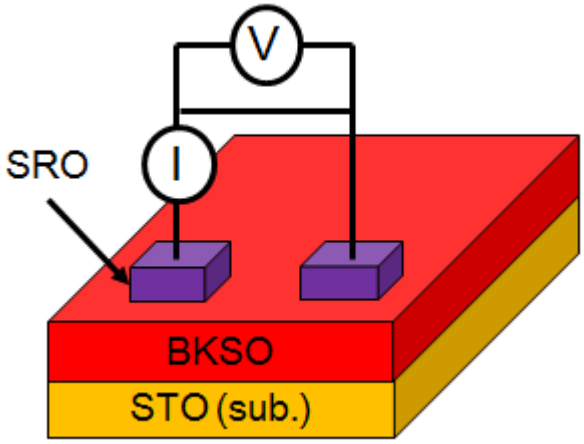

Figure 4.4. Schematics of SRO/BKSO/SRO planar junction for contact confirmation.

We confirm ohmic contact by measuring I-V characteristics of SRO/BKSO/SRO junction system at high temperature because its resistance is too high to measure at room temperature. Its schematic can be seen from Figure 4.4. I-V results in various temperatures indicated at Figure 4.5. In room temperature, the current is very low due to high resistance of BKSO thin film, shown in Figure 4.5 (a). At 100 ^{o}C measurement, the linear plot is slightly seen among the fluctuating noise because current is still very small (indicated in Figure 4.5 (b)). At 200 ^{o}C and 300 ^{o}C measurement, the contact between BKSO and SRO is definitely ohmic and their resistance is about 50 MΩ and 1 MΩ, respectively, which is quite agree with resistance of BKSO thin film discussed

at Chapter 3. We measured at 300 ^{o}C which is highest temperature for investigating junction property because the effect of the contact resistance is more dominant as temperature is increased cause of lowering the resistance of BKSO.

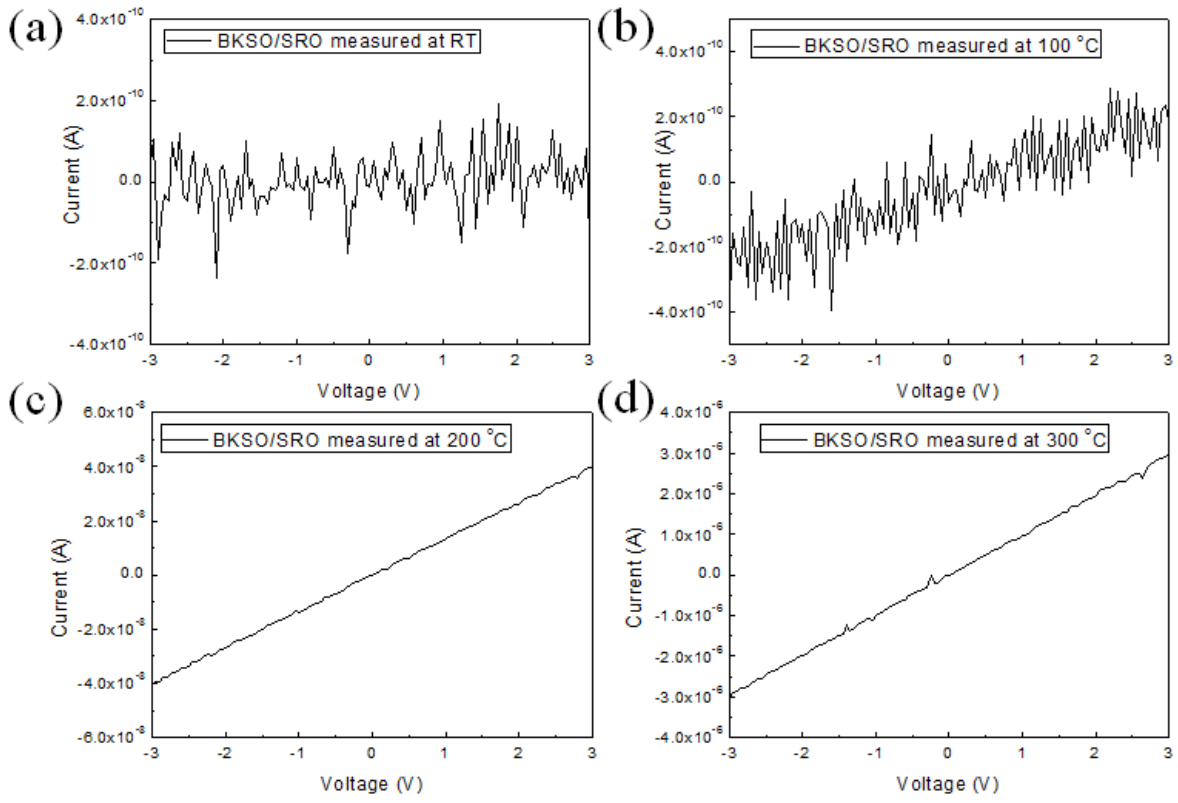

Figure 4.5. I-V characteristics of SRO /BKSO /SRO planar junction at (a) room temperature (b) 100 ^{o}C (c) 200 ^{o}C (d) 300 ^{o}C

4.3.2 I-V characteristics of pn junctions

We fabricated three kinds of pn junction with variation of thickness and carrier concentration in BKSO thin film. pn junction A composed of 11 % BKSO thin film with 500 nm thickness; pn junction B composed of 6 % BKSO thin film with 500 nm thickness; pn junction C composed of 6 % BKSO thin film with 100 nm thickness. We made those three kinds of junctions for investigating of the effect of thickness and carrier concentration of p-side. Though our pn junction is highly asymmetric and carrier concentration of n-side is very high, the n-side condition is same for all three junctions. We generally applied voltage from +3 V to -3 V. For forward bias, we sweep the voltage from 0 V to +3 V, and sweep the voltage from 0 V to -3 V for reverse bias.

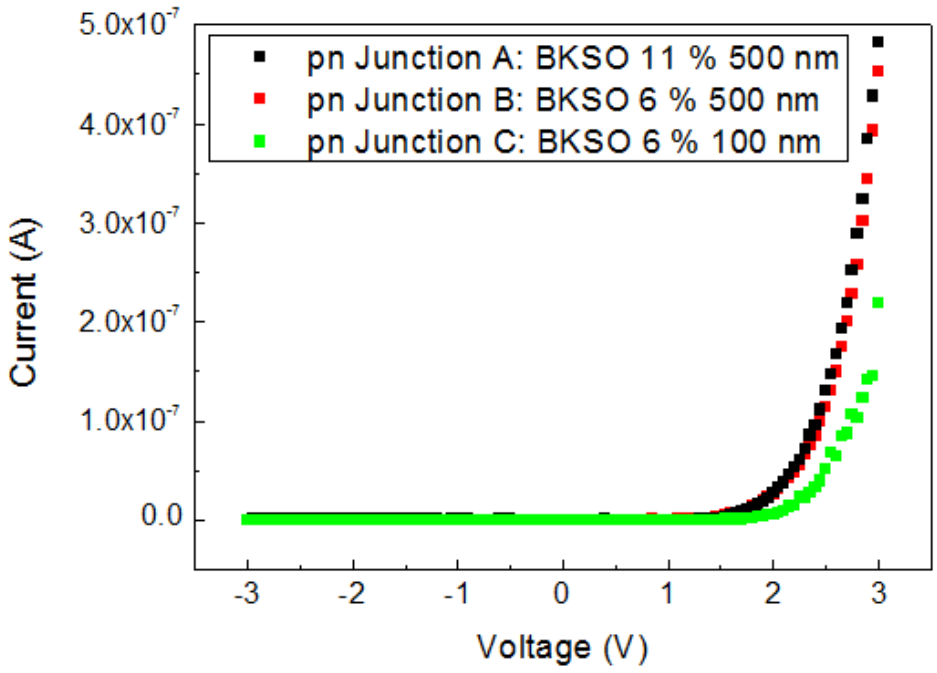

Figure 4.6. I-V characteristics of pn junction at room temperature. Junction A consists of BKSO 11 % with 500 nm; junction B consists of BKSO 6 % 500 nm; junction C consists of BKSO 6 % 100 nm for p-type. For n-type, all junction use BLSO 1 % with 100 nm thickness.

I-V characteristics for both junctions measured at room temperature are shown in Figure 4.6. Non-linear behavior is clearly observed at both junctions though current through junction is very low at room temperature. It means that these rectifying I-V characteristic in our pn junction demonstrates the diode-like behavior that is originating from the BLSO/BKSO interface. The rectification ratios (ratio between forward and reverse currents) are about 154.9, 126.8 and 46.1 at a bias of 2.0 V and 194.7, 158.7 and 101.8 at a bias of 3.0 V for junction A, B and C respectively. As you seen in Figure 4.6., the current is starting to rise after about 1 V at forward bias region for both junctions. It can be indicated that the intrinsic barrier potential is existed at pn junction because of no neutral region by high carrier asymmetry. As we will discussion below, the width of depletion region is much larger than thickness of junction itself, the current is not responded as raising voltage bias as junction seems like intrinsically charged. At reverse bias region, the current level is only 10^{-10} A order which is very low current level at room temperature and sustains even at high negative voltage region.

Although rectifying behavior is clearly observed at our pn junctions, current through junction is very low at room temperature. Because our pn junction is highly asymmetric between n-type and p-type carrier (about 10^6 ~ 10^7 order magnitude difference), the width of depletion region of p-side is larger than thickness of the p-side itself even though we use 11 % BKSO thin film. From the carrier densities of 1 % BLSO thin film for n-type and 6 % (and 11 %) BKSO thin film for p-type, we can calculate the width of depletion region of the pn junction using equation (4.9) and (4.10) with material parameters. The width of depletion region of pn junctions are even 25.1 μm for junction A and 18.5 μm for junction B (and C) at room temperature. Depletion width in the p-type

region is much larger than that of that of the n-type because the pn junction depletes further in the more lightly doped region. It means that the width of depletion region of n-type is almost negligible compared with that of p-type. In conclusion, all pn junctions show almost similar I-V characteristics in room temperature results. Moreover, we have difficulty with analyzing the experimental result with conventional pn junction formula though the rectifying behaviors of pn junctions observed.

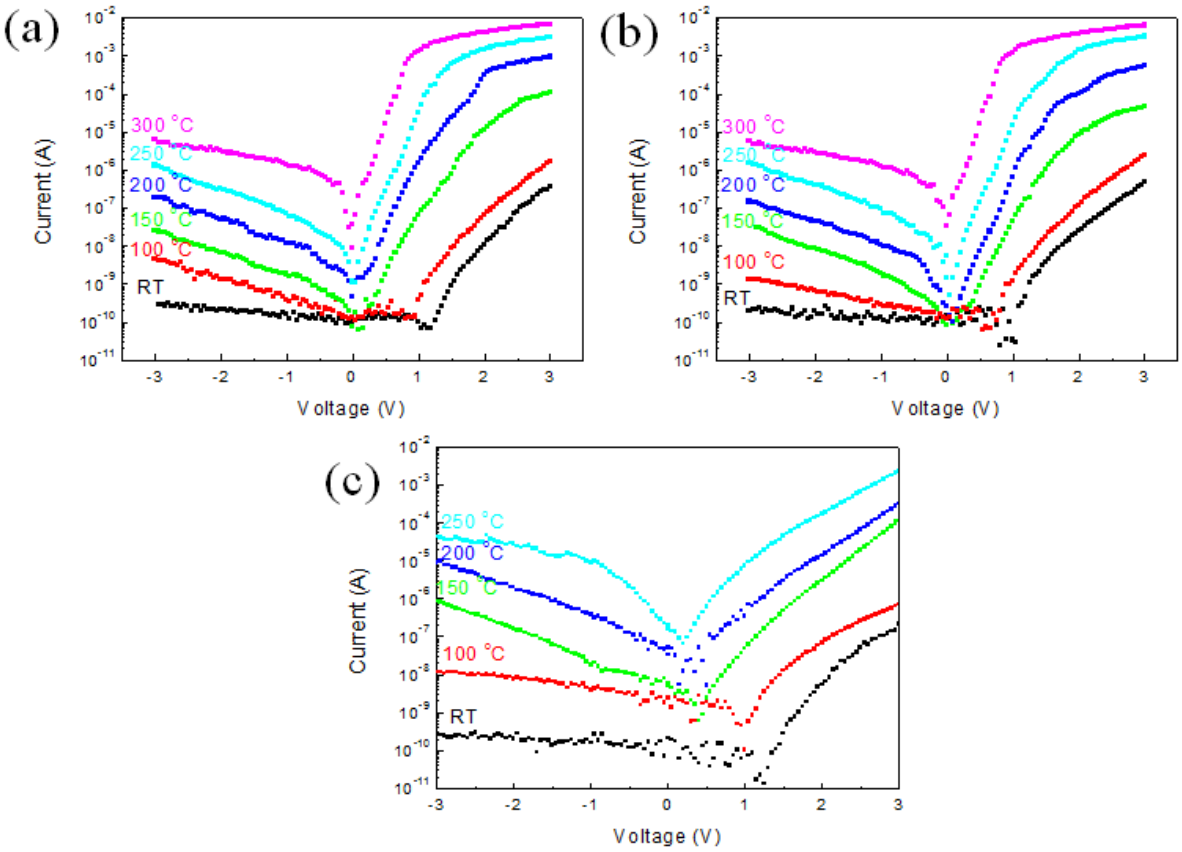

Figure 4.7. I-V characteristics of pn junction at various temperatures (a) for Junction A (b) for junction B consists (c) junction C.

Therefore, we measure the I-V characteristics of pn junctions by raising temperature [10]. We measure I-V characteristics at room temperature, 100 ^{o}C, 150 ^{o}C, 200 ^{o}C, 250 ^{o}C and 300 ^{o}C for junction A and B. We measure I-V characteristics at room temperature, 100 ^{o}C, 150 ^{o}C, 200 ^{o}C, 250 ^{o}C for junction C. Those results are exhibited in Figure 4.7. All measurement results show that non-linear behavior is clearly observed. All junctions show that the slope of the current is steeper for forward bias and the leakage current is increased as increasing temperature. Rectification ratios (ratio between forward and reverse currents) are about 31.1, 24.7 and 2.9 at a bias of 1.0 V in 150 ^{o}C for junction A, B and C respectively. Junction C has small ratio due to large leakage current by relatively thin p-side layer. Those rectification ratios are increased as increasing temperature for junction A and B; however, those values are decreased as increasing temperature for junction C.

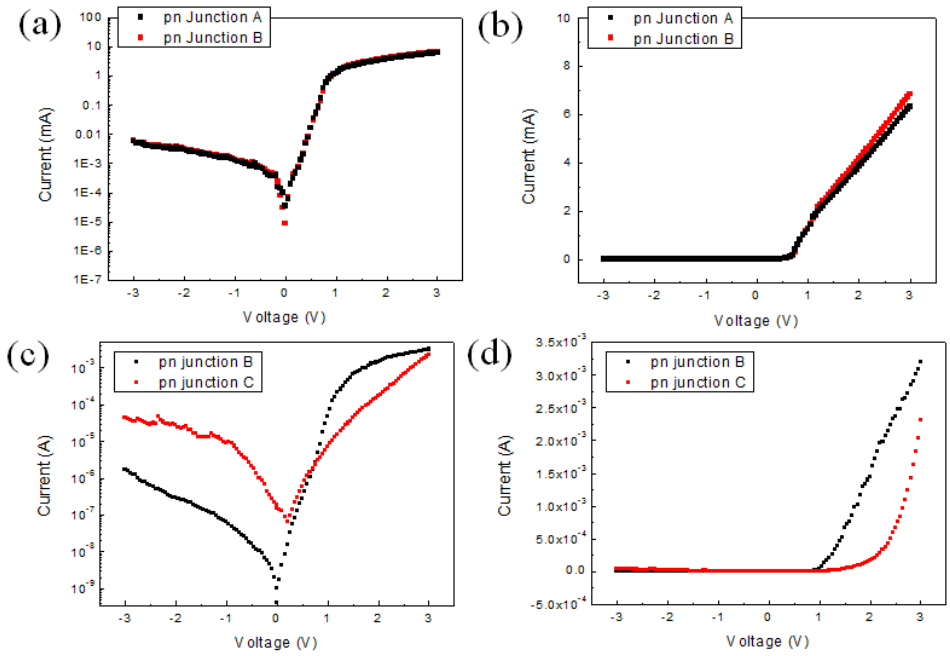

Figure 4.8. Compare I-V characteristics between junction A and B for different carrier concentration measured at 300 ^{o}C. (a) For logarithmic plot. (b) For linear plot. Compare I-V characteristics for different thickness between junction B and C measured at 250 ^{o}C. (c) For logarithmic plot. (d) For linear plot.

In order to precisely investigating the properties of pn junctions measured at high temperature, we classified I-V characteristics of pn junction for same carrier concentration with same thickness (pn junction A and B) and for thickness with same carrier concentration (pn junction B and C). The I-V characteristics of pn junction A and B measured at 300 ^{o}C are indicated in Figure 4.8 (a) for logarithmic plot and (b) for linear plot. Also, the I-V characteristics of pn junction B and C measured at 250 ^{o}C are indicated in Figure 4.8 (c) for logarithmic plot and (d) for linear plot. The result of I-V at junction A and B are almost same as shown in Figure 4.8 (a). The rectification ratios are about 1.16 x 10^{3} at a bias of 1.0 V which is higher than the values of low temperature region. And the I-V plot looks like linear plot at high forward bias region as exhibited in Figure 4.8 (b). It is originated from that the current is seems limited by series resistance of the devices for both junctions. However, the result of I-V at junction B and C are completely different as shown in Figure 4.8 (c). The rectification ratios are about 2.10 × 10^{3} at a bias of 3.0 V for junction B and 1.96 × 10^{2} at a bias of 3.0 V for junction B; which is about ten times lower than that of junction B. And the I-V result as linear plot is exhibited Figure 4.8 (d). As mentioned above, the I-V plot looks like linear plot at high forward bias region for junction B by limiting series resistance. However, I-V characteristic of junction C is still rectifying behavior at high temperature as shown in Figure 4.8 (d).

These differences are basically derived from the width of the depletion region. The carrier concentration of 6 % BKSO thin film is 1.32 × 10^{16} /cm^{3} at 250 ^{o}C and 3.48 x 10^{16} /cm^{3} at 300 ^{o}C. And for 11 % BKSO thin film, the carrier concentration is 3.03 × 10^{16} /cm^{3} at 250 ^{o}C and 7.81 × 10^{16} /cm^{3} at 300 ^{o}C. In

high temperature, the current is significantly raise by more p-type carrier is activated due to thermal activation. For n-type 1% BLSO thin film, the carrier concentration is almost same by changing temperature because it is degenerate semiconductor. From the equation (4.9) and (4.10), we calculate depletion region at various temperature using above parameters. The width of the depletion region is 6.58×10^{-5} cm at 250 ^{o}C and 4.06×10^{-5} cm at 300 ^{o}C for 6 % BKSO thin film and 4.35×10^{-5} cm at 250 ^{o}C and 2.71×10^{-5} cm at 300 ^{o}C for 11 % BKSO thin film. In conclusion, junction thickness is more significant factor for I-V characteristics of junctions than doping concentration because the depletion region is critical parameter for determining I-V characteristics in case of our pn junctions. These results are basically originated that balance of carrier is not matched between n-type and p-type carrier because of deep energy level of K in BKSO thin film. Therefore, we concluded that these pn junctions can be more useful when the dopant which has lower activation energy than K is found.

4.3.3 High-temperature stability of pn junction

The thermal stability of the device is one of the importance things to consider when device was operated especially at high temperature. We evaluated the thermal stability of our pn junction for thermal cycling which means sequentially measuring I-V characteristics at room temperature, at high temperature (300 ^{o}C) and room temperature again. As shown in Figure 4.9., both junction A and B exhibit excellent thermal stability that the I-V characteristics at room temperature are almost unchanged even after several thermal cycling. The slight change of the forward bias might come from the slight temperature difference of the device itself. It shows that our pn junction is highly stable for changing temperature and implicate that potassium in junction is not volatile even at 300 ^{o}C. Also, the interface of the junction is very unchangeable about temperature variation.

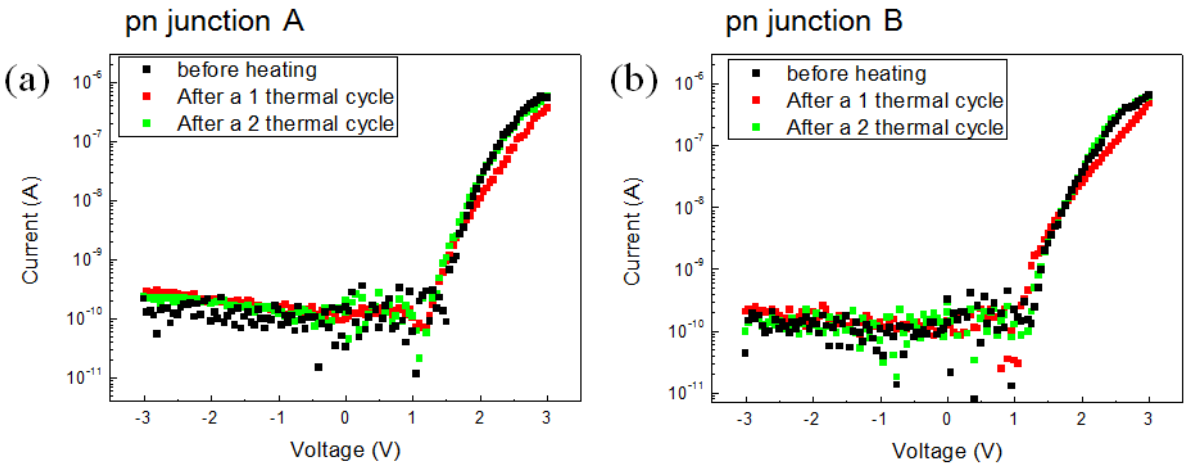

Figure 4.9. The thermal stability measurement of BLSO/BKSO pn junction. The thermal cycling is that I-V characteristics sequentially measured at room temperature, at high temperature (300 ^{o}C) and room temperature again. Repetition of I-V characteristics (a) for Junction A (b) for Junction B.

4.4 Analysis of pn junction

The observed behavior of the BLSO/BKSO pn junction device I-V characteristics is explained with a simple model of pn junction diode with a series resistance R, as shown in Figure 4.10. The measurement at different temperature changes the series resistance and junction parameter in device circuit. The current through junction at temperature T in series resistance R is given by following equation:

$$V = V_t \ln\left[\left(\frac{I}{I_s} + 1\right)\right] + IR \quad (4.17)$$

$$I_s = qAD_n n_{p0}/L_n \quad (4.18)$$

The data can be fitted with fitting variables such as I_s for reverse saturation current, V_t for thermal voltage and R for series resistance values [11-13]. The first part of equation (4.17) is originate from conventional pn junction formula, $I=I_s[\exp(V/V_t)-1]$. In equation (4.18), q is elementary charge, A is the area of junction, D_n is diffusion constant for electron, L_n is the diffusion length and n_{p0} is the electron minority carrier concentration at equilibrium. The hole part for I_s is negligible because the more lightly doped side of the pn junction will produce a larger number of minority carriers and the larger current component [14, 15].

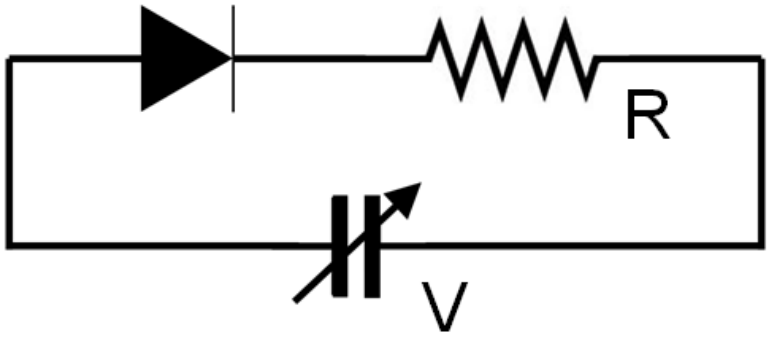

Figure. 4.10. The pn junction with series resistance model. V is the applied voltage and R is series resistance parasitic in junction diode.

The fitting analysis results for junction A are indicated in Figure 4.11 and for junction B are indicated in Figure 4.12. Firstly, we investigated junction parameter by fitting of the pn junction at 150 ^{o}C, 200 ^{o}C, 250 ^{o}C, and 300 ^{o}C. The reverse saturation current of junction A is 2.60 × 10^{-10} A at 150 ^{o}C, 6.64 ×10^{-10} A at 200 ^{o}C, 2.60 × 10^{-9} A at 250 ^{o}C and 2.28 × 10^{-8} A at 300 ^{o}C. From the results of high temperature (above at 250 ^{o}C) for junction A, the barrier height of the pn junction is about 1.16 eV for 250 ^{o}C and 1.19 eV for 300 ^{o}C. And the reverse saturation current of junction A is 8.43 × 10^{-11} A at 150 ^{o}C, 5.72 × 10^{-10} A at 200 ^{o}C, 4.62 × 10^{-9} A at 250 ^{o}C and 2.80 × 10^{-8} A at 300 ^{o}C. For estimation of the minority carrier concentration, the values of n_{p0} for junction A and B are 2.07 × 10^{8} /cm^{3} and 2.27 × 10^{8} /cm^{3} at 250 ^{o}C and 1.10 × 10^{9} /cm^{3} and 8.37 × 10^{8} /cm^{3} at 300 ^{o}C.

And we calculate the thermal voltage V_t from the fitting results. The thermal voltage for junction A is 0.142 V at 150 ^{o}C, 0.122 V at 200 ^{o}C, 0.089 V at 250 ^{o}C and 0.061 V at 300 ^{o}C. From the conventional pn junction formula, thermal voltage V_t is equal to mkT/q where k is Boltzmann constant, T is temperature and q is elementary charge and m is the ideality factor of the junction. Using above result, we can calculate ideality factors which are 3.90 at 150 ^{o}C, 3.02 at

200 ^{o}C, 2.1 at 250 ^{o}C and 1.3 at 300 ^{o}C, each. And, the thermal voltage for junction B is 0.120 V at 150 ^{o}C, 0.090 V at 200 ^{o}C, 0.076 V at 250 ^{o}C and 0.069 V at 300 ^{o}C. Their ideality factors are 3.3 at 150 ^{o}C, 2.2 at 200 ^{o}C, 1.95 at 250 ^{o}C and 1.4 at 300 ^{o}C, respectively. The ideality factor is temperature dependent and decreases consistently with increasing temperature mainly due to generally improving p-type transport with increasing temperature cause of the higher activation of acceptors at elevated temperatures [16]. Also the behavior of junction is more idealistic because the width of depletion region is decreased as increasing temperature.

Furthermore, we can obtain the series resistance values of the device circuit by analyzing the fitting of pn junctions. The series resistance for junction A is 4400 Ω at 150 ^{o}C, 1220 Ω at 200 ^{o}C, 520 Ω at 250 ^{o}C and 325 Ω at 300 ^{o}C. And the series resistance for junction A is 5800 Ω at 150 ^{o}C, 2450 Ω at 200 ^{o}C, 480 Ω at 250 ^{o}C and 350 Ω at 300 ^{o}C. We attribute that p-type transport properties generally improve with increasing temperature because of the higher activation of acceptors at elevated temperatures [16]. As mentioned above, the current through junction is limited by series resistance factor when current level is up to 10^{-3} A order. If tens of mA orders of current can be achieved, it has possibility that BKSO/BLSO homojunction exhibit luminescence behavior at the visible light or near UV region by 3 eV of BSO band gap as demonstrating GaN [17-19] and manganite [20, 21] results. The demonstration of the pn junctions based on a single transparent perovskite semiconductor (TPS) material further enhances the potential of the BSO system.

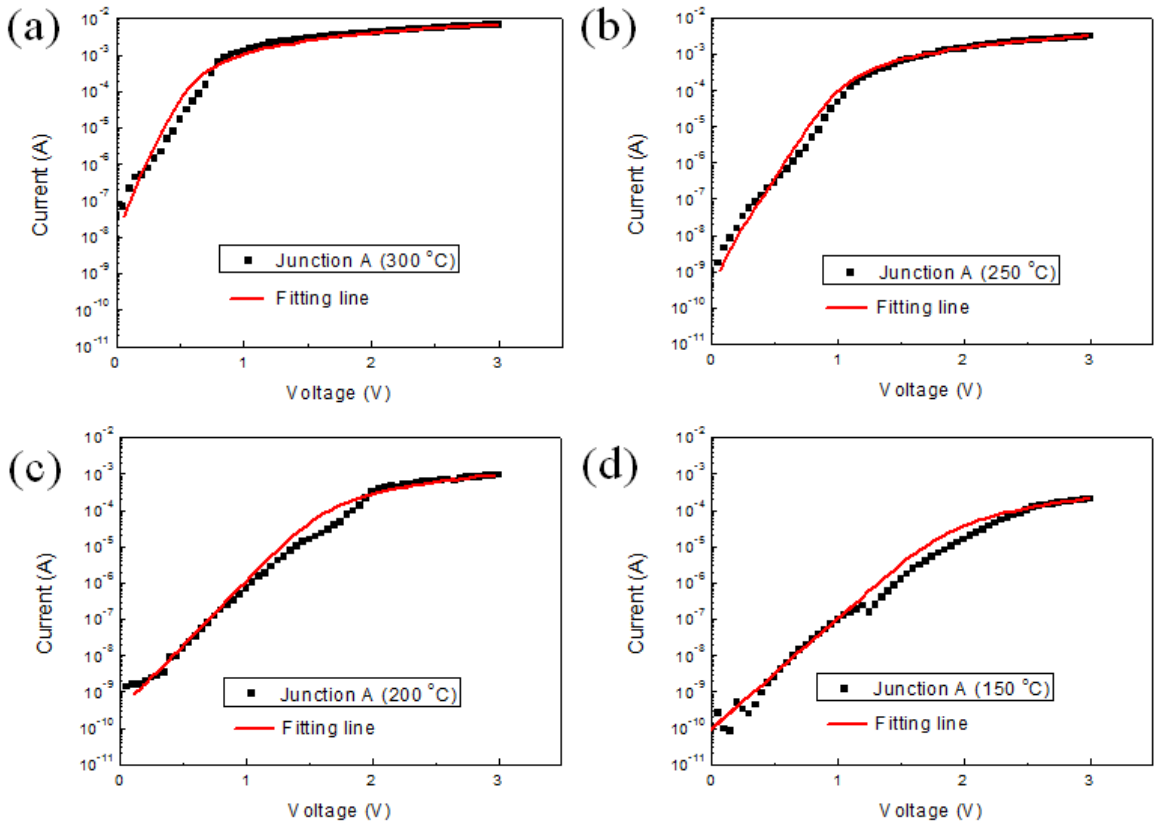

Figure. 4.11. I-V characteristics of the pn junction A with fitting lines using equations by series resistance model. Each graph is measured at (a) 300 ^{o}C (b) 250 ^{o}C (c) 200 ^{o}C (d) 150 ^{o}C.

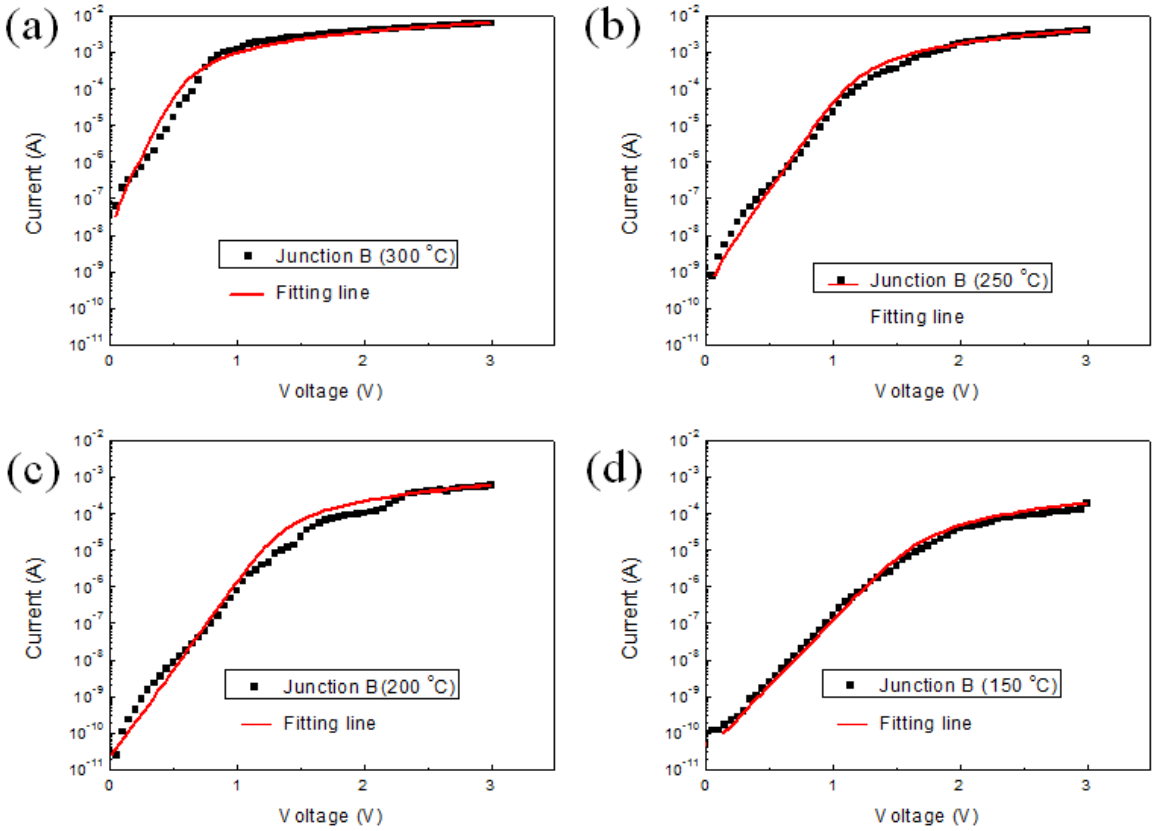

Figure. 4.12. I-V characteristics of the pn junction B with fitting lines using equations by series resistance model. Each graph is measured at (a) 300 ^{o}C (b) 250 ^{o}C (c) 200 ^{o}C (d) 150 ^{o}C.

Reference

[1] S. M. Sze, Semiconductor devices. 2nd Edition (Wiley, 2001), Chapter 4.

[2] M. Balkanski & R. F. Wallis, Semiconductor Physics and Applications. (Oxford, 2000), Chapter 12.

[3] R. F. Pierret, Semiconductor Device Fundamentals. (Addison Wesley, 1996), Chapter 5 and 6.

[4] D. J. Roulston, An introduction to the Physics of Semiconductor Devices. (Oxford, 1999) Chapter 2 and 3.

[5] J. A. J. Tejada, A. Godoy, A. Palma & J. A. L. Villanueva J. Appl. Phys. **92**, 320 (2002).

[6] H. J Kim, U. Kim, H. M. Kim, T. H. Kim, H. Mun, B. G. Jeon, K. T. Hong, W. J. Lee, C. Ju, K. H. Kim & Kookrin Char, Appl. Phys. Exp. **5**, 061102 (2012).

[7] H. Mun, U. Kim, H. M. Kim, C. Park, T. H. Kim, K. H. Kim & K. Char, Appl. Phys. Lett. **102,** 252105 (2013).

[8] M. Tapajna, P. Pisecny, R. Luptak, K. Husekova, K. Frohlich, L. Harmatha, J. C. Hooker, F. Roozeboom, & J. Jergel, Mater. Sci. Semicond. Process. **7**, 271 (2004).

[9] H. M. Christen, L. A. Boatner, J. D. Budai, M. F. Chisholm, L. A. Gea, D. P. Norton, C. Gerber & M. Urbanik Appl. Phys. Lett. **70** ,2147 (1997).

[10] J. Zhang, H. Tanaka and T. Kawai Appl. Phys. Lett. **80**, 4378 (2002).

[11] F. J. G. Sanchez, A. Ortiz-Conde & J. J. Liou, Proc. Circuits Devices

Syst. **143**, 68 (1996).

[12] H. Bayhan & A. S. Kavasoglu, Turk. J. Phys. **31**, 7 (2007).

[13] V. L. Borblik, Y. M. Shwarts, M. M. Shwarts, Semicon. Phys. Quan. Elec. & Optoelec. **12**, 339 (2009).

[14] D. O. Scanlon, Phys. Rev, B **87**, 161201 (2013).

[15] F. J. Garcia Sanchez, A. Ortiz-Conde, J.J Liou, IEE proc. Circuits Devices syst. **143**, 68 (1996).

[16] J. M. Shah, Y.L. Li, T. Gessmann & E. F. Schubert, J. Appl. Phys. **94**, 2627 (2003).

[17] E. S. M. Goh, H. Y. Yang, Z. J. Han, T. P. Chen & K. Ostrikov Appl. Phys. Lett. **101**, 263506 (2012).

[18] S. Nakamura, T. Mukai & M. Senoh Jap. J. Appl. Phys. **30**, 1998 (1991).

[19] T. Wang, H. Wu, Z. Wang, C. Chen & C. Liu, Appl. Phys. Lett. **101**, 161905 (2012).

[20] J. R. Sun, S. Y. Zhang, B. G. Shen & H. K. Wong Appl. Phys. Lett. **86**, 053503 (2005).

[21] K. Lord, D. Hunter, T. M. Williams, & A. K. Pradhan, Appl. Phys. Lett. **89**, 052116 (2006).

5. The properties of $SrSnO_3$ thin films & their pn junction

5.1 Structural properties of $SrSnO_3$ thin film

Perovskite $SrSnO_3$ (SSO) has an orthorhombic structure (space group Pbnm) with a high degree of pseudo-cubic symmetry at room temperature [1-3] indicated in figure 5.1 (b). The orthorhombic perovskite structure is elongated $\sqrt{2}$ times to the a and b axis and 2 times extended to the c axis direction from the cubic perovskite structure exhibited in Figure 5.1. The lattice parameters were reported to be a = 5.708 Å, b = 5.703 Å, and c = 8.065 Å by the least-squares refinement [3]. The octahedral tilting distortion will take place in the corner sharing octahedral network and the Sn-O-Sn bonds bend increasingly [3-5]. The first Brillouin zone (BZ) of the cubic perovskite structure is cubic; however, the first BZ of the orthorhombic perovskite is monoclinic shape, as indicated in Figure 5.2 [6]. Because of difference of the BZ, the band structures of the BSO and SSO are completely different, as shown in Figure 5.3 [7]. In Figure 5.3 (a), the band gap of the BSO is definitely indirect while band structure of SSO exhibit almost direct band gap (The values of the band gap in Figure 5.3 are underestimating. [8]). The band gap of the SSO is known to 4 eV [2, 8-9]. The investigations of direct band gap material for measuring the electrical properties and fabricating pn junction are very important because it is able to exhibit light emitting diode (LED) or photo-response behavior.

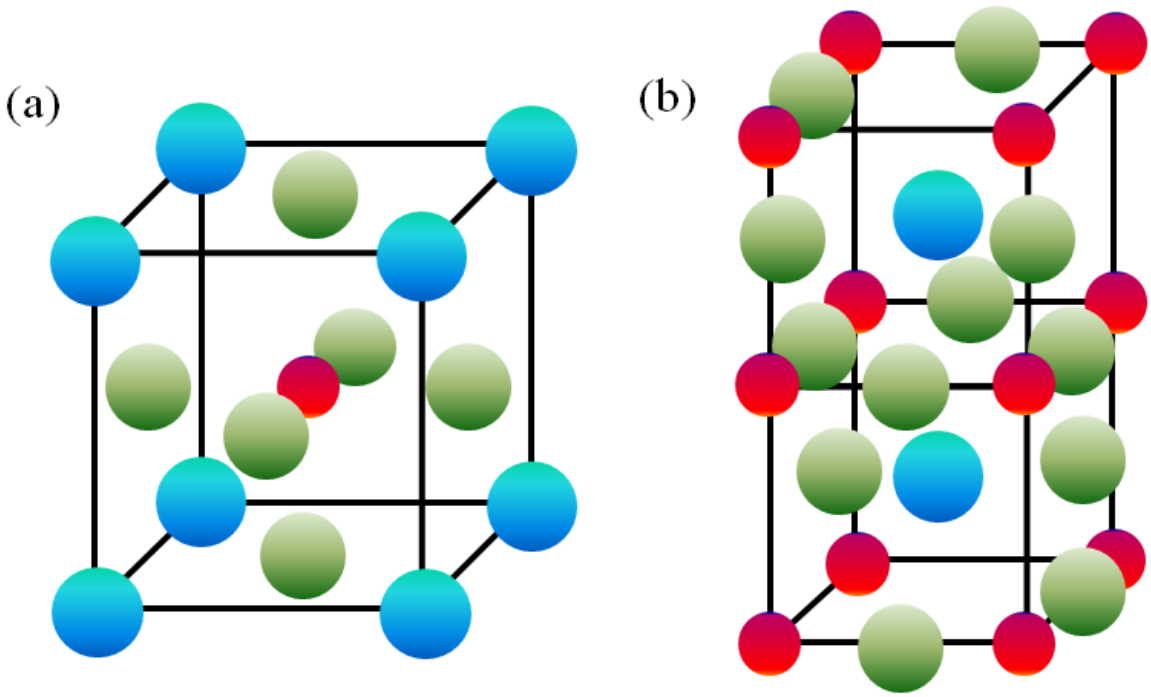

Figure 5.1. The structure of (a) cubic perovskite and (b) orthorhombic perovskite structure. The blue circle is A cation, red one is B cation and green one is oxygen. The orthorhombic perovskite is axis elongated $\sqrt{2}$ times for a and c and 2 times extended to the b axis direction from the cubic perovskite structure.

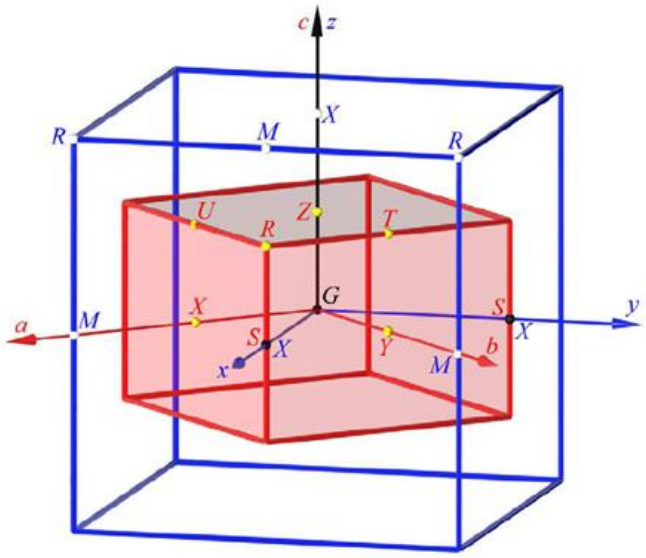

Figure 5.2. The first Brillouine zone of the cubic perovskite (blue) and orthorhombic perovskite (red) [6].

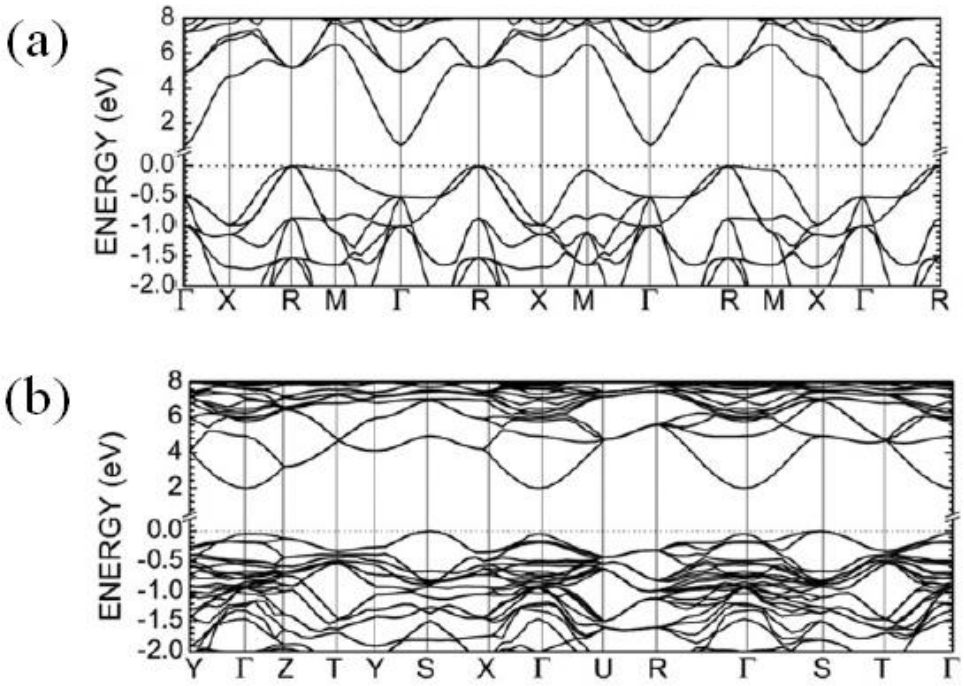

Figure 5.3. The band structure of (a) $BaSnO_3$ and (b) $SrSnO_3$ structure [7].

5.2 Properties of SSO thin films

5.2.1 SSO thin film deposition

We deposited various doped SSO thin films on 5 nm thick SSO buffer layer (deposited at 750 ^{o}C) on the $KTaO_3$ (KTO) substrate using $Sr(Sb,Sn)O_3$ (SSSO) and $SrSnO_3$ targets for SSSO thin films; $SrSnO_3$ and $La_2Sn_2O_7$ (LSO) targets are used for $(La,Sr)SnO_3$ (SLSO) thin films; and $SrSnO_3$ and $SrRuO_3$ targets are used for $Sr(Ru,Sn)O_3$ (SSRO) thin films by pulsed laser deposition system with a KrF excimer laser (λ = 248 nm) under 100 mTorr oxygen pressure with 1 ~ 1.5 J/cm^2 energy intensity. To specifically dope various dopants ions, we used a sequential deposition method which deposits thin films by sequentially alternating targets for each determined pulse shots [10]. The plume of the SSO, SSSO, LSO and SRO targets are shown in Figure 5.4 when laser is ablaze at target. We determine the doping rate is same as the nominal doping rate by measuring growth rate of each material and controlling shot ratios. Also, we assumed that dopant atoms are not volatile at high temperature.

We firstly grew the SSO thin film on STO substrate. However, because the lattice mismatch between STO and SSO is quite a big which shows in Table 5.1, the SSO thin film is still orthorhombic structure and their conductivity are not observed even at carrier doping. The SSO thin film seems to be more affected be lattice mismatch between substrate and thin film than BSO thin film because of their orthorhombic structure with tilting of SnO_6 octahedral [5, 11]. The conduction band of BSO is formed by the interaction between Sn 5s and O 2p orbitals, and thereby, the electron conduction channels pass through SnO_6 octahedral [11, 12]. Therefore, the tilting of SnO_6 octahedral may significantly affect to conduction of the SSO thin film. So we choose KTO as more suitable

substrate. KTO has cubic perovskite structure with lattice constant 3.989 Å for depositing various oxide thin films [13, 14]. The lattice mismatch between SSO and KTO shows only 1.1 % as it seen in Table 5.1, therefore, KTO is the more suitable substrate for depositing SSO thin film than STO. We etched the KTO substrate using 4 % HNO_3 for 30 minute. The surface of the KTO is almost atomically flat and their roughness is 0.107 nm as shown at figure 5.5.

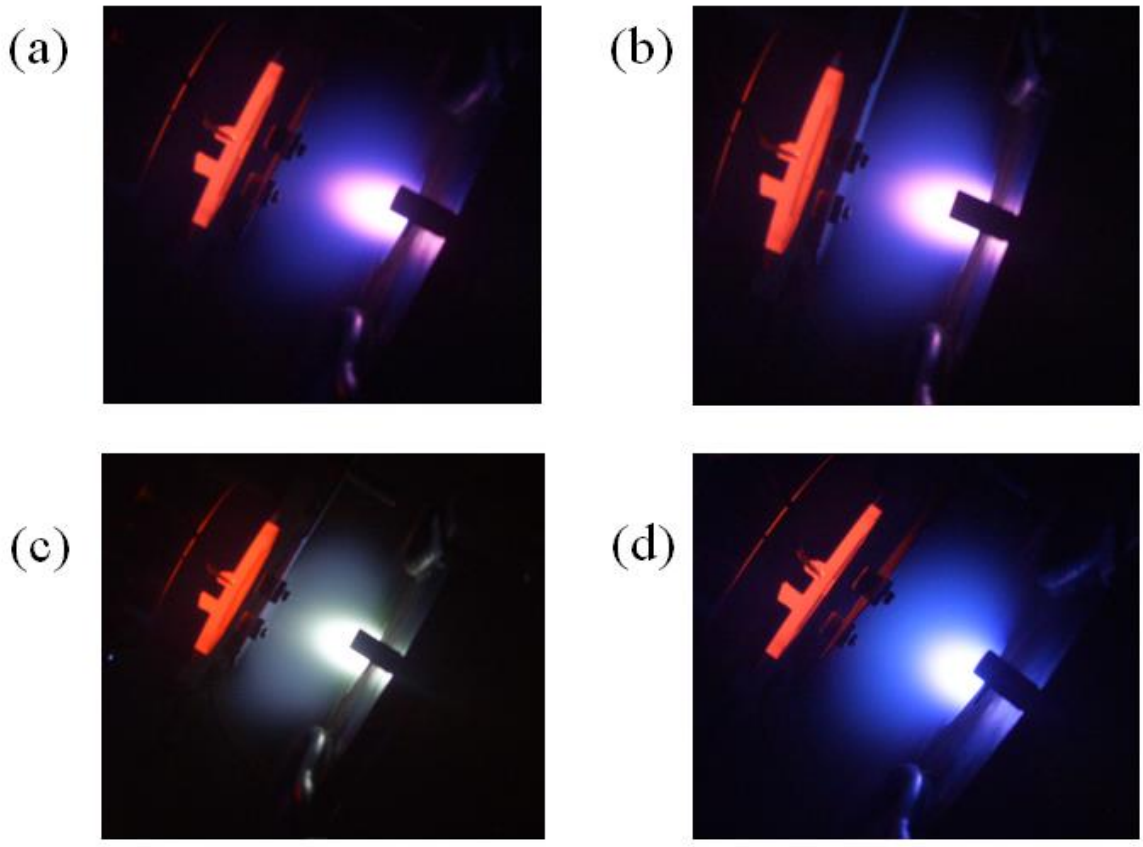

Figure 5.4. Shape of the plumes for laser ablation (a) plume of SSO (b) plume of SSSO (c) plume of LSO (d) plume of SRO.

	Cell plane(Å^2)	Lattice mismatch (%)
$SrSnO_3$	16.322	0
$SrTiO_3$	15.249	-3.45
$KTaO_3$	15.984	-1.11

Table 5.1. The cell plane area and their lattice mismatch with $SrSnO_3$.

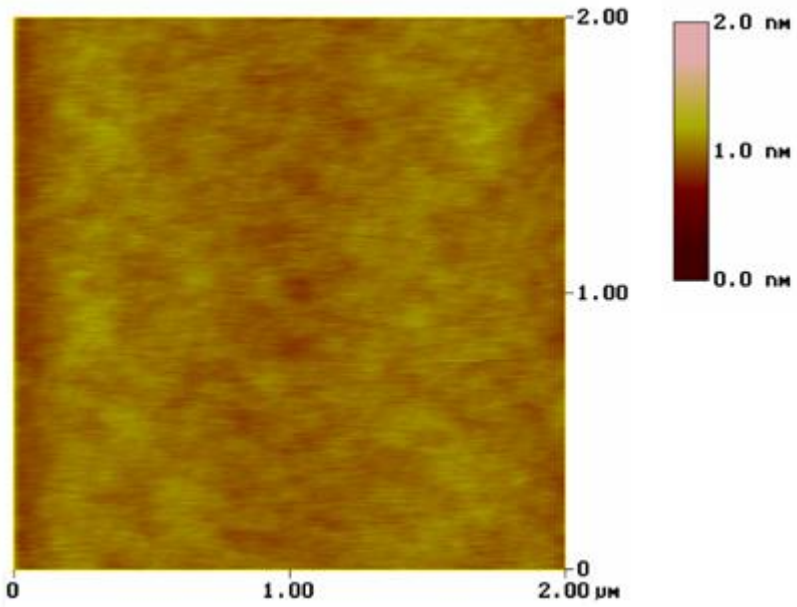

Figure 5.5. AFM image of HNO_3 etched KTO substrate. Its roughness value is 0.107 nm.

5.2.2 Structure and dislocations in SSO thin film

For proof of the epitaxiality of the SSO thin film, as already shown in BSO [15], we obtained the structural information of SSO thin film by the X-ray diffraction method, represented in Figure 5.6. The θ-2θ scan confirms that the epitaxial film was deposited along the direction of KTO substrate. The 2θ angle of the SSO (200) peak is 44.75^{o}. From this value, we can calculate the lattice constant of the SSO tin film for c axis direction that shows 4.050 Å. The values of full width at half maximum (FWHM) of the ω-scan at the SSO (002) peak is 0.09^{o} as indicated at inset of Figure 5.6 which shows that SSO film have highly crystalline and well oriented structure. In order to investigate the in-plane lattice constant and strain state of this film, we use reciprocal space mapping (RSM) method which peaks close to the (103) reflection of the SSSO thin films grown on KTO (001) substrates was measured and shown in Figure 5.7. It is seen that, due to a small lattice mismatch of 1.1 % between the SSO films and the KTO substrates, the film is strained elongated to the c axis. However, on the STO substrate, BSO films [12, 15-16] and SSO films [17, 18] are almost strain relaxed mainly due to the large lattice mismatch between thin film and substrate. It is calculated that the SSO film on KTO has quite a different in-plane and out-of-plane lattice constants of 3.992 Å and 4.049 Å, respectively. RSM method shows that the in-plane direction SSO films have large compressive strain, while they are slightly elongated along the out-of-plane direction. The circle-like shape (103) reflection of the films might mean low density of defects exists in thin film. To confirm the surface homogeneity of the SSO film, we use the AFM image as shown in Figure 5.8. Through the AFM image, we found the surface of the SSO films to be almost atomically flat and it has a very low roughness value which is 0.194 nm.

To proof the dislocation-free of the SSO thin film on KTO substrate, we investigated threading dislocations using TEM and AFM as shown at Figure 5.9. Contrary to TEM image of BSO case as shown in Figure 2.1, there are almost no dislocations at TEM image exhibited in Figure 5.9 (a). It is definitely confirmed that SSO thin film on KTO substrate has few dislocations. Also, we checked the dislocations in HNO_3 etched SSO thin film by using AFM image. The etching creates depressed holes near the dislocations core due to slightly faster etching of the defective atomic structure [18]. The AFM image shows very flat surface even after HNO_3 etching means that there are almost no dislocations in SSO thin film on KTO substrate shown at Figure 5.9 (b).

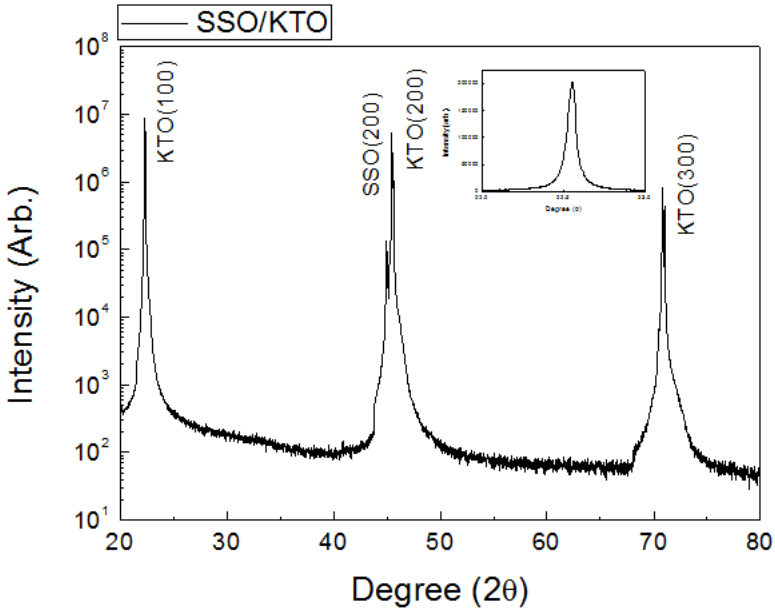

Figure 5.6. θ - 2θ scan of the $SrSnO_3$ thin film on $KTaO_3$ substrate. Inset: rocking curve of the SSO (200) peaks. The Full Width Half Maximum (HWFM) is 0.09^o.

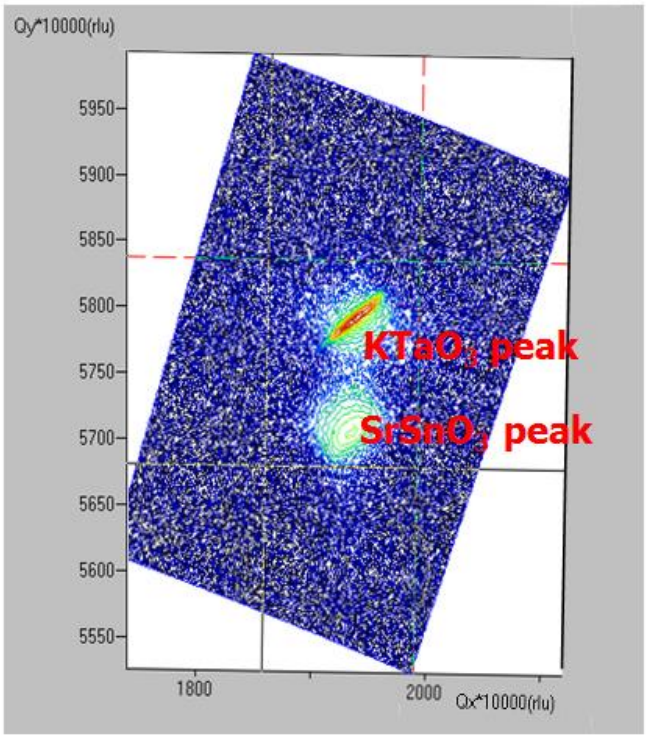

Figure 5.7. Reciprocal space mapping (RSM) of the SSO thin film on KTO substrate.

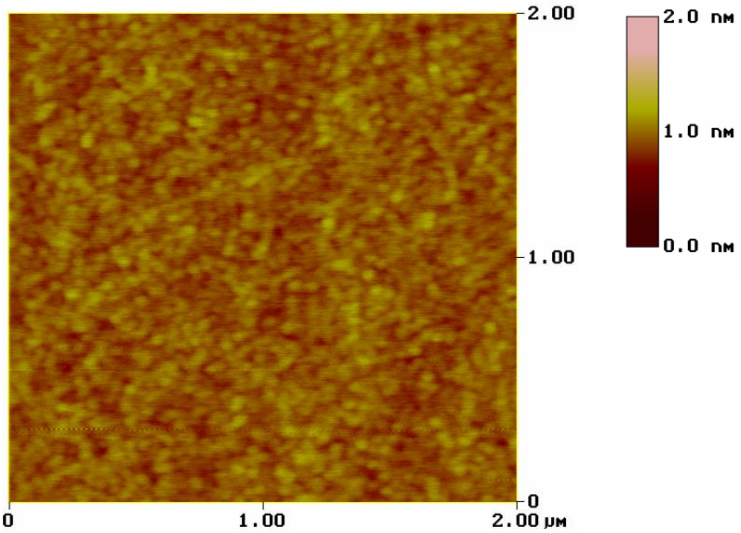

Figure 5.8. AFM image of SSO thin film on KTO with roughness value 0.194 nm.

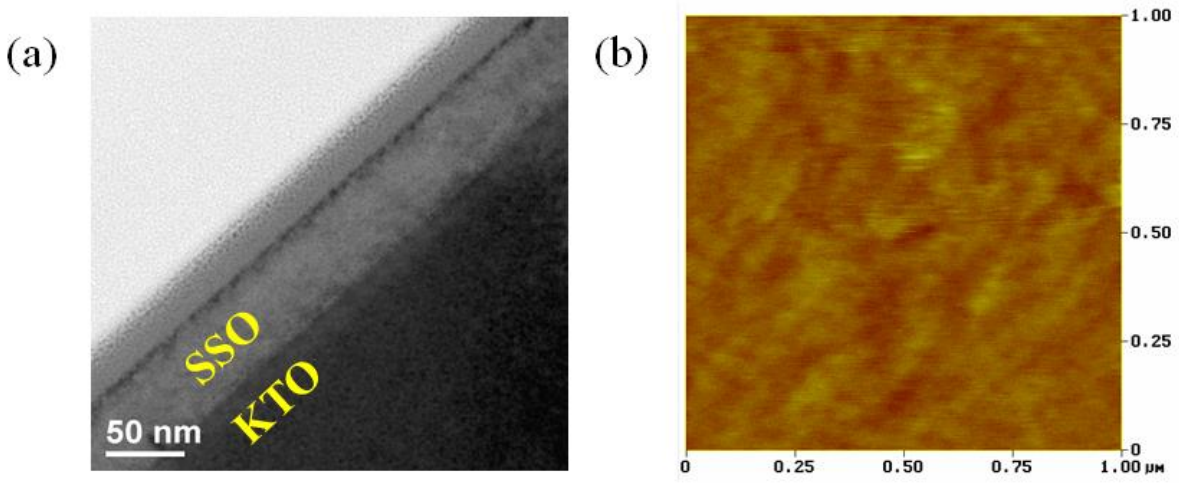

Figure 5.9. (a) TEM image of the SSO /KTO thin film. (b) AFM image of the SSO /KTO thin film. Results of (a) and (b) indicate that SSO thin film on KTO substrate has almost no threading dislocations. AFM imaged measured after 0.4 % HNO_3 etching for 30 s.

5.2 Electrical properties of SSO thin films

5.2.1 Sb-doped SSO (SSSO) thin films

We deposited various Sb doped SSO thin films and measured their resistivity, mobility and carrier concentrations by Hall measurement system. We analyzed resistivity, mobility and carrier concentrations by Sb doping rate as shown in Figure 5.10. Surprisingly, the 4 % Sb doped SSSO thin film shows lowest resistivity, (0.231 Ω·cm), highest mobility (0.516 $cm^2/V \cdot s$) and highest carrier concentration (5.24×10^{19} $/cm^3$). Although we dope Sb ions more than 4 %, these films show higher resistivity and lower mobility and carrier concentration than 4 % SSSO. We suggested that this phenomenon is mainly related with Sb ions because almost same behavior is observed in BSO case [12]. We suggested that the reasons for this phenomenon come from existing multi valence of Sb ions or some kind of charge density wave.

The plot of resistivity and mobility by their carrier concentration is exhibited in Figure 5.11. As shown in Figure 5.11, the mobility is decreased when carrier concentration is increased, as same as BSO [12, 19]. In BSO case, this behavior is explained as scattering at threading dislocations or grain boundaries. However, we need another explanation in case of SSO thin films because there are almost no dislocations in SSO thin films on KTO substrate. We suggested that the SnO_6 octahedral tilting in SSO structure as scattering center is the dominant factor to deteriorate the transport properties in SSSO thin films.

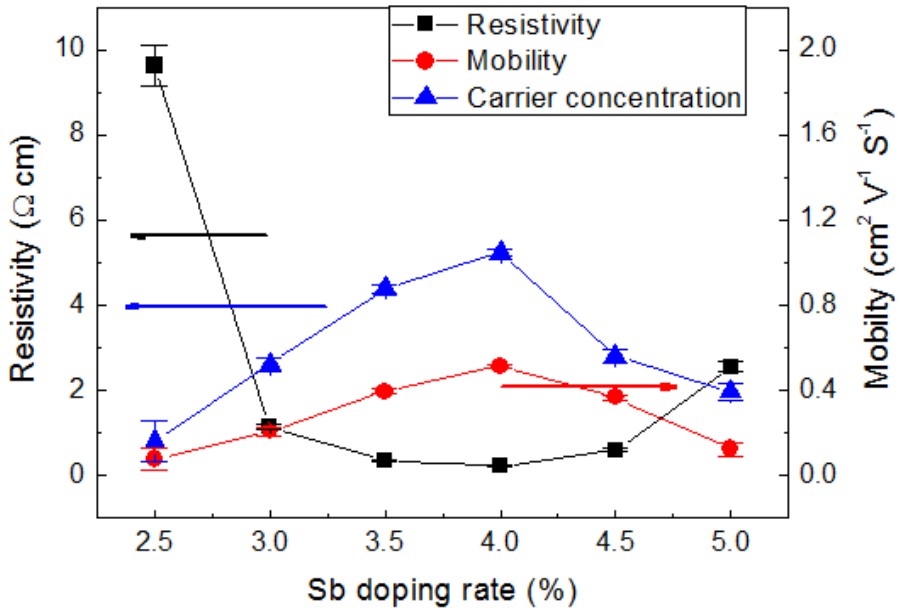

Figure 5.10. (a) Resistivity, mobility and carrier concentration about Sb doping rate of SSSO thin films on KTO substrate.

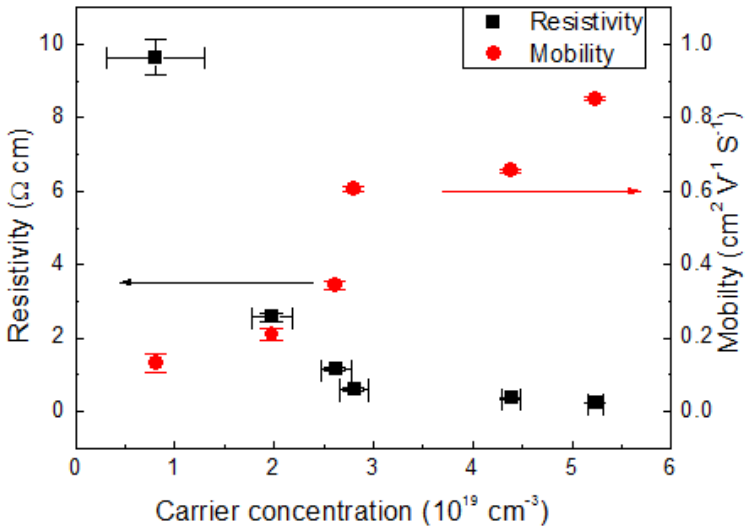

Figure 5.11. Resistivity and mobility as function of the carrier concentration of the SSSO thin film on KTO substrate. Error bar of carrier concentration is indicated at points of resistivity.

5.2.2 La-doped SSO (SLSO) thin films

We deposited various La doped thin films and measured their resistivity, mobility and carrier concentrations by Hall measurement system as same as SSSO case. We analyzed resistivity and mobility by their carrier concentration as shown in Figure 5.12. The SLSO thin film shows no distinctive variation and special tendency of resistivity or mobility as variation of carrier concentration. The range of resistivity (1.36 to 5.82 $cm^2/V \cdot s$) and carrier concentration (1.86×10^{19} to 3.86×10^{19} $/cm^3$) is small for various doped thin films. Although mobility and resistivity are slightly higher than that of Sb doped case, it needs more investigation about exact doping rate and their electrical conduction mechanism. And interestingly, the difference of the mobility and resistivity in SSO system between Sb- and La- doped thin film is very different to those of BSO system [12, 15]. In BSO system, mobility of the La-doped thin film is about ten times higher than that of Sb-doped thin film. We explained this phenomenon from large enhancement of scattering by the threading dislocations in Sb-doped $BaSnO_3$ films and the Sb impurities around the threading dislocation [12]. It is indicated that there are other mechanism for the restriction of electrical conduction of the SSO system such as SnO_6 octahedral tilting. The lanthanum oxides may form a kind of segregation when thin films deposit using sequential deposition method by pulsed laser deposition system using SSO and LSO targets.

5.2.3 Ru-doped SSO (SSRO) thin films

Ru is doped for various thin film oxides for enhance ferromagnetism [20, 21] and sensor response [22]. Among them, SRO is widely used as conducting electrode due to its low resistivity. Moreover, SRO is originally known at p-type metal even alloying with SSO [23]. In SRO, the t_{2g} orbital of Ru lay over the Fermi level. The electrical properties mainly originated from the very strongly hybridized Ru 4d with O 2p orbital extending from -8 to 14 eV relative to the Fermi energy [24]. We deposited various Ru doped SSRO thin films and measured their resistivity, mobility and carrier concentrations by Hall measurement system. We analyzed resistivity and mobility by their carrier as shown in Figure 5.13. All SRSO thin films have p-type carrier with large concentration and relatively low mobility. The Ru dominant region is almost metallic which have high carrier concentration (~10^{22} /cm^3) and low mobility (below 0.1 cm^2/V·s). The lowering the Ru doping, the more semiconducting behavior is appeared that show low carrier concentration and relatively high mobility. The possibility of forming the half-metal state or dilute magnetic semiconductor state is existed because the SSRO is the semiconductor system between SRO as the metallic state and SSO as the wide gap semiconductor. Ru is reported that it is quite volatile [25], it needs more investigation about variation of low doping Ru concentration region and growth temperature for depositing thin films.

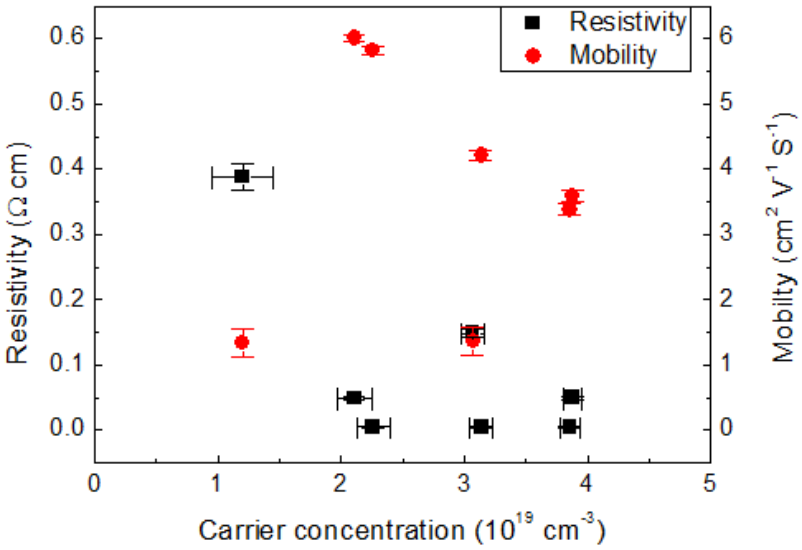

Figure 5.12. Resistivity and mobility as function of the carrier concentration of the SLSO thin film on KTO substrate. Error bar of carrier concentration is indicated at points of resistivity.

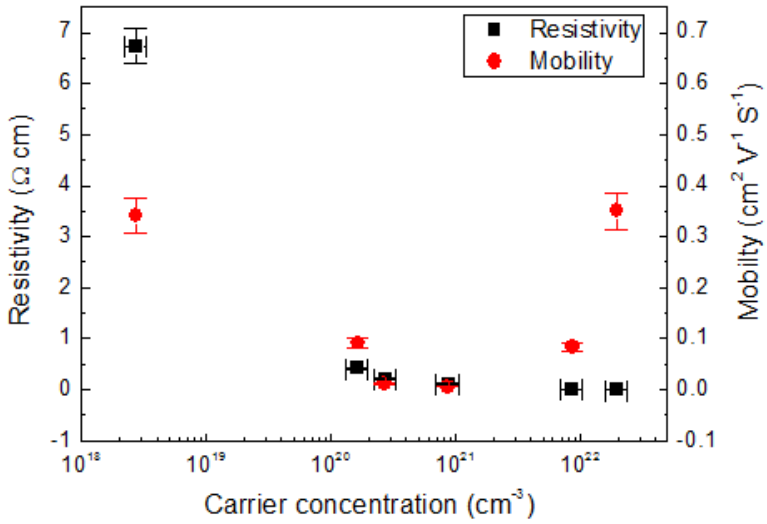

Figure 5.13. Resistivity and mobility as function of the carrier concentration of the SSRO thin film on KTO substrate. Error bar of carrier concentration is indicated at points of resistivity.

5.3 pn junctions fabricated with SSSO and SSRO

5.3.1 Fabrication of pn junction

We fabricate the SSSO/SSRO pn junction which consists of 2.5 % of SSSO for the n-type and SSRO which has lowest carrier concentration exhibited in Figure 5.13 for the p-type. Firstly, 4 % SSSO layer was deposited on the KTO (001) substrate for conduction path. The resistivity of 4 % SSSO layer is about 0.231 Ω·cm, the resistance through this conducting layer is about 13 kΩ including contact resistances. Then we deposited 2.5 % SSSO film with 100 nm thickness using Si stencil mask. The resistivity, mobility and carrier concentration of 2.5 % SSSO film which is used for n-type were 9.63 Ω·cm, 0.079 $cm^2/V{\cdot}s$ and 8.1×10^{18} cm^3, respectively. And SSRO film was deposited at 0.7×0.7 mm^2 patterned cell by using another Si stencil mask. The picture of the cell is shown in Figure 5.14 (a). And then, about 5 nm thick metallic SRO layer was deposited on SSRO thin film to improve the contact between junction and probe. The whole schematic of pn junction structure is illustrated in Figure 5.14 (b). I-V measurement system used same as for BSO based pn junction system which indicated at Figure 4.3.

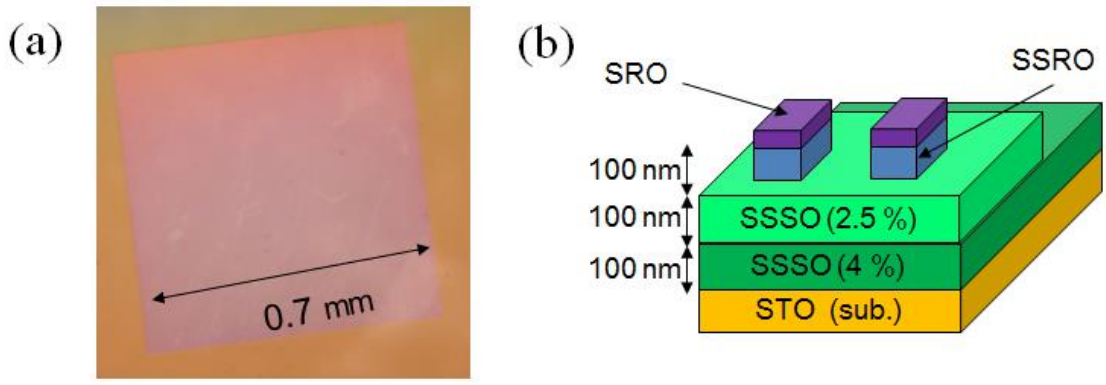

Figure 5.14. (a) The picture of cell for pn junction fabricated by using stencil mask. The area of the cell is 0.7 × 0.7 mm^2. (b) Schematics of the SSSO /SSRO pn junction. Each pn junction contains 2 cells.

5.3.2 I-V characteristics of pn junction

We applied voltage from +3 V to -3 V for measuring I-V characteristics. For forward bias, we sweep the voltage from 0 V to +3 V, and sweep the voltage from 0 V to -3 V for reverse bias. I-V characteristics measured at room temperature are shown in Figure 5.15. Rectifying behavior is clearly observed at junctions with relatively large current through junction about tens μA scales. It means that these rectifying I-V characteristic in our pn junction demonstrates the diode-like behavior originating from the SSSO/SSRO interface. The rectification ratio (ratio between forward and reverse currents) is about 6.46 at a bias of 2.0 V and 2.28 at a bias of 3.0 V. These values are much lower than those of BSO based pn junction, discussed at Chapter 4. This means that SSO-based pn junction has large leakage current at reverse bias region. At reverse bias region, the current level is up to 10^{-4} A order which is very large current level at

high voltage region. As you seen at Figure 5.15 (b), the current is starting to rise just after about 0 V which means that there might have neutral region by relatively more carrier matching than BSO-based pn junction.

As you seen at Figure 5.15 (a), it is originated from that the current is seems limited by series resistance of the devices for both junctions. The estimated value of the series resistance of the pn junction is about 15.8 kΩ. It is mainly originated from the line resistance of the conducting path layer (SSSO 4 %) which has very large resistance as using conducting path. Although the pn junction based SSO system shows large junction current forward bias region, there are many drawbacks such as large leakage current at reverse bias region and no excellent epitaxial film for conducting path. And, there are reported that SSO system exhibit linear band gap variation with BSO system [7, 8]. By the band gap engineering with BSO system, it can be possible to make the direct band gap with low leakage current pn junction attaching low resistivity conduction line with carrier matching.

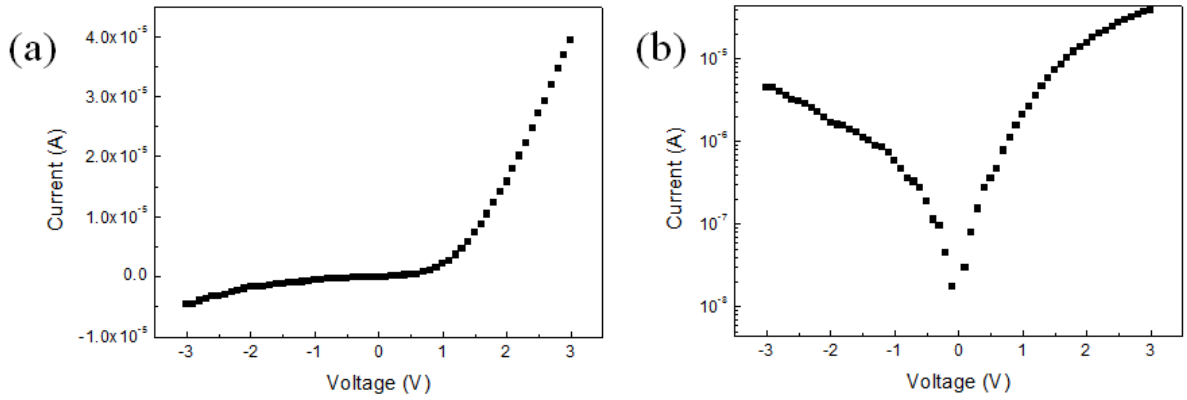

Figure 5.15. I-V characteristics of SSRO /SSSO pn junction at room temperature. (a) Linear plot. (b) Logarithmic plot.

Reference

[1] W. Zhanga, J. Tanga & J. Yea, J. Mater. Res. **22**, 1859 (2007).

[2] L. Shi, Y. F. Duan, X. Q Yang & L. X. Qin ,Chin. Phys. Lett. **27**, 096201 (2010).

[3] P. S. Beurmann, V. Thangadurai & W. Weppner, J. Solid State Chem. **174**, 392 (2003).

[4] E. Moreira, J. M. Henriques, D. L. Azevedo, E. W. S. Caetano, V. N. Freire & E. L. Albuquerque., J. Sol. Stat. Chem. **184**, 921 (2011).

[5] E. H. Mountstevents & S. A. T. Redfern, Phys. Rev. B **71**, 220102 (2005).

[6] E. Pavarini, A. Yamasaki, J. Nuss & O. K. Andersen, New J. Phys. **7**, 188 (2005).

[7] E. Moreira, J. M. Henriques, D. L. Azevedo, E. W. S. Caetano, V. N. Freire & E. L. Albuquerque, J. Sol. Stat. Chem. **187**, 186 (2012).

[8] Q. Liu, B. Li, J. Liu, H. Li, Z. Liu, K. Dai, G. Zhu, P. Zhang, F. Chen and J. Dai, Euro. Phys. Lett. **98**, 47010 (2012).

[9] W. F. Zhang, J.Tang & J. Ye, Chem. Phys. Lett. **418**, 174 (2006).

[10] L. Mieville, T. H. Gaballe, L. Antagnazza, and K. Char, Appl. Phys. Lett. **70**, 126 (1997).

[11] H. Mizoguchi, H. W. Eng and P. M. Woodward, Inorg. Chem. **43**, 1667 (2004).

[12] U. Kim, C. Park, T. Ha, R. Kim, H. Mun, H. M. Kim, H. J. Kim, T. H. Kim, N. Kim, J. Yu, K. H. Kim, J. H. Kim & K. Char APL materials

submitted.

[13] M. Naito *et al.,* Supercond. Sci. Technol. **15**, 1663 (2002).

[14] S. Inoue, M. Kawai, Y. Shimakawa, M. Mizumaki, N. Kawamura, T.Watanabe, Y. Tsujimoto, H. Kageyama, & K. YoshimuraAppl. Phys. Lett. **92**, 161911 (2008).

[15] H. J Kim, U. Kim, H. M. Kim, T. H. Kim, H. Mun, B. G. Jeon, K. T. Hong, W. J. Lee, C. Ju, K. H. Kim & Kookrin Char, Appl. Phys. Exp. **5**, 061102 (2012).

[16] H. Mun, U. Kim, H. M. Kim, C. Park, T. H. Kim, K. H. Kim & K. Char, Appl. Phys. Lett. **102,** 252105 (2013).

[17] Q. Z. Liu, H. F. Wang, F. Chen, & W. Wu, J. Appl. Phys. **103**, 093709 (2008).

[18] Q. Liu, J. Dai, X. Zhang, G. Zhu, Z. Liu & G. Ding, Thin Solid Films **519**, 6059 (2011).

[19] H. J. Kim, U. Kim, T. H. Kim, J. Kim, H. M. Kim, B. G. Jeon, W. J. Lee, H. S. Mun, K. T. Hong, J. Yu, K. Char & K. H. Kim, Phys. Rev. B 86, 165205 (2012).

[20] F. Yan, M. O. Lai, L. Lu & T.Jun, J. Phys. Chem. C **114**, 6994 (2010).

[21] H. Yamada, M. Kawasaki & Y. Tokura Appl. Phys. Lett. **86**, 192505 (2005).

[22] N. S. Ramgir, I. S. Mulla & K. P. Vijayamohanan, Sensors and Actuators B **107**, 708 (2005).

[23] H. M. Christen, L. A. Boatner, J. D. Budai, M. F. Chisholm, L. A. Gea, D. P. Norton, C. Gerber & M. Urbanik Appl. Phys. Lett. **70** ,2147 (1997).

[24] David J. Singh, Appl. Phys. Lett. **79**, 4818 (1996)

[25] P. Pohl & W. Zyrnicki, J. Anal. At. Spectrom **17**, 746 (2002).

6. Summary

In this work, we are attempting to find a suitable substrate that is more suitable than $SrTiO_3$ (STO) for improving the electrical properties of the BLSO thin films. However, BLSO thin films on r-sapphire, $MgAl_2O_4$ spinel and MgO substrates show a poorer mobility than those on STO. The small amount of La-doped BSO thin film acts like a p-type semiconductor due to the effect of threading dislocations even though dopant is an n-type. The high asymmetry of the pn junction carrier partially originates from this phenomenon.

We deposited BKSO thin films on BSO buffer layer using a STO-(100) substrate and investigated the structure, surface properties, and electrical characteristics. The resistances of the BKSO thin films generally followed the Arrhenius formula, and the activation energy of K in the BKSO films was estimated as 0.49 eV. The p-type semiconductor behavior was manifested in the increasing that resistance when the background gas changed from O_2 to Ar.

Using the BKSO and BLSO films p- and n-type semiconductors, we successfully fabricated a pn junction based on single TPS. Although the BKSO/BLSO junction is highly asymmetrically doped, it exhibits typical rectifying behavior. An analysis and fit of the measurement conducted at 300 ^oC, revealed the possibility of using this pn junction for a wide semiconductor LED. If a dopant with activation energy lower than K can be found, the BSO based pn junction will be more useful. These demonstrations of a p-type BKSO thin film and a pn junction based on a TPS material further enhances the potential of the BSO system.

We have also successfully deposited dislocation free SSO thin films on KTO substrates, as confirmed by TEM and AFM images. The electrical properties of

this n-type SSO thin film are not as good as those of the BSO system. Ru-doped SSO thin film show distinctive p-type behavior even at room temperature. A pn junction consisting of Sb-doped SSO (n-type) and Ru-doped SSO (p-type) also showed rectifying behavior. The current of this junction was even larger than that of BKSO-BLSO pn junction; however, the leakage current was very high and an epitaxial layer with a higher conductivity is needed. Combining the BSO and SSO systems will allow us to modulate the band gap in a linear manner.

국문초록

투명 산화물 반도체는 가시광선 및 자외선 영역에서 광학적으로 투명하고 그 전기전도도를 조정할 수 있는 특징이 있어 투명 전극으로 널리 이용되어 왔다. 하지만 이러한 투명 산화물 반도체의 응용은 p형 투명 산화물 반도체가 부재하기 때문에 투명 전극과 화면 패널로 제한되어 왔다. Cu를 기반으로한 p형 투명 산화물 반도체가 발견됨으로써 투명 산화물 반도체를 이용한 pn 접합 또는 전계효과 트랜지스터의 제작이 가능하게 되었다. 하지만 한 투명 산화물 반도체 물질로서 동시에 p형 그리고 n형을 구현한 경우는 거의 보고되지 않고 있다.

최근에 La을 도핑한 $BaSnO_3$ (BSO)가 높은 산소의 안정성과 뛰어난 전기전도도를 가짐이 보고된 바 있었다. 하지만 $BaSnO_3$ 박막이 기판에 대한 뛰어난 결맞음을 지니기는 하지만 박막에 수많은 결정립계 (grain boundaries)와 전위 (dislocations)가 존재하여 이들이 전하를 속박하거나 산란의 요인이 되는 단점이 있었다. 우리는 La을 도핑한 BSO 박막의 전기적인 성질을 증가시키기 위하여 널리 쓰이는 $SrTiO_3$ (STO) 기판 이외에 좀 더 BSO 에 걸맞은 기판을 찾아보았지만 이들 기판은 모두 STO 기판에 비하여 낮은 전기전도도를 나타내었다. 또한, 아주 적은 양의 La만을 도핑 하였을 경우에는 La을 도핑한 BSO 박막이 박막 내의 전위의 영향에 의하여 n형 전하를 도핑 하였음에도 p형 반도체와 같이 행동함을 알 수 있었다.

d-orbital이 Sn과 O사이의 결합에 관계하지 않으므로, BSO 는 다른 페로브스카이트 물질에 비하여 Sn과 O사이의 결합이 강하고 이는 곧 BSO 에 p형 전하를 도핑할 수 있는 가능성을 보임을 의미한다. 우리는 p형 전하를 도핑하기 위해 BSO 에 K을 펄스 레이저 증착법 (Pulsed Laser Deposition: PLD)를 이용하여 도핑하였다. K을 도핑한 BSO 가 상온에서는 상당히 높은 저항을 보이지만 고온으로 올라갈수록 그 저항이 급격하게 감소하였다. 도핑된 K의 활성화 에너지는 약 0.5 eV로 계산되었다. 더욱이 고온에서 박막의 산소를 약간만 제거시켜도 전도도가 눈에 띄게 떨어짐으로써 이 물질이 p형 산화물과 같은

행동을 보임을 관측하였다. K이외에 Ga과 Cu를 도핑한 결과 역시 비슷한 양상을 보였다.

우리는 K를 도핑한 BSO를 p형으로, La을 도핑한 BSO를 n형으로 하여 pn 접합을 제작하였다. 이 소자의 전류-전압 특성을 측정한 결과 pn접합의 전형적인 정류 현상을 보였다. 고온에서 이 pn 접합은 1에서 2사이의 이상계수 (ideality factor)를 보이는 데 이는 고온에서의 BSO의 높은 신뢰성 때문이라 생각한다. 더욱이 이 접합은 높은 인가 전압과 고온에서의 반복 측정에도 아주 안정적인 특성을 나타내었다. 한 페로브스카이트 물질인 BSO를 이용한 pn junction의 구현은 높은 전하 이동도와 산소의 안정성을 갖는 투명 페로브스카이트 반도체로서의 BSO의 가능성을 더욱 높이게 되었다.

그리고 약 4 eV의 직접 밴드 갭 (direct band gap)을 갖는 $SrSnO_3$ (SSO) 시스템에 대하여도 같은 방법을 이용하여 연구하였다. SSO박막은 STO에 비하여 SSO와 더욱 격자상수가 맞는 $KTaO_3$ (KTO) 기판을 이용하였다. 투과 전자 현미경(Transmission electron microscope)과 원자간 힘 현미경 (Atomic Force Microscope)를 이용하여 측정한 결과, KTO기판위의 SSO박막은 전위가 거의 없음을 확인할 수 있었다. SSO박막의 전기적인 성질을 조사하기 위하여 Sb, La, Ru을 도핑하였는데 이들 물질은 SnO_6 팔면체의 기울어짐 때문에 BSO의 경우보다 대체적으로 전하 이동도가 낮았다. 이들 가운데 Ru을 도핑한 SSO는 상온에서도 p형 반도체의 특징이 잘 관측되었기 때문에 Sb를 도핑한 SSO를 n형으로, Ru을 도핑한 SSO를 p형으로 하여 pn 접합을 제작하였다. SSO를 기반으로 한 pn 접합은 BSO 기반 접합에 비하여 전류가 크게 증가하였지만 큰 누설전류와 큰 기생저항 등의 문제가 발견되었다. BSO와 SSO를 결합한 시스템을 이용한다면 직접 밴드 갭을 가지면서도 누설전류와 기생저항이 적은 소자의 제작이 가능하여 향후 발광 다이오드 (LED)등의 응용 등에 큰 가능성이 있다.

Keywords: 투명 산화물 반도체, $BaSnO_3$, K을 도핑한 p형 산화물, 한 페로브스카이트를 이용한 pn 동형 접합, $SrSnO_3$, Ru을 도핑한 p형 산화물

Student number: 2007-20416

감사의 글

학위 심사를 준비 하고 논문을 작성하면서 감사의 글을 쓰는 지금 그 동안 마치 멀게만 느껴졌던 졸업이 새삼 다가옴을 알 수 있었습니다. 이제 학교를 졸업하고 사회로 나아간다고 생각을 하니 두려운 마음과 함께 아쉬움이 교차합니다. 그 동안 많은 분들에게 도움을 받았는데 드디어 이 자리를 빌어서 지난 시간 동안 제가 느낀 고마움을 전할 수 있게 되었습니다.

우선 박사과정 기간 동안 많이 부족하였던 저를 가르쳐주시고 지도해 주신 차국린 교수님께 감사하다는 말씀을 드립니다. 연구에 수행함에 있어서 올바른 방법과 방향을 제시해 주셨으며 연구 외적인 측면으로도 많을 것을 배울 수 있었습니다. 자율적인 연구실 분위기에서 교수님의 지도 하에 많은 연구를 하며 배움을 얻을 수 있었습니다. 믿고 기대해 주신 것에 제가 한참 모자라고 부족한 모습을 보여 항상 죄송스럽지만 지금까지 배운 것을 잊지 않고 앞으로도 부끄럽지 않은 제자로 살아갈 수 있도록 하겠습니다. 그리고 심사 기간 동안 연구 방향과 자세에 대하여 많은 조언을 해 주신 국 양 교수님, 같은 분야의 연구를 진행하면서 항상 염려하여 주신 김 기훈 교수님, 저에게 자신감을 갖도록 격려해 주신 박 제근 교수님, 그리고 몸소 서울까지 오셔서 심사에 참여해 주신 방 윤규 교수님께 감사 드립니다. 심사 때 해주신 소중한 충고와 조언들을 깊이 새겨 앞으로 더욱 노력하겠습니다. 그리고 제가 미국의 Rutgers 대학에서 연구 경험을 쌓을 수 있도록 허락해 주신 정 상욱 교수님께도 감사를 표합니다.

오랜 실험실 생활을 하면서 많은 사람들과의 인연과 도움으로 제가 더욱 배우고 성장할 수 있었습니다. 함께 수 많은 밤을 지새며 저에게 STM을 가르쳐 주시고 연구하는 방법과 자세에 있어 모범이 되셨던 제욱이형, 실험실 생활을 비롯한 많은 것을 가르쳐 주신 진오형, 저의 반도체 연구의 기반을 다져주신 태수형, 그리고 PLD 및 연구 진행 및 프로세스를 가르쳐 주신 승란 누나에게 감사 드립니다. 또한 오랜 기간 동안 같이 있으면서 함께 많은 일을 하였던 찬종, 많은 일을 맡아 하면서 항상 의지할 수 있는 효식, 저희를 항상 배려해 주시고

같이 어울려 주신 동호 형, 연구와 지식에 대한 열정이 넘치는 우성, 모든 일에 집중력을 발휘하는 혁우, 앞장서서 실험을 하며 연구실의 분위기를 책임지는 철권, 끈기를 가지고 항상 최선을 다하는 지성, 그리고 앞으로 연구실의 미래를 이끌어 갈 주연이와 영모에 이르기 까지 많은 이들이 도움이 없었다면 제가 앞으로 나아가는 일은 불가능하였을 것입니다.

대학원 과정에서 졸업하기까지 여러 연구를 하면서 수많은 사람들에게 도움을 받았습니다. 미국 Rutgers 대학에 있을 때 많은 배려를 봐주시고 도움을 주신 채 승철 박사님, 최 영재 박사님, 이 나라 박사님에게 감사 드립니다. 그리고 같은 주제에 대하여 연구를 하면서 많은 도움을 주시고 discussion을 같이 하였던 형준이 형, 태훈이 형, 웅재씨에게 감사를 드립니다. 연구실 이동 시 많은 도움을 주셨던 강 진홍 사장님과 따뜻한 관심을 가져주신 김 융기 상무님, 그리고 김 명옥씨에게도 감사 인사를 드리고 싶습니다. 맛있는 커피와 함께 많은 이야기를 나누었던 봉수 형, 도움이 필요할 때 많은 의지가 되었던 성민 형에게도 감사를 표합니다. 그리고 스터디와 모임을 같이 하며 견문을 넓히고 많은 이야기를 나눌 수 있었던 승훈, 성민, 범용, 예리도 각자의 길에서 모두 잘 되기를 바랍니다.

이제 박사 후 연구원 과정을 통해 독일로 가게 될 승현, 역시 미국에서 박사 후 연구원으로 있는 성모와 태경, 곧 여기서의 일을 마무리 짓고 더 넓은 곳으로 나가게 될 성준에게 좋은 결과 있기를, 열심히 연구에 매진하고 있는 록연도 좋은 결과를 내고 빨리 졸업하기를 바랍니다. 주완, 광원, 예령, 소진, 희태, 영한도 각자의 자리에서 많은 것을 이루며 뛰어난 성과를 내고 있으리라 생각합니다. 외국에서 유학 생활을 하는 상윤, 연정, 형빈이도 건강하고 잘 지내기를 바랍니다. 그리고 고등학교 때부터 알고 지낸 진호, 성학, 성훈, 명진, 동협이도 더 자주 보았어야 한다는 아쉬움과 함께 앞으로도 변치 않는 우정을 이어가자는 말을 전하고 싶습니다.

그리고 오랜 시간 동안 같이 생활하면서 연구에 정진할 수 있도록 배려와 지원을 아끼지 않고 인생과 진로에 대해 아낌없는 조언을 해 준 형, 새로이

가족이 되어 많은 도움을 주시고 부족한 저를 따뜻함으로 대해 주신 형수님, 무엇보다도 저의 긴 대학원 생활 동안 부족한 저를 항상 믿어주시고 지원과 격려, 그리고 사랑을 아끼지 않으신 부모님에게 감사를 표합니다. 주신 사랑에 비하면 보잘것없지만 그래도 박사 과정을 마치어 아들 이름이 적힌 학위 논문이나마 드릴 수 있어서 다행입니다. 지금보다 더 큰 사람이 되어 앞으로 사회에서 열심히 활동하여 도와주신 모든 분들께 보답할 수 있는 사람이 될 수 있도록 하겠습니다. 이 논문을 나를 걱정해 주시고 사랑해 주신 모든 분들에게 바칩니다. 감사합니다.

이학박사 학위논문

p-type doping for transparent perovskite semiconductor of alkali-earth stannate and its pn-junctions

투명 페로브스카이트 반도체 알칼리토 주석 산화물의 p 형 도핑과 그 pn 접합 연구

2014 년 2 월

서울대학교 대학원

물리천문학부

김 훈 민

p-type doping for transparent perovskite semiconductor of alkali-earth stannate and its pn-junctions

투명 페로브스카이트 반도체 알칼리토 주석 산화물의 p 형 도핑과 그 pn 접합 연구

지도 교수 차 국 린

이 논문을 이학박사 학위논문으로 제출함.
2014년 2 월

이 논문을 이학박사 학위논문으로 제출함

서울대학교 대학원
물리천문학부
김 훈 민

김훈민의 이학박사 학위 논문을 인준함
2014 년 2 월

위 원 장 _____ 국 양

부위원장 _____ 차 국 린

위 원 _____ 김 기 훈

위 원 _____ 박 제 근

위 원 _____ 방 윤 규

p-type doping for transparent perovskite semiconductor of alkali-earth stannate and its pn-junctions

by

Hoon Min Kim

Supervised by

Professor Kookrin Char

A dissertation submitted to the Faculty of
Seoul National University
in Partial Fulfillment of the Requirements
for the Degree of
Doctor of Philosophy

February 2014

Department of Physics and Astronomy
Graduate School
Seoul National University

Abstract

Transparent oxide semiconductors (TOSs) are widely used as transparent electrodes because they are optically transparent in the visible light and UV regions and their electrical conductivity can be manipulated. However, applications of TOSs are limited to transparent electrodes and panel displays because of a lack of p-type conducting transparent oxide materials. The discovering and developing Cu-based p-type TOSs has allowed the fabrication of fundamental semiconductor devices such as pn junctions and field effect transistors; however, there are few reports of TOS materials that can be injected with dopants to from both p- and n-type materials.

Recently, it was reported that La-doped $BaSnO_3$ (BLSO) has high oxygen stability and good electrical conductivity. However, even though BSO thin films exhibit a high epitaxiality, the films contains many grain boundaries and dislocations that act as charge traps and scattering centers. We are attempting to find a substrate more suitable than $SrTiO_3$ (STO) for improving the electrical properties of BLSO thin films; however, BLSO thin films on alternative substrates show a poorer mobility than those on STO. In addition, the low doped BLSO thin film acts like a p-type semiconductor due to the effects of threading dislocations even though the dopant is an n-type carrier.

Because the d-orbital does not participate in the bonding between Sn and O in $BaSnO_3$ (BSO), this bond can be stronger than that in other perovskite materials, and allows for the possible doping with a p-type carrier. We have been successfully in doping BSO with K using pulsed laser deposition. Although K-doped BSO exhibits a rather high resistivity at room temperature, its conductivity increased dramatically at higher temperatures. The activation

energy of the K-dopant was estimated to be about 0.5 eV. Furthermore, the conductivity decreased when a small amount of oxygen was removed from the film, consistent with the behavior of p-type doped oxides. The results of doping BSO with other elements such as Ga and Cu are presented.

We have fabricated pn junctions using K-doped BSO (BKSO) and BLSO as the p- and n-type semiconductors, respectively. I-V characteristics of these devices showed the typical rectifying behavior of pn junctions in room temperature. In addition, I-V characteristics of these devices exhibit an ideal diode behavior with the ideality factor between 1 and 2 in high temperature, implying high integrity of the BSO materials. Moreover, the junction properties were found to be very stable after repeated high-bias, high-temperature thermal cycling. Our demonstration of pn junctions based on a single perovskite BSO further enhances the potential of a transparent perovskite semiconductor BSO system, whose high mobility and stability have previously been shown.

We investigated $SrSnO_3$ (SSO), which has a 4 eV direct band gap. SSO thin films were deposited on $KTaO_3$ (KTO) to minimize the lattice mismatch with SSO. Images obtained with TEM and AFM showed that the SSO thin films on KTO exhibit almost no threading dislocations. In measuring the electrical properties of the SSO thin films with various dopants such as Sb, La and Ru, we found that the mobility was generally lower than that of BLSO thin films due to tilting of the SnO_6 octahedral. Ru-doped SSO showed p-type behavior even at room temperature. We fabricated a pn junction using Sb-doped SSO and Ru-doped as the n- and p-type semiconductors, respectively. We found that the current of the SSO based pn junction was higher than that based on BSO system; there were several problems with the pn junction, such as large leakage current and large parasitic resistance. If we combine the BSO and SSO system, however,

it will be possible to fabricate LED devices because of the direct band gap, low leakage current pn junction and low resistivity conduction.

Keywords: Transparent oxide semiconductor, $BaSnO_3$, p-type oxide with potassium doping, pn homojunction with single perovskite oxide, $SrSnO_3$, p-type oxide with ruthenium doping

Student number: 2007-20416

Contents

List of Tables

List of Figures

1. Introduction

1.1 p-doping on oxides and their pn junctions

Oxide materials have been intensively investigated because they exhibit insulating, semiconducting, or metallic behavior and novel phenomena such as colossal magneto-resistance and high temperature superconductivity. Among them, perovskite oxides possess great potential for advancing science and technology because of their various unique functionalities, including superconductivity [1], magnetism [2], ferroelectricity [3], and multiferrocity [4]. For example, $SrTiO_3$ (STO) has been extensively studied for these characteristics as well as its high-mobility 2DEG behavior [5, 6] at the interface with $LaAlO_3$. Recently, transparent conducting oxides (TCOs) such as Sn-doped indium oxide (ITO) [7, 8] and In-Ga-Zn-O (IGZO) [9] are widely used as transparent electrodes for display applications and solar cells because they are optically transparent in the visible and UV regions and modulate the electrical conductivity [10, 11]. However, the large electronegativity of oxygen and charge compensation by oxygen vacancies makes it difficult to dope oxide materials with a p-type dopant. Therefore, we reviewed the progress of p-type oxide research and investigated the mechanisms of various p-type oxides and their applications.

Although TCOs have a good conductivity and wide controllable range, their application is limited to transparent electrodes and panel displays because of a lack of p-type conducting transparent oxide materials [12]. In 1997, there was a report of fabrication of p-type transparent conducting oxide films of $CuAlO_2$ [13] and the discovery of p-type TCOs has led to a class of materials known as transparent oxide semiconductors (TOSs) [10, 13]. Since then, a series of p-type

TCOs based on Cu^{+}-bearing oxides, such as $CuGaO_2$ [14], $CuInO_2$ [15, 16], $SrCu_2O_2$ [17] and LnCuOCh (where Ln = lanthanide and Ch = S or Se) [18-21] have been fabricated as the result of material exploration efforts. In general, because of the large electronegativity of oxygen, the valence band edge of oxides is strongly localized to the oxygen ions in the oxide materials. However, in Cu-based TOSs, the $3d^{10}$ closed shell orbital of the Cu^{+} ion is hybridized with the oxygen 2p state, which pushes a more dispersive band up to an energy above the non-bonding O 2p or Cu 3d states. The electronic structures of $CuAlO_2$ which probed by normal/inverse photoemission spectroscopy show that the hybridized orbitals are distinctly nearer to the Fermi level than the typical oxygen 2p state [22]. In a similar manner to the Cu^{+} ion, Rh^{3+} metal ions with a $4d^6$ shell hybridize with oxygen because of the quasi-closed shell configuration [23].

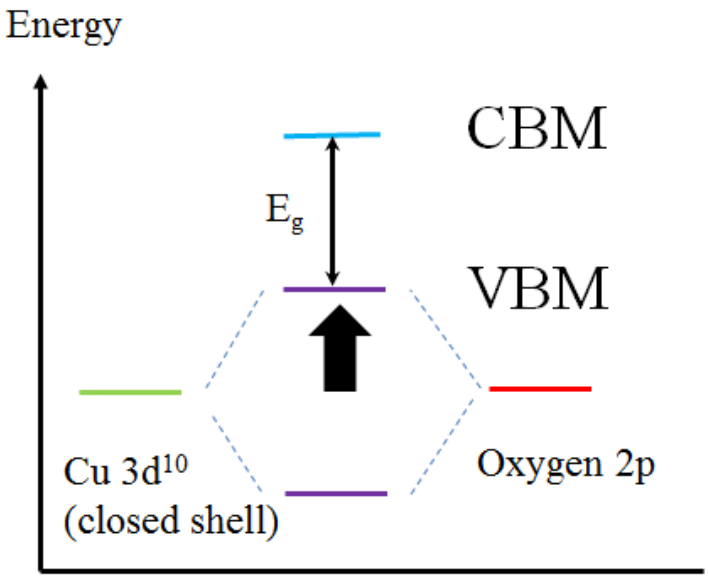

Figure 1.1. Schematic of the chemical bond between an oxide ion and a cations that has a closed shell electronic configuration.

As p-type TOSs have been developed, fundamental semiconductor devices such as light emitting diodes (LEDs) and UV detectors using pn junctions can be fabricated. Near-UV-LEDs are composed of pn heterojunctions of TOSs: p-type $SrCu_2O_2$ and n-type ZnO. Efficient electroluminescence centered at 382 nm was observed when a forward current was injected into the pn-heterojunction diode [24, 25]. A transparent UV light detector was also fabricated using a high-quality pn heterojunction diode composed of TOSs, p-type NiO and n-type ZnO, and its UV-light response was characterized at room temperature [26]. However, there are few reports of TOS materials that can be injected with dopants to fabricate p- and n-type materials [16].

Perovskite oxides are important functional materials that exhibit the various physical properties noted above. An investigation of p-doping perovskite has mainly focused on manganite materials [27-30] because of the relative lack of p-type perovskite oxide materials. The 3d band of Mn splits into the t_{2g} and e_g bands under a crystalline field, and the e_g band is split further into the e_{g1} and e_{g2} bands because of the Jahn-Teller effect. The e_{g1} band is fully occupied while the e_{g2} band is completely empty. Mn^{3+} ions can be oxidized into Mn^{4+} ions by doping divalent ions such as Sr at the La^{3+} sites, which is equivalent to introducing holes into the e_{g1} band [27, 28]. Manganese materials have been intensively researched because of their colossal magneto-resistance effect. A pn junction fabricated using such materials, as shown in Figure 1.4, has a large leakage current and stability problems even at room temperature, although it does exhibit photo-response [28, 29], because the p-doping mechanism is different to the conventional doping mechanism. As shown in Figure 1.5, pn junctions composed of Nb-doped $SrTiO_3$ (STO) (n-type) and In-doped STO (p-type) are demonstrated [31, 32]. However, the use of a STO substrate (not a

film) for the n-type semiconductor limits device fabrication. Therefore, it will be very useful for scientific research and engineering applications if both the thermal and electrical stability and n- and p- type doping mechanism can be shown to similar to those of a conventional semiconductor.

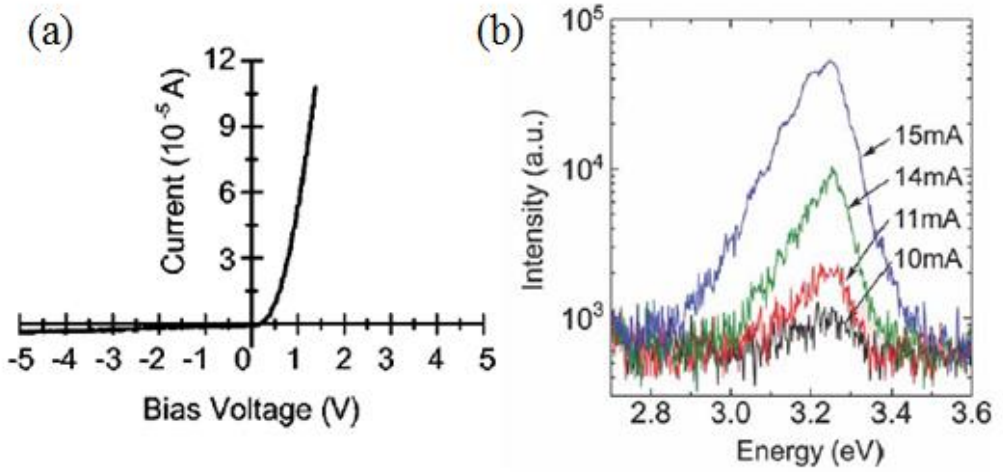

Figure 1.2. (a) A typical I-V characteristic of the transparent pn heterojunction p-$SrCu_2O_2$/n-ZnO. (b) UV emission spectra of the pn junction LED for tens of currents [24].

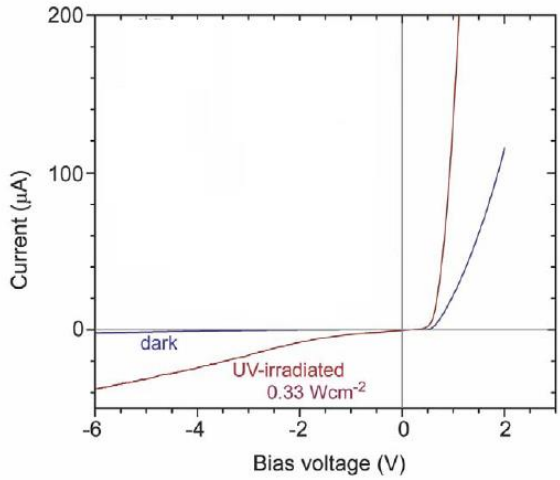

Figure 1.3. Typical I-V characteristics of a pn-heterojunction p-NiO/n-ZnO diode in the dark and under UV illumination; total power density is 0.33 W·cm^{-2} at room temperature [25].

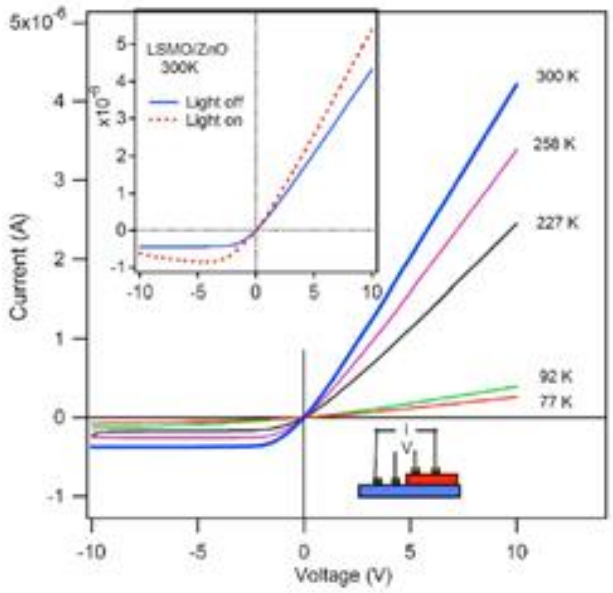

Figure 1.4. I-V characteristics of p-LSMO/n-ZnO junction of various temperatures. The inset shows the current-voltage curves at 300 K with irradiance of 80 mW/cm^2 and without light irradiation [28].

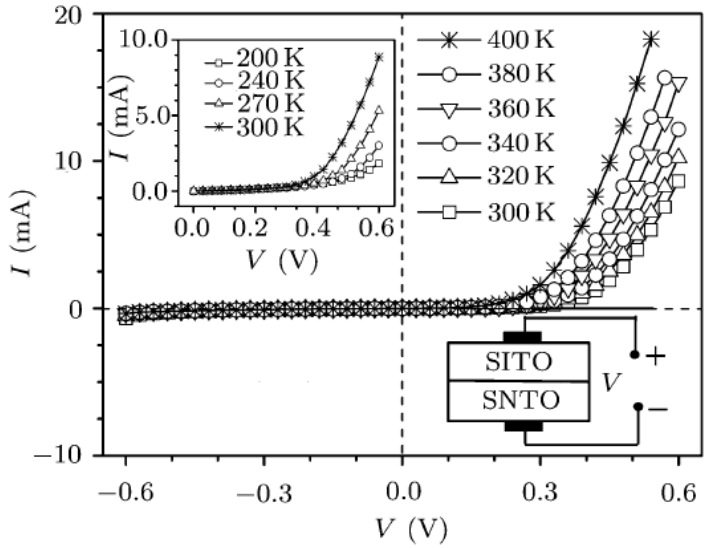

Figure 1.5. I-V curves of the SITO/SNTO pn junction at 300–400K. The upper inset shows the forward-bias I-V curves at 200–300 K and the lower inset is the schematic circuit of the measurement [32].

1.2 $BaSnO_3$: transparent perovskite semiconductor

Wider application of perovskite oxides is limited mainly because of the instability of oxygen, which results in uncertainty in the oxygen stoichiometry and movement at interfaces. This oxygen instability has made thermally stable p- and n-doping in a single perovskite system elusive in spite of its enormous significance in optoelectronic applications. Recently, we reported that $BaSnO_3$ (BSO) exhibits a high oxygen stability and good electrical conductivity in La-doped BSO (BLSO) for an n-type degenerate semiconductor [33]. In contrast to conventional transition metal perovskite oxides, the 5s-orbital of the Sn^{4+} ion is directly bonded to the 2p-orbital of the O_2 ions in BSO system [34]. As the d-orbital does not participate in this bonding between Sn and O, the bond can be stronger than that in other perovskite materials, and it becomes possible to dope the system with a p-type carrier.

La-doped $BaSnO_3$ (BLSO) is reported to have a high oxygen stability and good electrical conductivity [33]. The oxygen diffusion constant measured at 530 ^oC is approximately 10^{-15} cm^2/s^{-1}, which is lower than other perovskite oxides such as titanates (10^{-8}) [35], cuprates (10^{-11}) [36] and manganites (10^{-13}) [37]. In single crystals, the mobility reached 320 $cm^2/V{\cdot}s$ at a doping level of 8 $\times$ 10^{19} cm^{-3}, constituting the highest value among wide-band-gap semiconductors [38-41] (see Figure 1.6). Also, BLSO thin films have a good electrical conductivity of 0.2 $m\Omega{\cdot}cm$ and avery high mobility of 70 $cm^2/V{\cdot}s$. Therefore, BSO has the potential to open the way for the development of transparent perovskite semiconductors (TPSs) because it can be applied to strongly correlated perovskite systems combined with the TOS regime.

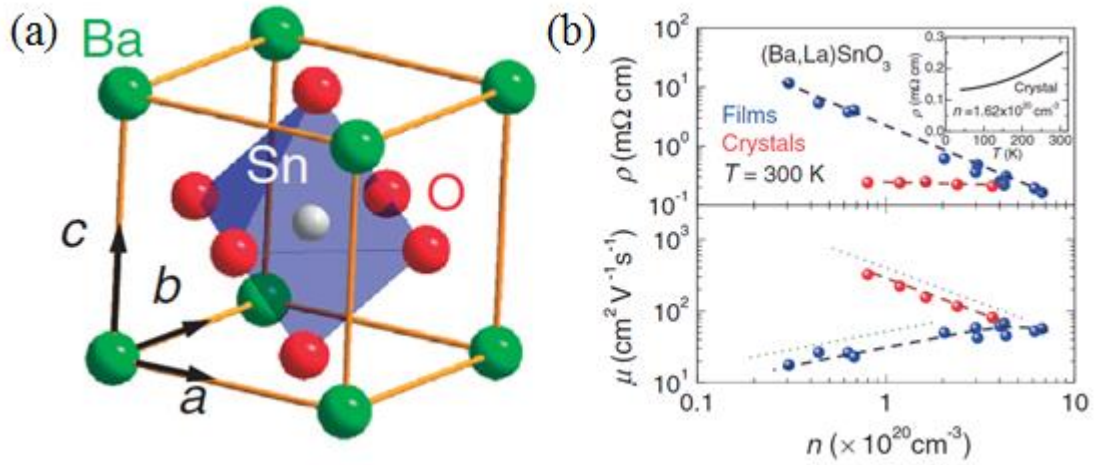

Figure 1.6. (a) Cubic perovskite $BaSnO_3$ which lattice is constant is 4.116 Å. (b) Resistivity and mobility of the BLSO thin films and single crystals are plotted as functions of carrier density at 300 K [32].

Reference

[1] R. J. Cava, B. Batlogg, J. J. Krajewski, R. Farrow, L. W. Rupp Jr, A. E. White, K. Short, W. F. Peck, & T. Kometani, Nature **332,** 814-816 (1988).

[2] Y. Tokura & Y. J. Tomioka, Magn. Magn. Mater. **200**, 1 (1999).

[3] G. H. Haertling, J. Am. Ceram. Soc. **82**, 797 (1999).

[4] T. Kimura, T. Goto, H. Shintani, K. Ishizaka, T. Arima & Y. Tokura, Nature **426**, 55 (2003).

[5] A. Ohtomo & H. Y. Hwang , Nature **427**, 423 (2004).

[6] S. Thiel, G. Hammerl, A. Schmehl, C. W. Schneider, & J. Mannhart, Science **313**, 1942 (2006).

[7] T. Minami, Semicond. Sci. Technol. **20 S35** (2005).

[8] A. L. Dawar, J. C. Joshi. J. Mater. Sci. **19**, 1 (1984).

[9] T. Kamiya, K. Nomura & H. Hosono, Sci. Technol. Adv. Mater. **11**, 044305 (2010).

[10] H. Ohta & H. Hosono., materials today **7**, 42 (2004).

[11] D. S. Ginley & C. Bright, Mater. Res. Soc. Bull. **25**, 8 (2000).

[12] S. Sheng, G. Fang, C. Li, S. Xu, & X. Zhao1, phys. stat. sol. **8**, 1891 (2006).

[13] H. Kawazoe, M. Yasukawa, H. Hyodo, M. Kurita, H. Yanagi & H. Hosono, Nature **389**, 939 (1997).

[14] K. Ueda, T. Hase, H. Yanagi, H. Kawazoe, H. Hosono, H. Ohta, M.

Orita & M. Hirano J. Appl. Phys. **89**, 1790 (2001).

[15] C. N. R. Rao, A. Govindaraj, F. Leonard Deepak, N. A. Gunari & Manashi Nath , Appl. Phys. Lett. **78**, 1583 (2001).

[16] H. Yanagi, K. Ueda, H. Ohta, M. Orita, M. Hirano & H. Hosono, Solid State Commun. **121**, 15 (2001).

[17] A. Kudo, H. Yanagi, H. Hosono & H. Kawazoe., Appl. Phys. Lett. **73**, 220 (1998).

[18] K. Ueda, S. Inoue, S. Hirose, H. Kawazoe & H. Hosono, Appl. Phys. Lett. **77**, 2701 (2000).

[19] K. Ueda, S. Inoue, H. Hosono, N. Sarukura & M. Hirano, Appl. Phys. Lett. **78**, 2333 (2001).

[20] K. Ueda & H. Hosono, J. Appl. Phys. **91**, 4768 (2002).

[21] K. Ueda, K. Takafuji, H. Hiramatsu, H. Ohta, T. Kamiya, M. Hirano, & H. Hosono , Chem. Mater. **15**, 3692 (2003).

[22] H. Yanagi, H. Kawazoe, A. Kudo, M. Yasukawa & H. Hosono, J. Electroceram. **4**, 407 (2000).

[23] H. Mizoguchi, M. Hirano, S. Fujitsu, T. Takeuchi, K. Ueda & H. Hosono, Appl. Phys. Lett. **80** 1207 (2002).

[24] H. Ohta, K. Kawamura, M. Orita, M. Hirano, N. Sarukura & H. Hosono., Appl. Phys. Lett. **77**, 475 (2000).

[25] H. Hosono, H. Ohta, K. Hayashia, M. Oritaa & M. Hiranoa, J. Cryst. Growth **237**, 496 (2002).

[26] H. Ohta, M. Hirano, K. Nakahara, H. Maruta, T. Tanabe, M. Kamiya, T. Kamiya & H. Hosono Appl. Phys. Lett. **83**, 1029 (2003).

[27] K. Lord, D. Hunter, T. M. Williams, & A. K. Pradhan, Appl. Phys. Lett. **89**, 052116 (2006).

[28] D. J. Wang, Y. W. Xie, C. M. Xiong, B. G. Shen & J. R. Sun, Europhys. Lett. **73**, 401 (2006).

[29] J. R. Sun, S. Y. Zhang, B. G. Shen & H. K. Wong, Appl. Phys. Lett. **86**, 053503 (2005).

[30] J. Zhang, H. Tanaka & T. Kawai, Appl. Phys. Lett. **80**, 4378 (2002).

[31] Q. Zhou, K. Jin, H. Lu, P. Han, Z.Chen, K. Zhao, Y. Zhou & G. Yang, Europhys. Lett. **71**, 283 (2005).

[32] G. Liu, K. Jin, M. He, J. Qiu, J. Xing, H. Lu & G. Yang, Chin. Phys. Lett. **25,** 2209 (2008).

[33] H. J Kim, U. Kim, H. M. Kim, T. H. Kim, H. Mun, B. G. Jeon, K. T. Hong, W. J. Lee, C. Ju, K. H. Kim & Kookrin Char, Appl. Phys. Exp. **5**, 061102 (2012).

[34] H. Mizoguchi, H. W. Eng and P. M. Woodward, Inorg. Chem. **43**, 1667 (2004).

[35] C. Schaffrin, Phys. Status Solidi **35,** 79 (1976).

[36] K. N. Tu, N. C. Yeh, S. I. Park & C. C. Tsuei, Phys. Rev. B **39,** 304 (1989).

[37] L. Malavasi & G. Flor., J. Phys. Chem. B **107**, 13880 (2003).

[38] D. K. Gaskill, A. E. Wickenden, K. Doverspike, B. Tadayon, & L. B. Rowland, J. Electron. Mater. **24**, 1525 (1995)..

[39] R. L. Weiher, J. Appl. Phys. **33**, 2834 (1962)..

[40] H. Toyosaki, M. Kawasaki, and Y. Tokura, Appl. Phys. Lett. **93**, 132109 (2008).

[41] A. Ohtomo, K. Tamura, K. Saikusa, K. Takahashi, T. Makino, Y. Segawa, H. Koinuma, & M. Kawasaki, Appl. Phys. Lett. **75**, 2635 (1999).

2. Properties of n-type BSO thin films

As mentioned in Chapter 1, BLSO thin films exhibit an excellent electrical mobility and high oxygen stability. However, there are some significant differences between BSO single crystals and thin films: the mobility of a BLSO single crystal is about 320 $cm^2/V{\cdot}s$ and that of BLSO thin film is about 70 $cm^2/V{\cdot}s$ for a high doping concentration [1]. Furthermore, there are distinct differences in the behavior of the electron mobility of single crystals and thin films in response to changes in the carrier concentration. Unlike a single crystal, the mobility of a thin film decrease as the carrier concentration decreased. Even though our films have a high epitaxiality, there will be a large number of grain boundaries and dislocations that act as charge traps and scattering centers for the carriers, as shown in Figure 2.1 [2]. Moreover, there is suggestion that the effect of dislocations on the electrical transport properties in BLSO films is much larger than that in other materials such as GaN [2]. That means that more carriers are trapped in dislocation traps and that a higher carrier density is required to shield the scattering by the dislocation. Therefore, the conductivity of a BLSO thin film is very low when the doping concentration is relatively low. The structure and defect content of the interface between a substrate and the epitaxially grown thin film is of considerable importance, particularly in the technology of solid state electronic devices [3]. In this section, we describe the efforts made in finding a more suitable substrate for resolving the dislocation problems and the comment on measurements of the conductivity of BLSO thin films at high temperature in different background atmospheres to determine the type of carrier in the BLSO thin films.

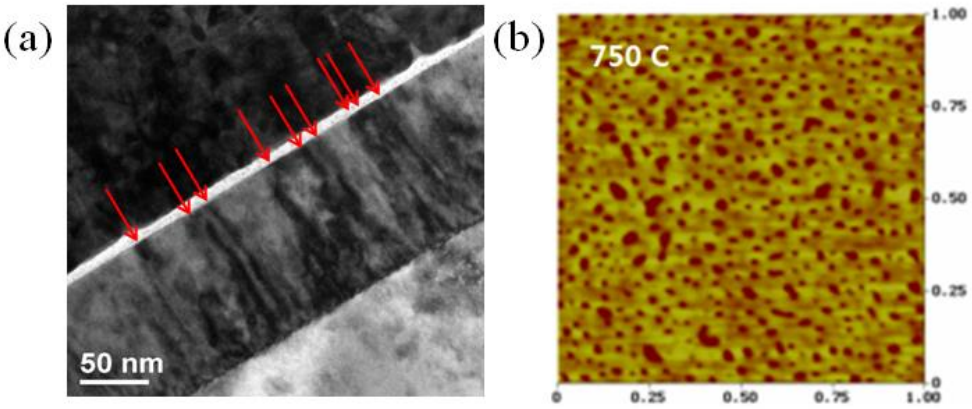

Figure 2.1. (a) The cross-sectional TEM image of BLSO thin film obtained by using two beam condition, showing threading dislocations by arrows. (b) Images of surface morphologies after etching with 0.4 % HNO_3 for 10 s [2].

	Cell plane(Å^2)	Lattice mismatch (%)
$BaSnO_3$	16.941	0
$SrTiO_3$	15.249	-5.12
r-Al_2O_3 (1/4)	18.297	3.92
$BaTiO_3$	15.952	-2.96
$MgAl_2O_4$ (1/4)	16.322	1.84
MgO	17.74	2.33

Table 2.1. The area of cell planes and their lattice mismatch with $BaSnO_3$. (1/4) in r-Al_2O_3 and $MgAl_2O_4$ indicate that value is ¼ of the cell plane.

2.1 Properties of BLSO thin films at various substrates

2.1.1 BLSO thin film deposition

We deposited various doped BLSO thin films (deposited at 750 ^{o}C) on various buffer layers and substrates which described below using BLSO and BSO targets by pulsed laser deposition system with a KrF excimer laser (λ = 248 nm) under 100 mTorr oxygen pressure with 1 ~ 1.5 J/cm^2 energy intensity. To specifically doped lanthanum ions, we used a sequential deposition method which deposits thin films by sequentially alternating targets for each determined pulse shots [4]. The plume of the BLSO and BSO targets are shown in Figure 2.2 when laser is ablaze at target. As you can see, the size of the plume of BLSO and BSO are almost identical. Therefore, we concluded that the deposition rate matched to the nominal shot ratio of the BLSO and BSO targets assuming that La is not volatile at high temperature.

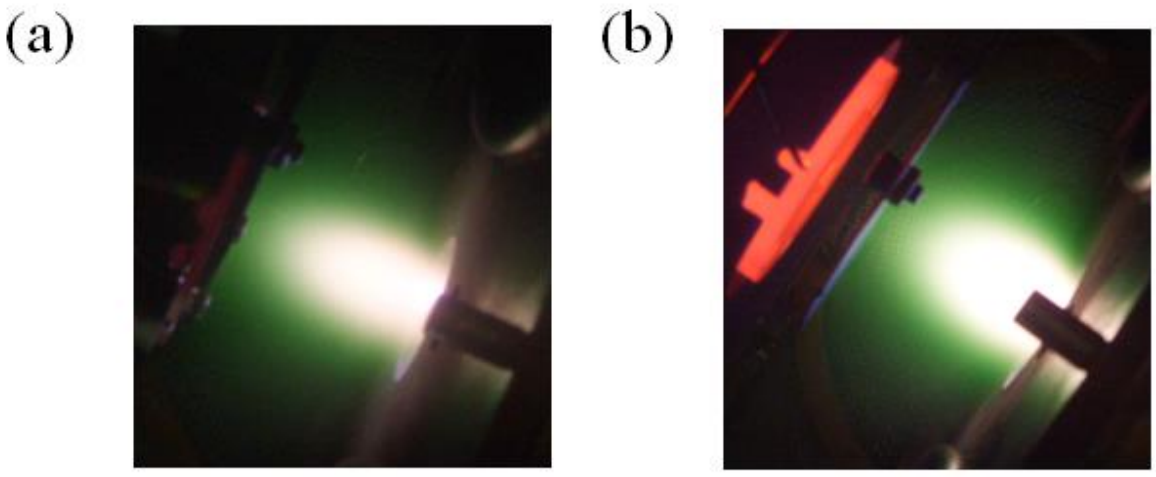

Figure 2.2. Shapes of the plume for laser ablation. (a) plume of BSO (b) plume of BLSO.

2.1.1 r-cut sapphire

As shown in Figure 2.3 (a), the structure sapphire crystal is a hexagonal system, where an axis C for forming a central axis, a plane C (0001) vertical to it [5]. And the plane R (1102) inclined at a constant angle to the axis C, and an axis R is vertical to it when the major axis and plane of the crystal system are expressed with hexagonal indices. As shown at Table 2.1, the lattice mismatch between r-cut sapphire (1/4 plane) and BSO is about 3.92 %. However, because the BLSO thin film is not grown epitaxially on r-cut sapphire directly, we used MgO thin film as a buffer layer. There were many reports to using the MgO buffer layer for obtaining higher crystalline thin films [6-8]. The gonio scan result of BLSO/MgO/r-cut sapphire is indicated in Figure 2.3 (b). There are clearly shown that peaks of MgO buffer layer and BLSO thin films matching to the sapphire substrate are observed and no other peaks are existed. It means that the BLSO thin film on MgO/r-cut sapphire have epitaxial structure and their full width half maximum (FWHM) of rocking curve for omega scan is about 0.25^{o}, which indicate it has highly crystalline. Its electrical properties are shown in Table 2.2. However, it exhibit that the mobility of the BLSO thin film on MgO/r-cut sapphire is 7.96 $cm^2/V{\cdot}s$ which about ten times low compare with that of BLSO on STO (about 70 $cm^2/V{\cdot}s$). Because the structure of r-cut sapphire and BSO is different and the difficulty of MgO growth, the electrical properties of BLSO on MgO/r-cut sapphire is not good as BLSO on STO although it have relatively low lattice mismatch with BSO.

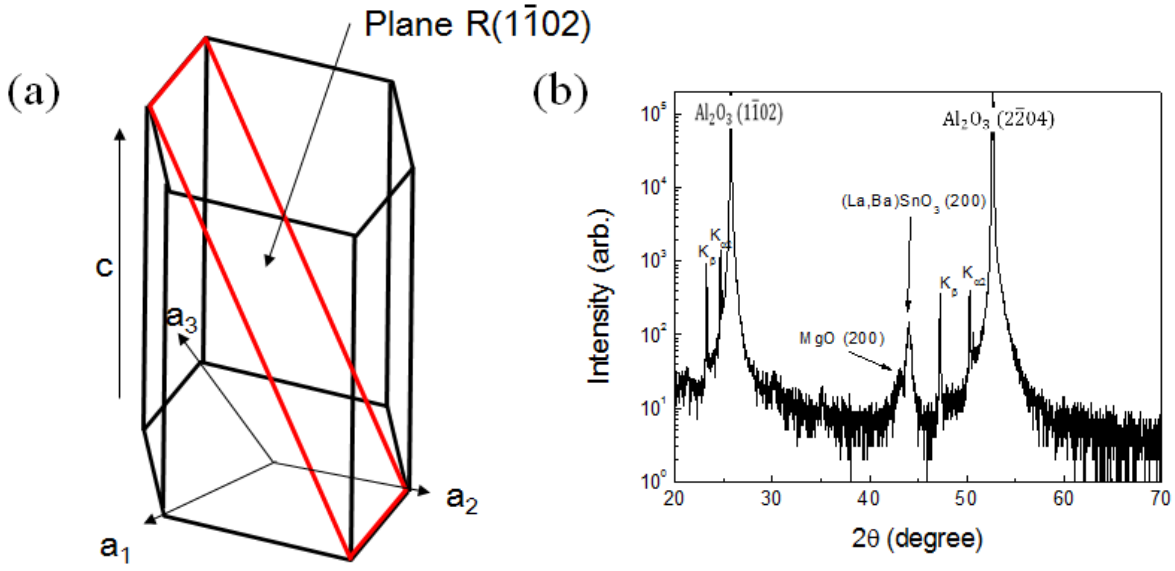

Figure 2.3. (a) The structure of r-cut sapphire in hexagonal sapphire structure (b) θ-2θ scan of BLSO /MgO /r-Al_2O_3 by X-ray diffraction method.

2.1.2 $MgAl_2O_4$

$MgAl_2O_4$ (100) substrate, which generally used for depositing GaN system [9-11], have spinel structure that means the oxygen packs face-centered cubic (FCC) and cations put partial occupancy of tetrahedral and octahedral sites i.e. 1/8 of tetrahedral and 1/2 of the octahedral sites are occupied. A spinel unit-cell is made up of eight FCC cells made by 2 × 2 × 2 oxygen ions configuration, so it is a big structure which consisting of 32 oxygen atoms, 8 A atoms and 16 B atoms. As shown at Table 2.1., the lattice mismatch between $MgAl_2O_4$ (1/4 plane) and BSO is about only 1.84 %. We deposit BLSO on many buffer layers on $MgAl_2O_4$ substrate; no buffer layer, $BaTiO_3$ (BTO), and STO on various temperature. The gonio scan results of various BLSO thin films on buffer layers/$MgAl_2O_4$ are indicated in Figure 2.4. Only using STO which grown at

600 ^{o}C as buffer layer show truly epitaxial structure. Surprisingly, using BTO buffer layer thin film is worse crystalline structure than using STO buffer layer even though BTO have only 2.96 % lattice mismatch which is clearly lower than that of STO (5.12 %). It may originate from the non-stoichiometry of the BTO thin film and its oxygen and Ba vacancies [12-13]. Its mobility of BLSO thin film on STO (grown at 600 ^{o}C) on $MgAl_2O_4$ shows about up to half of that of BLSO/STO (31.5 $cm^2/V{\cdot}s$) as shown at Table 2.3. We conclude that qualities of thin films using STO buffer layer is not exceed of that using STO single crystal substrate and other buffer layer is not work very well.

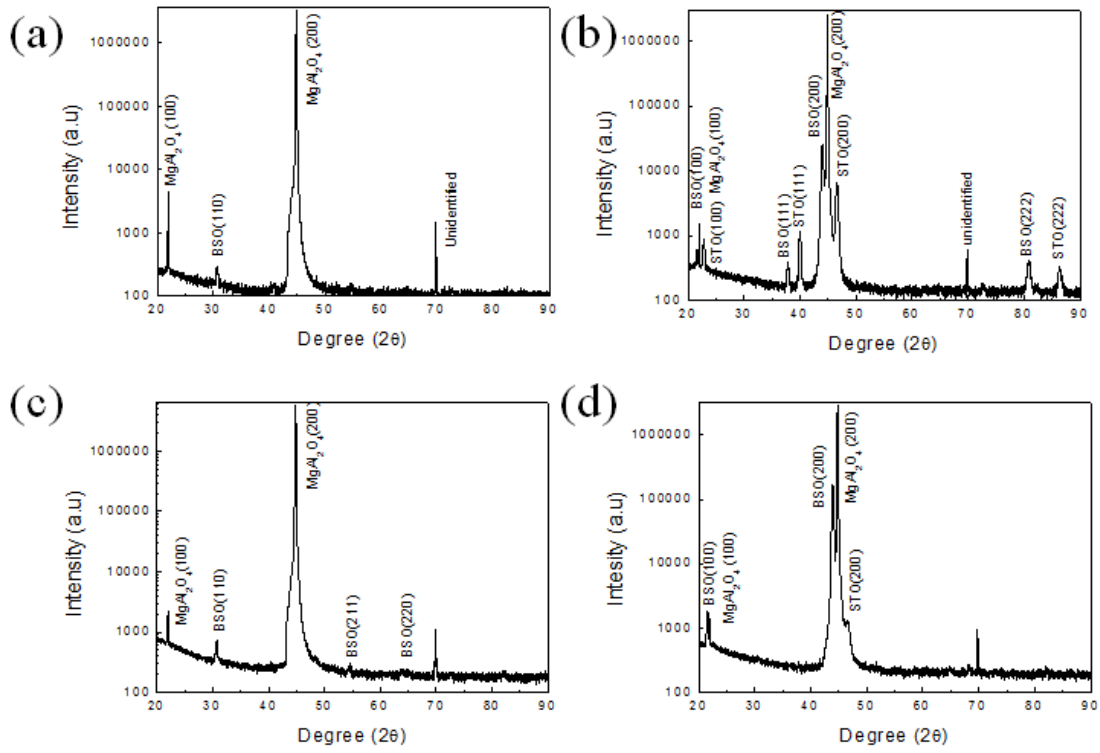

Figure 2.4. θ-2θ scan of (a) BLSO/$MgAl_2O_4$ (b) BLSO/STO(750 ^{o}C) $MgAl_2O_4$ (c) BLSO/BTO(700 ^{o}C)/$MgAl_2O_4$ (d) BLSO/STO(600 ^{o}C) /$MgAl_2O_4$ by X-ray diffraction method.

2.1.3 MgO

MgO (100) substrate has simple rock-salt structure for usually depositing superconducting system such as YBCO [14-16]. The lattice mismatch between r-cut sapphire (1/4 plane) and BSO is about 2.33 %. The gonio scan results BLSO thin film on MgO are indicated at Figure 2.5. The FWHM of rocking curve for BLSO (200) peak is 0.24^{o}, which shows highly crystalline structure. The highest mobility of BLSO thin film is up to 15.7 cm^2/V·s when we use BSO grown at 700 ^{o}C as buffer layer as shown at Table 2.4. From the electrical properties of BLSO /MgO system, we suggest that BLSO grown at 700 ^{o}C is more matched to MgO substrate than BLSO grown at 750 ^{o}C. We think that there are many parameters for matching between substrate and thin film besides lattice mismatch. In conclusion, the suitable substrate which has good lattice match and same perovskite structure must be found to obtaining BLSO thin film with better performance.

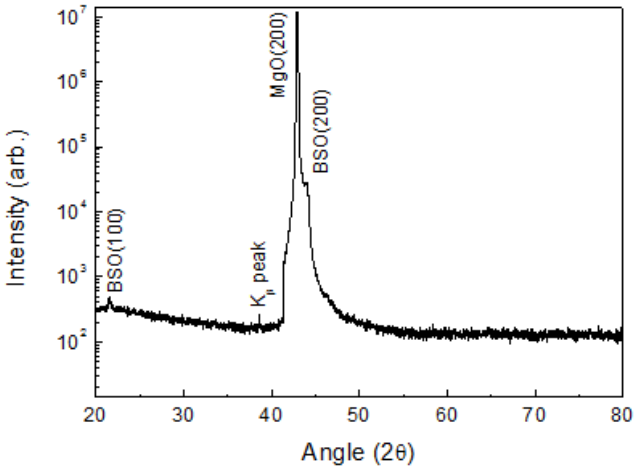

Figure 2.5. (b) θ-2θ scan of BLSO(750 ^{o}C) /BSO(700 ^{o}C)/MgO by X-ray diffraction method.

Sample	LBSO/MgO/r-Al_2O_3
Resistivity (Ω·cm)	0.00252
Mobility (cm^2/V·s)	7.96
Carrier concentration (/cm^3)	-3.11E+20

Table 2.2. The resistivity, mobility and carrier concentration on BLSO thin films on r-Al_2O_3 substrate.

Sample	BLSO on MgAl2O4	BLSO/STO (750 °C) on $MgAl_2O_4$
Resistivity (Ω·cm)	0.75	0.00111
Mobility (cm^2/V·s)	-	13.4
Carrier concentration (/cm^3)	-	4.22 x 10^{20}

Sample	BLSO/BTO on MgAl2O4	BLSO/STO (600 °C) on $MgAl_2O_4$
Resistivity (Ω·cm)	32	0.000653
Mobility (cm^2/V·s)	-	31.5
Carrier concentration (/cm^3)	-	3.03 x 10^{20}

Table 2.3. The resistivity, mobility and carrier concentration on BLSO thin films on $MgAl_2O_4$ substrate.

Sample	BLSO4%(50nm)/ MgO(100)	BLSO4%(40nm at 750°C)/BLSO 4%(10nm at 700°C)/MgO(100)
Resistivity (Ω·cm)	0.00443	0.00212
Mobility (cm^2/V·s)	11.5	15.7
Carrier concentration (/cm^3)	-1.23 x 10^{20}	-1.87 x 10^{20}

Table 2.4. The resistivity, mobility and carrier concentration on BLSO thin films on MgO substrate.

2.2 High temperature experiment of BLSO thin films

As we described above, the conductivity is significantly diminished by threading dislocations or grain boundaries for charge trapping and inelastic scattering. We measure the resistance at high temperature because it confirmed the type of the carrier by changing background atmosphere at high temperature although its resistance is too high to measure at room temperature. We recorded the resistance as increasing temperature in oxygen atmosphere to decide that sample has metallic or semiconducting behavior. And we change atmosphere oxygen to argon and oxygen again when temperature maintains constant. The oxygen vacancies act as electron donor in oxide materials. It means that vacancies generally induce the n-type carrier. Therefore, resistance of the p-type material should be increased if we change background atmosphere from oxygen to argon and that of n-type material should be decreased in same condition.

Surprisingly, the electrical behavior of 2 % BLSO thin film and 0.6 % BLSO at high temperature thin film is completely different. The resistance of 2 % BLSO thin film increased constantly when temperature is raised; however, the resistance of 2 % BLSO thin film decreased constantly. It indicates that 2 % BLSO thin film is degenerate semiconductor which shows almost metallic behavior and 0.6 % BLSO thin film exhibits conventional semiconducting behavior. And the resistance change of BLSO thin films by alternating background atmosphere is shown in Figure 2.6. As you can see, the resistance of 2 % BLSO thin film changes from 130 Ω in oxygen atmosphere to 125 Ω in argon atmosphere. On the contrary, the resistance of 0.6 % BLSO thin film changes from about 1000 Ω in oxygen atmosphere to 3500 Ω in argon atmosphere. The abrupt changes of resistance occur when we change background atmosphere. This phenomenon might come from the effect of

surface bonding such as dangling bond which hold the oxygen ions. In conclusion, the small amount of La-doped BSO thin film acts like p-type semiconductor even though n-type carriers are doped because of the effect of threading dislocations. Therefore we only fabricate BLSO thin film which has high carrier concentration about 10^{19} /cm^3 for n-type system.

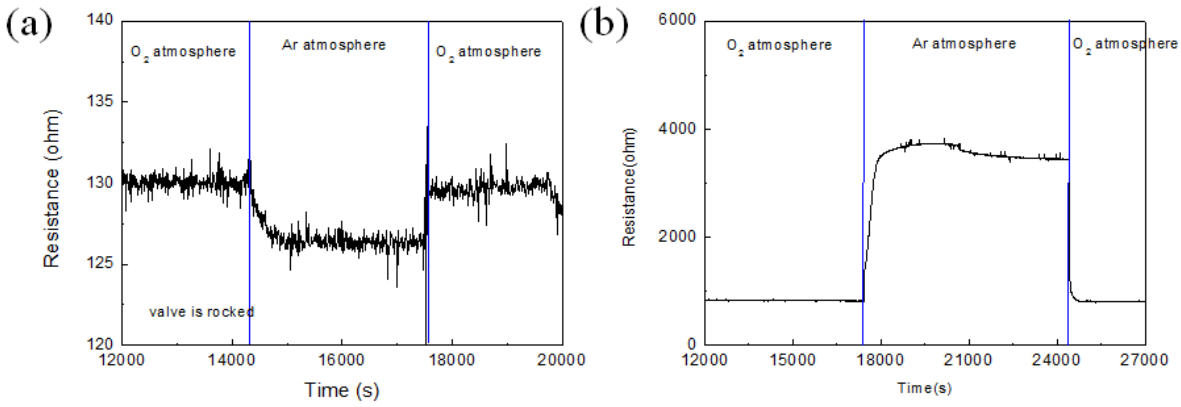

Figure 2.6. High temperature experiment results of (a) 2 % BLSO thin film measured at 500 ^{o}C (b) 0.6 % BLSO thin film at 700 ^{o}C.

Reference

[1] H. J Kim, U. Kim, H. M. Kim, T. H. Kim, H. Mun, B. G. Jeon, K. T. Hong, W. J. Lee, C. Ju, K. H. Kim & Kookrin Char, Appl. Phys. Exp. **5**, 061102 (2012).

[2] H. Mun, U. Kim, H. M. Kim, C. Park, T. H. Kim, K. H. Kim & K. Char, Appl. Phys. Lett. **102,** 252105 (2013).

[3] D. Hull & D. J. Bacon., Introduction to dislocations. (Elsevier, 2011) Chapter 9.6.

[4] L. Mieville, T. H. Gaballe, L. Antagnazza, and K. Char, Appl. Phys. Lett. **70**, 126 (1997).

[5] Kinoshita & M. Umehara, US patent, US 2004/0109486 A1 (2004).

[6] J. G. Lisoni, M. Siegert, C.H Lei, W. Biegel, J. Schubert, W. Zander & C. Buchal., Thin Solid films, **389**, 219 (2001).

[7] C. H. Lei, C. L. Jia, J. G. Lisoni, M. Siegert, J. Schubert, C. Buchal & K Urban., J. Crys. Growth **219**, 397 (2000).

[8] P. A. Stampe, M. Bullock, W. P. Tucker & R. J. Kennedy, J. Phys D **32**, 1778 (1999).

[9] S. Nakamura, M.i Senoh, S. Nagahama, N. Iwasa, T. Yamada, T. Matsushita, H. Kiyoku & Y. Sugimoto Appl. Phys. Lett. **68**, 2105 (1996).

[10] A. Kuramata, K. Horino, K. Domen, K. Shinohara & T. Tanahashi, Appl. Phys. Lett. **67**, 2521 (1995).

[11] A. N. Efimov, A. O. Lebedev, V. V. Lundin & A. S. Usikov, Cryst.

Reports **45**, 312 (2000).

[12] G.V Lewis & C.R.A Catlow, J. Phys. Chem. Solids **47**, 89 (1986).

[13] N. H. Chan, R. K. Sharma & D. M. Smyth, J . Am. Ceram. Soc. **64**, 556 (1981).

[14] B. H. Moeckly, S. E. Russek, D. K. Lathrop, R. A. Buhrman, J. Li & J. W. Mayer, Appl. Phys. Lett. **57**, 1687 (1990).

[15] D. M. Hwang, T. S. Ravi, R. Ramesh, S. W. Chan, C. Y. Chen, L. Nazar, X. D. Wu, A. Inam and T. Venkatesan, Appl. Phys. Lett. **57**, 1690 (1990).

[16] S. Miki, M. Fujiwara, M. Sasaki, B. Baek, A. J. Miller, R. H. Hadfield, S. W. Nam & Z. Wang, Appl. Phys. Lett. **92**, 061116 (2008).

3. Properties of p-type BSO thin films

3.1 K-doped BSO (BKSO) thin films

3.1.1 BKSO thin film deposition

We deposited 100 nm think BKSO thin film (deposited at 700 ^{o}C) on 5 nm thick BSO buffer layer (deposited at 750 ^{o}C) on the STO (001) substrate using BSO and K_2SnO_3 (KSO) targets by pulsed laser deposition system with a KrF excimer laser (λ = 248 nm) under 100 mTorr oxygen pressure with 1 ~ 1.5 J/cm^2 energy intensity. To partially dope potassium ions, we used a sequential deposition method which deposits thin films by sequentially alternating targets for each determined pulse shots [1]. The plume of the BSO and KSO targets are shown at Figure 3.1 when laser is ablaze at target. As you can see, the size of the plume of BSO and KSO are very different. Therefore, the deposition rate is not exactly matched to the shot ratio of the BSO and KSO targets. Also, we consider that doping rate is not precisely determined by nominal shot ratios because potassium is quite volatile at high temperature.

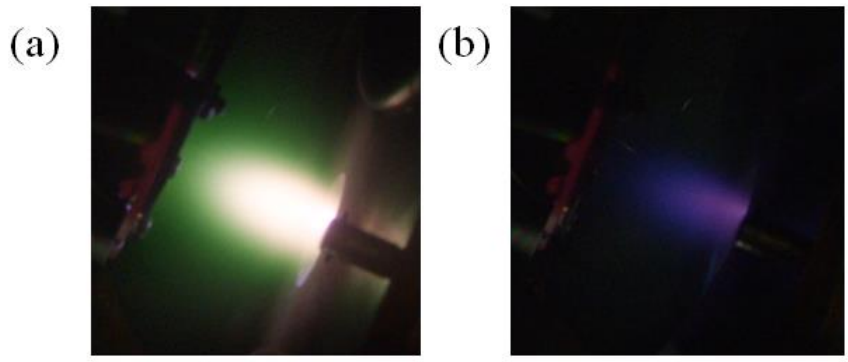

Figure 3.1. Plumes for laser ablation in pulsed laser deposition method. (a) Plume of BSO and (b) KSO.

3.1.2 Electron spectroscopy for chemical analysis

In order to quantify the concentration of potassium at BKSO thin film, electron spectroscopy for chemical analysis (ESCA) method was used. The equation of the relative density between the dopant and host atoms derived by measured intensity ratio is as follows:

$$\frac{\eta_d}{\eta_h} = \frac{I_d \sigma_d \lambda(\varepsilon_d) D(\varepsilon_d)}{I_h \sigma_h \lambda(\varepsilon_h) D(\varepsilon_h)} \quad (3.1)$$

where I is the intensity of the X-ray peak, σ is the photo-excitation probability, λ is the mean free path of an excited electron with energy ε, D is the fraction of electrons detected by the analyzer, and the lower subscripts d and h are used for dopants and host atoms in equation (3.1) [2]. We assumed that detection efficiencies for Ba and K elements are same, and the mean free path and photo-excitation probability (denoted in parenthesis) of Ba and K are 25.8 (0.473) and 17.2 (0.248) [2, 3]. Using above formula and X-ray intensity obtained by ESCA shown in Figure 3.2, we can estimate doping ratio of potassium at the several different BKSO thin films, which are shown in Figure 3.3. Using this peaks and equation (3.1), we concluded that the estimated doping rate of K is generally proportional to the shot ratio of BSO and KSO targets as you can see at Figure 3.3. Therefore, we derive the exact doping ratio of K in BKSO thin films from ESCA.

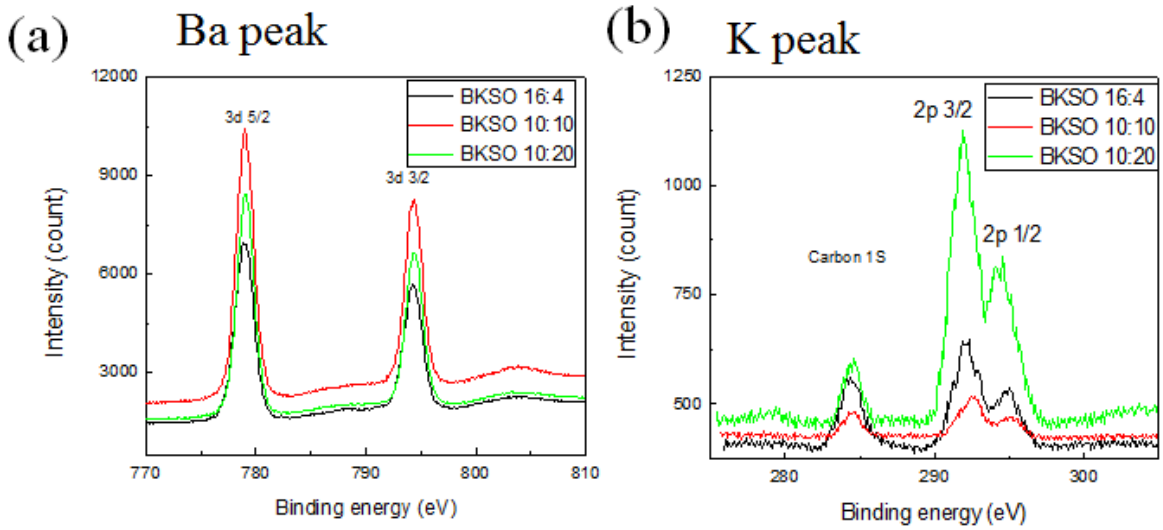

Figure 3.2. XPS peaks for (a) Ba and (b) K by ESCA method. We calculated the concentration of K about Ba by 3d 5/2 peak for Ba and 2p 3/2 for K.

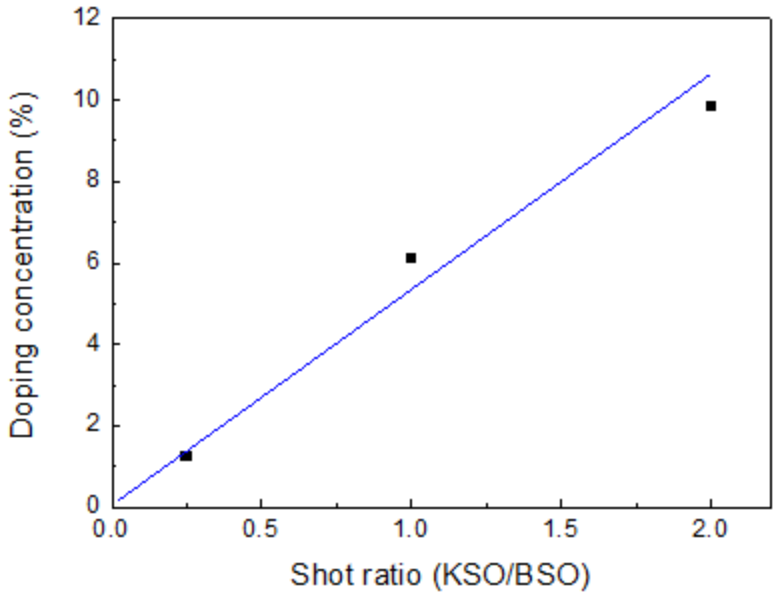

Figure 3.3. Doping centration vs. shot ratio graph plotted by ESCA method. Blue line is linear estimation for fitting. The shot ratio indicates for proportion to the number of laser shots for KSO and BSO target.

3.1.3 Structural and Surface properties of BKSO thin films

For proof of the epitaxiality of the BKSO thin film, as already shown at BSO and BLSO thin film [4], we obtained the structural information of BKSO thin film by the X-ray diffraction method, represented in Figure 3.4. The θ-2θ scan confirms that the epitaxial film was deposited along the direction of STO substrate. Compared with the peak of the BSO film buffer layer, definitely higher X-ray peak intensities as we deposit thicker BKSO films strongly supports that BKSO thin films on BSO buffer layer are grown to highly epitaxial structure. The values of full width at half maximum (FWHM) of the ω-scan at the BKSO (002) peak position for BSO buffer, BKSO 1.5 %, 6 % and 11 % are 0.11^{o}, 0.13^{o}, 0.40^{o} and 0.42^{o}, as indicated in Figure 3.5 which shows that BKSO film have highly crystalline and well oriented structure. Also, to confirm the surface homogeneity of the BKSO film, we use the AFM image as shown in Figure 3.6 and the SEM picture as shown in Figure 3.7. Through the AFM image, we found the surface of the 6 % BKSO films to be almost atomically flat and have a very low roughness value which is 0.738 nm. The roughness of the BLSO thin film is 0.223 nm. Though the roughness of the BKSO is larger than BLSO thin film, it has excellent surface to fabricating device and consisting their interface. By the SEM image, the 6 % BKSO films exhibit highly flat surface morphology and no potassium segregation was observed contrary to the image of KSO thin film with segregations.

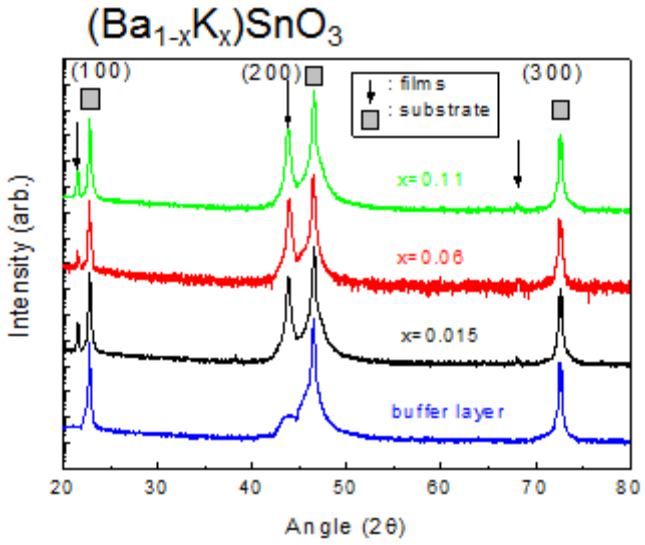

Figure 3.4. A θ-2θ scan of various BKSO thin films on STO substrate with BSO buffer layer (BSO/STO) and BSO buffer film.

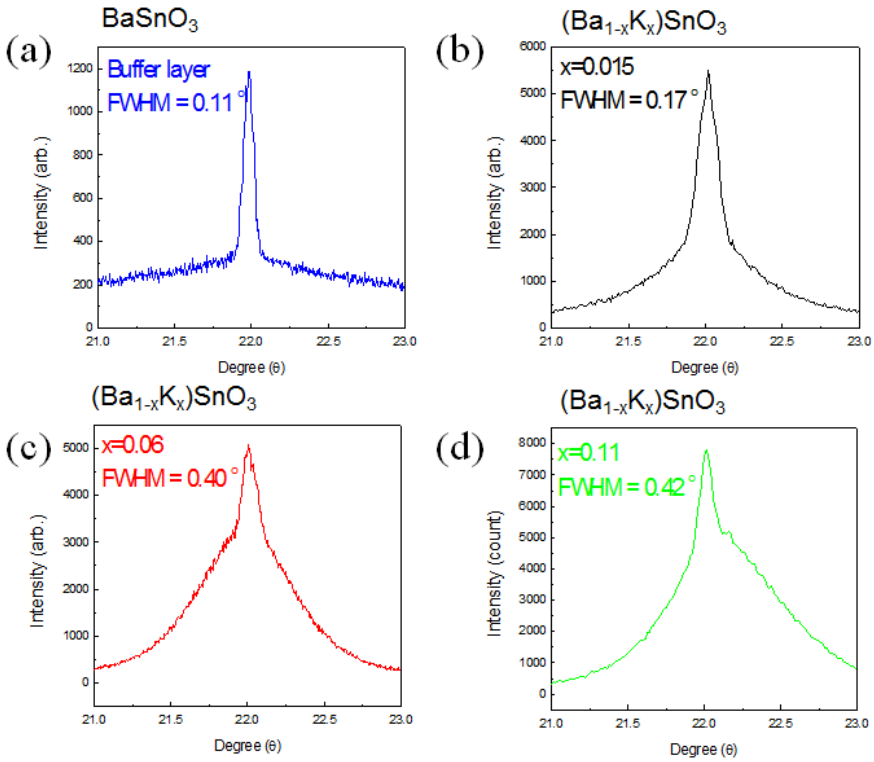

Figure 3.5. A rocking curve for BSO and BKSO (200) peak of various BKSO thin films on STO substrate. (a) BSO buffer film (b) 1.5 % BKSO film (c) 6 % BKSO film (d) 11 % BKSO film.

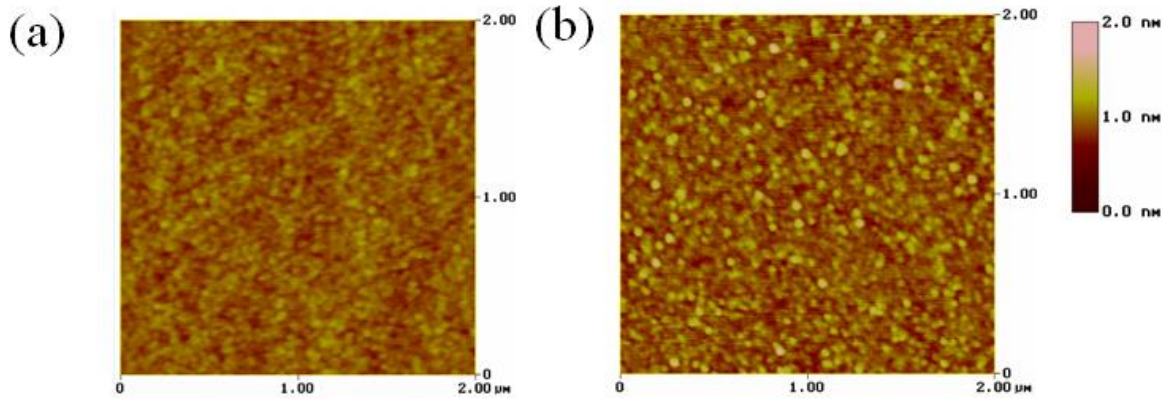

Figure 3.6. (a) AFM image of BLSO thin film on STO with roughness value 0.223 nm (b) AFM image of the 6 % BKSO thin film on BSO/STO with roughness value 0.738 nm.

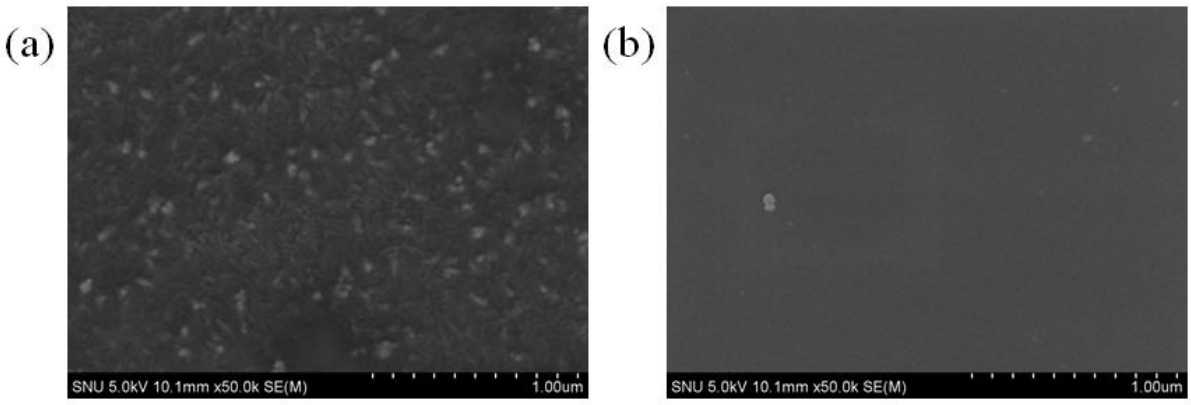

Figure 3.7. (a) SEM image of KSO thin film on STO with many congregations (b) SEM image of the 6 % BKSO thin film on BSO/STO with no K congregation.

3.1.4 High temperature measurement of BKSO thin film

To investigate the electrical properties of BKSO thin film, we execute measurement of the resistance of the 1.5 %, 6 % and 11 % BKSO thin films at high temperature because resistance was too high to measure at room temperature. We used for measuring resistances by the voltage-driven 2-probe method which is able to detect much higher resistance. Because of very high resistance even at high temperature, we suppose that contact resistance is not significantly affected for high temperature measurement. To evaluate the activation energy of K in BKSO thin film, we plot the graph for resistance versus reciprocal temperature [5-9], as shown in Figure 3.8. As you can see, resistance is almost exponentially decayed for rising temperature. We calculate the activation energy for the low temperature region by extrapolation method denoted by dash line, because the resistance is too high to measure at low temperature and low temperature region is important for pn junction operation. We estimate the activation energy which value is 0.49 eV using the conventional Arrhenius formula [10]. From this activation energy, we obtained the carrier concentration of holes in this 6 % and 11 % BKSO thin film to be about 5.67×10^{12} and 1.03×10^{13} /cm^3 at room temperature, assuming a full activation of intrinsic K doping concentration at given activation energy. The corresponding mobility from the measured conductivity is about 0.0556 and 0.303 cm^2/V·s for 6 % and 11 % BKSO films at room temperature. The lower mobility for the lowest doping indicates that charge trapping mechanism is enhanced by grain boundaries/dislocations [4, 11].

To confirm that the BKSO thin films are indeed p-type, we measured changing resistance by switching the background atmosphere from O_2 to Ar and O_2 again at 750 ^{o}C in a tube furnace system. In oxide thin film, the oxygen

vacancies are existed which regarded as act for n-type carrier. In general, oxygen vacancies are reduced at O_2 and induced at Ar background, especially at very high temperature. Therefore, we determine the carrier type by observing the change of resistances when changing the background gas. As shown in Figure 3.9, the all resistances of BKSO films increased when the background gas atmosphere was changed from O_2 to Ar. This finding indicates that the BKSO thin film is indeed a p-type doped semiconductor. The resistance ratios between O_2 and Ar gas of 1.5 %, 6 %, 11 % BKSO thin films are 7.6, 9.6 and 11.7, respectively. It means that the amounts of K are clearly affected to the resistance ratios, indicating that K in BKSO thin film acts as p-type dopants. When the background gas atmosphere was switched back to the oxygen, the resistance abruptly switched to the original value in the oxygen atmosphere although the resistance increase in Ar atmosphere was rather gradual. This sudden change of resistance might be originated from the oxygen ions trapping at the surface by forming a kind of dangling bonds Ar background atmosphere because of the strong oxygen bonding of at BKSO thin films.

3.1.5 Summary

We deposited an epitaxial K-doped BSO thin film on BSO buffer layer and confirmed its crystallinity and K incorporation by X-ray diffraction and ESCA. Although BKSO exhibited rather high resistivity at room temperature, its conductivity increased dramatically at high temperature, yielding high activation energy of 0.49 eV. The conductivity decreased when a small amount of oxygen was removed from the films consistent with the behavior of p-type doped oxides in contrast to that of n-type BLSO. We need to increase the p-doping level for better performance by finding a more suitable dopant.

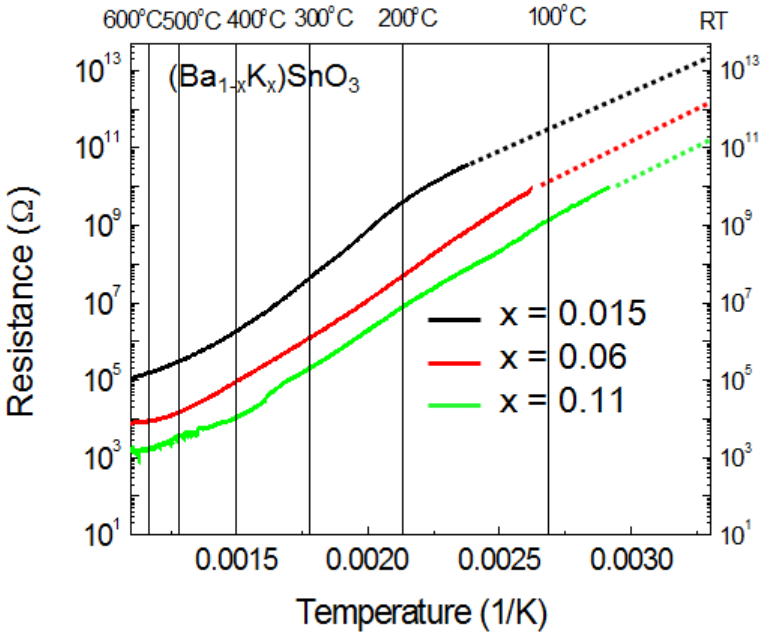

Figure 3.8. High temperature measurement result for BKSO thin films. The graph indicates that resistance versus inverse temperature graph of the BKSO thin films. Each line is two probe measurement results and each dash line is estimation line for extrapolation.

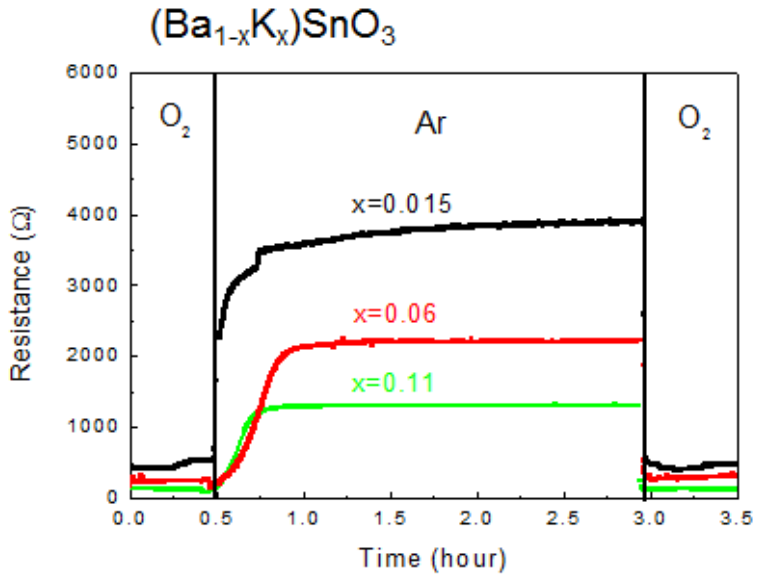

Figure 3.9. High temperature measurement result for BKSO thin films by resistance versus time graph of the BKSO thin films for changing background atmosphere.

3.2 Other p-type doping BSO thin film

3.2.1 Ga-doped BSO (BSGO) thin film

Gallium was used as conventional p-type carrier dopant for ZnO [12] and coping technique with N for ZnO [13, 14]. We deposited 100 nm think BSGO thin film (deposited at 700 ^{o}C) on the STO (001) substrate using BSO and Ga_2O_3 targets by pulsed laser deposition system using sequential deposition method. For proof of the epitaxiality of the BSGO thin film, we obtained the structural information of BSGO thin film by the X-ray diffraction method, represented in Figure 3.10. The θ-2θ scan confirms that the film was deposited epitaxially along the direction of STO substrate. The values of FWHM of the ω-scan, as indicated at Figure 3.10 (b), at the BSGO (002) peak position is 1.38 ^{o} which indicate relatively bad crystalline orientation mainly due to the absence of the BSO buffer layer. To investigate the electrical properties of BSGO thin film, we execute measurement of the resistance BSGO thin films at high temperature using 4 probe methods. We estimate the activation energy which value is 0.81 eV using the conventional Arrhenius formula using reciprocal temperature vs. resistance graph as indicated in Figure 3.11 (a). Also, to confirm that the BSGO thin films are indeed p-type, we measured changing resistance by switching the background atmosphere from O_2 to Ar and O_2 again at 700 ^{o}C in a tube furnace system. The resistance ratios of BSGO thin films between O_2 and Ar gas is 4.33 as shown at Figure 3.11 (b). In conclusion, the activation energy of Ga in BSGO thin film is too high, we regarded that Ga is not suitable dopant for p-type of BSO thin film.

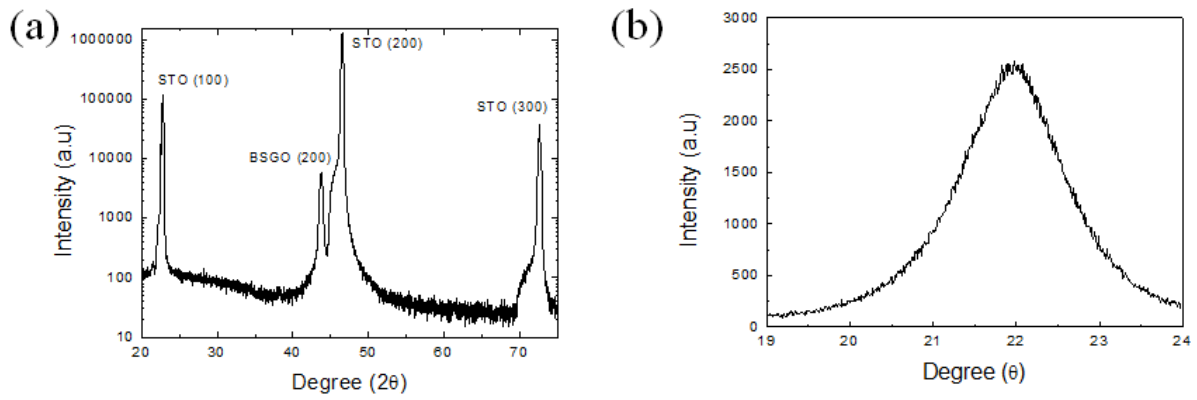

Figure 3.10. (a) A θ-2θ scan of BSGO thin films on STO substrate without BSO buffer layer. (b) A rocking curve for BSO and BSGO (200) peak which FWHM is 1.38^{o}.

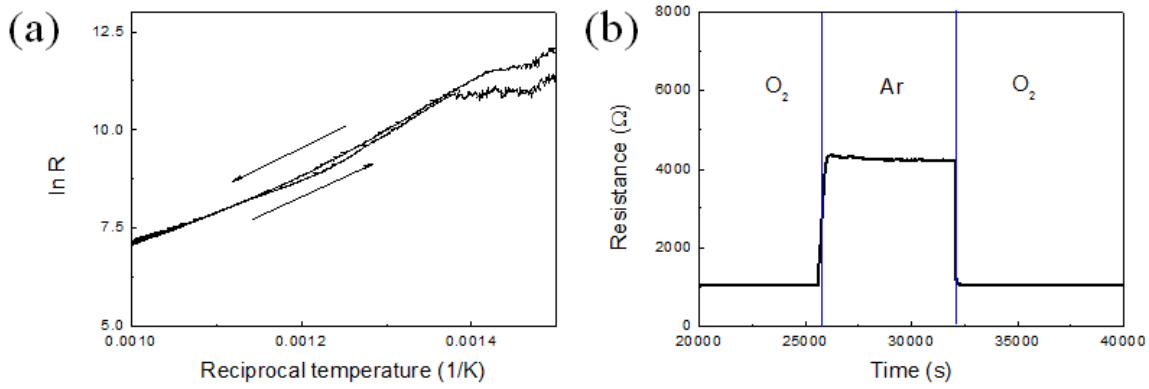

Figure 3.11. High temperature measurement result for BSGO thin films. (a) Resistance versus inverse temperature graph of the BSGO thin films. (b) Resistance versus time graph of the BKSO thin films for changing background atmosphere.

3.2.2 Cu-doped BSO (BSCO) thin film

Cu have great attention when Cu^{+} bearing oxide show p-type in TCO regime such as $CuGaO_2$ [15] and $SrCu_2O_2$ [16]. We deposited 100 nm think BSCO thin film (deposited at 700 ^{o}C) on the STO (001) substrate using BSO and CuO targets by pulsed laser deposition system using sequential deposition method, almost same as BKSO and BSGO case. For proof of the epitaxiality of the BSCO thin film. We obtained the structural information of BSGO thin film by the X-ray diffraction method, represented in Figure 3.12. The θ-2θ scan confirms that the film only have epitaxial phase along the direction of STO substrate. The values of FWHM of the rocking scan, as indicated in Figure 3.12 (b), at the BSCO (002) peak position is 0.18 ^{o} which shows that BSCO film has highly crystalline and well oriented structure. To investigate the electrical properties of BSCO thin film, we executed measurement of the resistance BSCO thin films at high temperature using 4 probe methods. We estimate the activation energy which value is 0.64 eV using the conventional Arrhenius formula using reciprocal temperature vs. resistance graph as indicated in Figure 3.13. Also, to confirm that the BSCO thin films are indeed p-type, we measured changing resistance by switching the background atmosphere from O_2 to Ar and O_2 again at 700 ^{o}C in a tube furnace system. The resistance ratios of BSCO thin films between O_2 and Ar gas is 8.60 as shown at Figure 3.13 (b). The reason that activation energy of Cu is too high is that Cu ion doped as 2^{+} ions, not 1^{+} ion, as we confirmed by the XPS result.

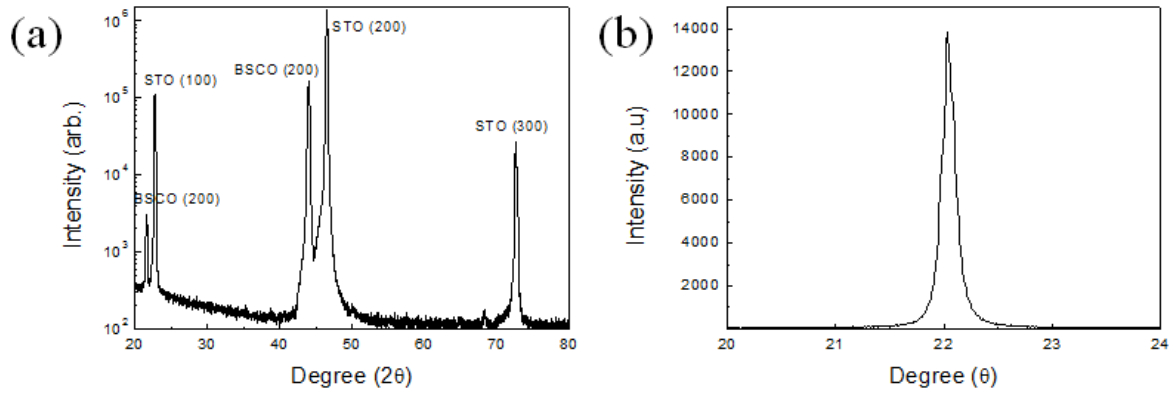

Figure 3.12. (a) A θ-2θ scan of BSCO thin films on STO substrate on BSO buffer layer. (b) A rocking curve for BSO and BSCO (200) peak which FWHM is 0.18°.

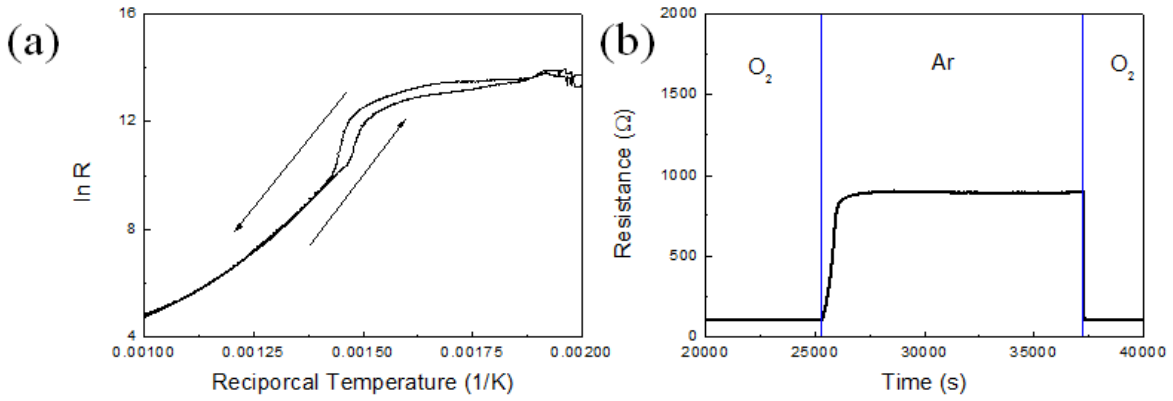

Figure 3.13. High temperature measurement result for BSCO thin films. (a) Resistance versus inverse temperature graph of the BSCO thin films. (b) Resistance versus time graph of the BSCO thin films for changing background atmosphere.

Reference

[1] L. Mieville, T. H. Gaballe, L. Antagnazza, and K. Char, Appl. Phys. Lett. **70**, 126 (1997).

[2] D. R. Chen, Journal of Electron Spectroscopy and Related Phenomena **9**, 29 (1976).

[3] J. H. Scofield, Lawerence Livermore Laboratory, Report No. UCRL-51326 (1973).

[4] H. J Kim, U. Kim, H. M. Kim, T. H. Kim, H. Mun, B. G. Jeon, K. T. Hong, W. J. Lee, C. Ju, K. H. Kim & Kookrin Char, Appl. Phys. Exp. **5**, 061102 (2012).

[5] O. Lopatiuk-Tirpak, W. V. Schoenfeld, L. Chernyak, F. X. Xiu, J. L. Liu, S. Jang, F. Ren, S. J. Pearton, A. Osinsky & P. Chow, Appl. Phys. Lett. **88**, 202110 (2006).

[6] Y. Pei, A. D. LaLonde, H. Wang & G. Jeffrey Snyder, Energy Environ Sci. **5**, 7963 (2012).

[7] P. Huang & A. Petric J. Electrochem. Soc. **143**, 1644 (1996).

[8] V. Thangadurai &W. Weppner, J. Electrochem. Soc. **148**, 1294 (2001).

[9] H. He, X. Huang & L. Chen, Electrochimica Acta **46**, 2871 (2001).

[10] D. B. Rogers, J. M. Honig & J. B. Goodenough, Mat. Res. Bull. **2**, 223 (1967).

[11] H. Mun, U. Kim, H. M. Kim, C. Park, T. H. Kim, K. H. Kim & K. Char, Appl. Phys. Lett. **102,** 252105 (2013).

[12] M. Joseph, H. Tabata& T. Kawai Jpn. J. Appl. Phys. **38**, 1205 (1999).

[13] Y. Yan & S. B. Zhang, Phys. Rev. Lett. **86**, 5723 (2001).

[14] M Joseph, H. Tabata, H. Saeki, K. Ueda & T. Kawai Physica B **302**, 140 (2001).

[15] K. Ueda, T. Hase, H. Yanagi, H. Kawazoe, H. Hosono, H. Ohta, M. Orita & M. Hirano, J. Appl. Phys. **89**, 1790 (1999).

[16] A. Kudo, H. Yanagi, H. Hosono & H. Kawazoe., Appl. Phys. Lett. **73**, 220 (1998).

4. pn junction fabricated with BLSO and BKSO

4.1 Theory

In semiconductor, the Fermi level E_F is near the valence band edge in the p-type material and near the conduction band edge in the n-type material. When the p- and n-type semiconductors are jointed together, the large carrier concentration gradients at the junction due to carrier diffusion; Holes from the p-side diffuse into the n-side, and electrons from the n-side diffuse into the p-side [1]. Diffusion will continue until basic criterion for thermal equilibrium is attained, i.e. the Fermi energy is constant throughout the system. During this process, the uncompensated charged ions are referred as space charge and the region in which they are located is the depletion region [2]. The voltage drops across the junction under equilibrium conditions and the appearance of charge near the metallurgical boundary. This voltage drop across the depletion region under equilibrium conditions is known as built-in potential [3]. The most important characteristic of pn junction is that they have rectifying behavior [1]. The current increases rapidly as the voltage increases, when we apply forward bias (positively voltage on the p-side). However, there are virtually no current flows when we apply a reverse bias.

4.1.1 Electrostatic analysis of pn junction

We assumed an abrupt junction the concentration of doping atoms changes discontinuously from a uniform value N_A on the p-side to another uniform value N_D on the n-side [3]. In thermal equilibrium condition, we will show that how to use the Poisson equation and current density equations to calculate the built-in electric, the potential and the width of the depletion layer. We assumed abrupt

pn junction which charge densities are abruptly changed. And there are the space charge regions adjacent to the junction interface only uncompensated donor and acceptor ions existed. The space charge region is a so-called depletion layer.

From the fact that charge density passing through pn junction is zero, the charge density of p side is

$$j_p = q\mu_p \left(pE - \frac{kT}{q}\frac{\partial p}{\partial x} \right) = 0 \qquad (4.1)$$

From equation (4.1), we find electric field

$$E_x = \frac{kT}{q}\frac{1}{p}\frac{\partial p}{\partial x} = -\frac{\partial \varphi}{\partial x} \qquad (4.2)$$

φ is the electrostatic potential. Because the intrinsic charge density$n_i = \sqrt{n_p N_D} = \sqrt{N_A p_n}$ and equation (4.2), we know the relation of the built-in potential in the junction

$$V_b = \frac{E_q}{q} + \frac{kT}{q}\ln\left[\frac{N_A N_D}{n_i^2}\right] \qquad (4.3)$$

If we only consider 1 dimensional junction, we find the charge density at depletion region by depletion approximation at junction interface,

$$\begin{aligned} \rho\,(x) &= -qN_A \left(-x_p \le x \le 0\right) \\ &= qN_D \ (0 \le x \le x_n) \qquad (4.4) \\ &= 0 \ (x \le x_p \ and \ x \ge x_n) \end{aligned}$$

Because the distribution of charges formed the step junction under equilibrium condition from (4.4) , the continuity of the electric field is found to

require [2]

$$N_A x_p = N_D x_n \qquad (4.5)$$

Put equation (4.4) to Poisson equation we get the formula

$$\frac{d^2\varphi}{dx^2} = qN_A/(\varepsilon\varepsilon_0)\ (-x_p \le x \le 0)$$

$$= -\mathrm{q}N_D/(\varepsilon\varepsilon_0)\ (0 \le x \le x_n \qquad (4.6)$$

$$= 0\ (x \le x_p\ and\ x \ge x_n)$$

Hence the electric field of the depletion region is

$$\mathrm{E(x)} = -\frac{qN_A}{\varepsilon\varepsilon_0}(x_p + x)\ (-x_p \le x \le 0) \qquad (4.7)$$

$$= -\frac{qN_D}{\varepsilon\varepsilon_0}(x_n - x)\ (0 \le x \le x_n)$$

Also, the electrostatic potential is obtained from the equation (4.6),

$$\varphi(\mathrm{x}) = \frac{qN_A}{2\varepsilon\varepsilon_0}(x_p + x)^2\ (-x_p \le x \le 0) \quad (4.8)$$

$$= V_b - \frac{qN_D}{2\varepsilon\varepsilon_0}(x_n - x)^2\ (0 \le x \le x_n)$$

The results of the electric field and electrostatic potential as a function of position for an abrupt p-n junction (equation (4.4) to (4.8)) are shown in Figure. 4.1.

Lastly, Solving about x_p and x_n combining equation (4.7)

$$x_n = \left[\frac{2K_s\varepsilon_o}{q}\frac{N_A}{N_D(N_A+N_D)}V_{bi}\right]^{1/2} \qquad (4.9)$$

$$x_p = \left[\frac{2K_s\varepsilon_o}{q}\frac{N_D}{N_A(N_A+N_D)}V_{bi}\right]^{1/2} \quad (4.10)$$

And the total width of the depletion region is $W \equiv x_p + x_n = W_p + W_n$.

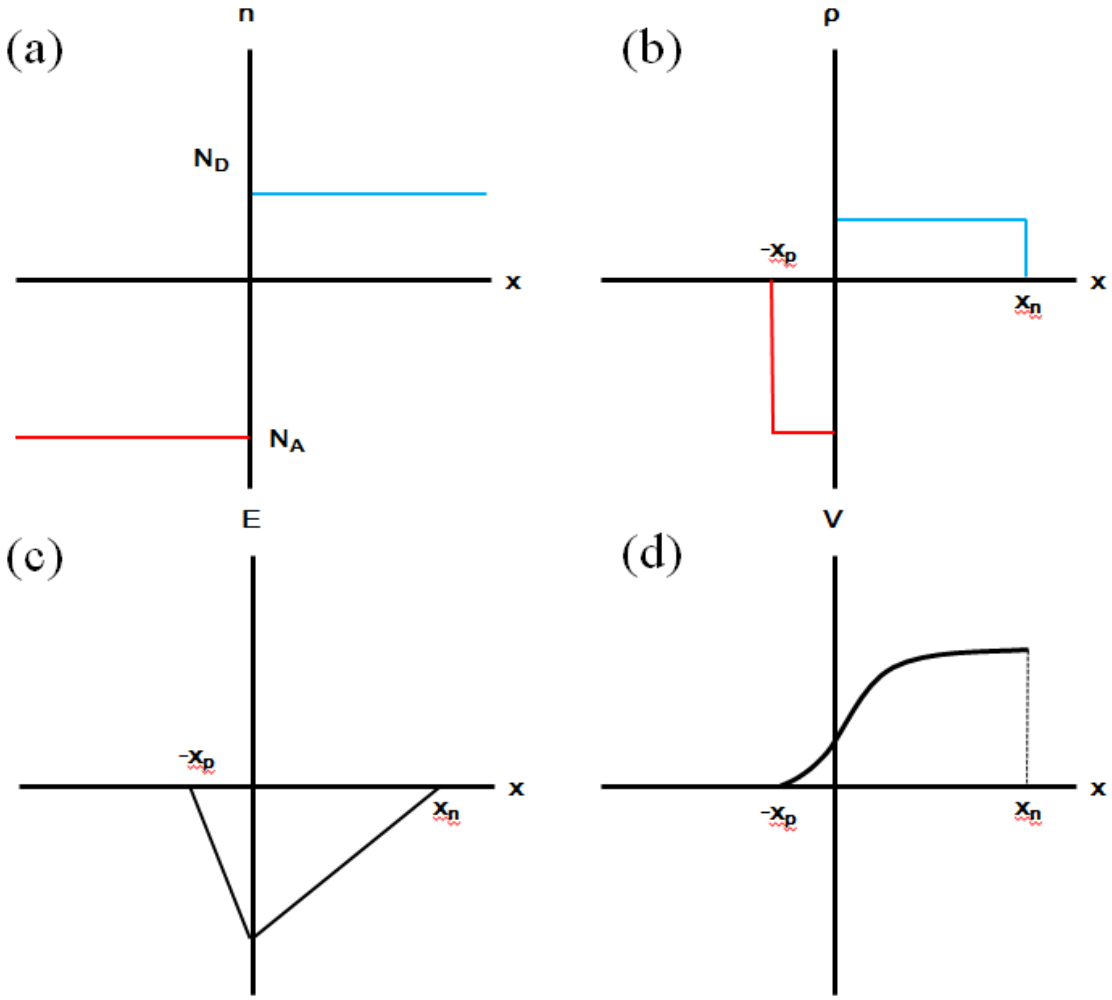

Figure 4.1. Depletion approximation based qualitative solution for the electrostatic variables in a pn step junction under equilibrium conditions. (a) Step junction profile (b) charge density (c) electric field and (d) electrostatic potential as a function of position.

4.1.2 The ideal I-V characteristics

We use the subscript n and p to denote the semiconductor type and the subscript o to specify the condition of thermal equilibrium. Using built-in potential and the mass action low $p_{p0}n_{n0} = n_i^2$, we obtain the electron density at the boundary of the depletion region [1]:

$$n_p - n_{p0} = n_{p0}\left[\exp\left(\frac{qV}{kT}\right) - 1\right] \quad (4.11)$$

$$p_n - p_{n0} = p_{n0}\left[\exp\left(\frac{qV}{kT}\right) - 1\right] \quad (4.12)$$

Since the neutral region is small, there is no reason for any substantial minority carrier drift current to flow. Therefore, the current is originated due almost entirely to diffusion [4]. From (4.11) and (4.12) the current density of each side is as below:

$$J_p = -qD_p[p_n - p_{n0}]/L_p \quad (4.13)$$

$$J_n = -qD_n[n_p - n_{p0}]/L_n \quad (4.14)$$

The D means that the diffusion constant and L is the diffusion length which is equal to$\sqrt{D\tau}$. Therefore, the ideal current through pn junction at forward bias is described by following equations:

$$\mathrm{I} = I_0\left[\exp\left(\frac{qV}{kT}\right) - 1\right] \quad (4.15)$$

$$I_0 = \frac{qAD_p p_{n0}}{L_p} + \frac{qAD_n n_{p0}}{L_n} \quad (4.16)$$

The barrier thus produced can be modulated by and applied voltage, thereby causing the currents through the junction to be modulated [3].

4.1.3 The asymmetry pn junction

We called the asymmetry pn junction when the one side is doped much heavily than the other side [4]. In the asymmetry pn junction, the depletion layer thickness and the potential on the heavily doped side is neglected in calculation. For example, for the n^+-p junction, $I = I_0[\exp(qV/kT) - 1]$ with $I_0 = qAD_n n_{p0}/L_n$. In the highly asymmetrical junction, carriers coming from the highly doped region create a layer of mobile charge in the depletion region of the less-doped zone [5]. Since acceptor doping is much lower than donor doping, electrons are not neglected in the n-region or in the p-region without imposing the depletion approximation [5], may not obeying conventional ideal pn junction formula.

For asymmetrical abrupt p-n junctions, due to accumulation of free carriers there is an inversion layer at the junction interface close to the lowly doped side. To solve the problem, the free carrier, p and n, must be taken into account during calculations. In a case of n^+-p junction, a larger number of electrons will be accumulated at the p-side of the junction to form an n-type inversion layer. Such a charge accumulation is able to change the value of the built-in voltage and width of the depletion region.

4.2 Fabrication of pn junction

We fabricate the BKSO/BLSO pn junction which consists of 1 % BLSO for the n-type and 6 % or 11 % BKSO for the p-type. Firstly, 4 % BLSO layer was deposited on the STO (100) substrate which has highly conductive and sustains good epitaxiality. The resistivity of 4 % BLSO layer is about 0.2 mΩ·cm, the resistance through this conducting layer is less than 100 Ω including contact resistances. Then we deposited 1 % BLSO film with 100 nm thickness using Si stencil mask. The resistivity, mobility and carrier concentration of 1 % BLSO film which is used for n-type were 0.0274 Ω·cm, 23.4 $cm^2/V \cdot s$ and 9.76×10^{19} $/cm^3$, respectively. As discussed in Chapter 2, n-type films which have less carrier concentration is able to deposit due to the effect of threading dislocation [7, 8]. And BKSO film was deposited at 0.7×0.7 mm^2 patterned cell by using another Si stencil mask. The picture of the cell is shown in Figure 4.2 (a). We deposit BKSO thin films with changing parameters such as film thickness (100 nm, 500 nm) and concentration of dopant (6 %, 11 %). And then, about 2 nm thick metallic $SrRuO_3$ (SRO) layer was deposited on BKSO film to improve the contact between junction and probe. We used SRO as p-type contact because its work function is larger than 5 eV [8]. The whole schematic of pn junction structure is illustrated at Figure 4.2 (b).

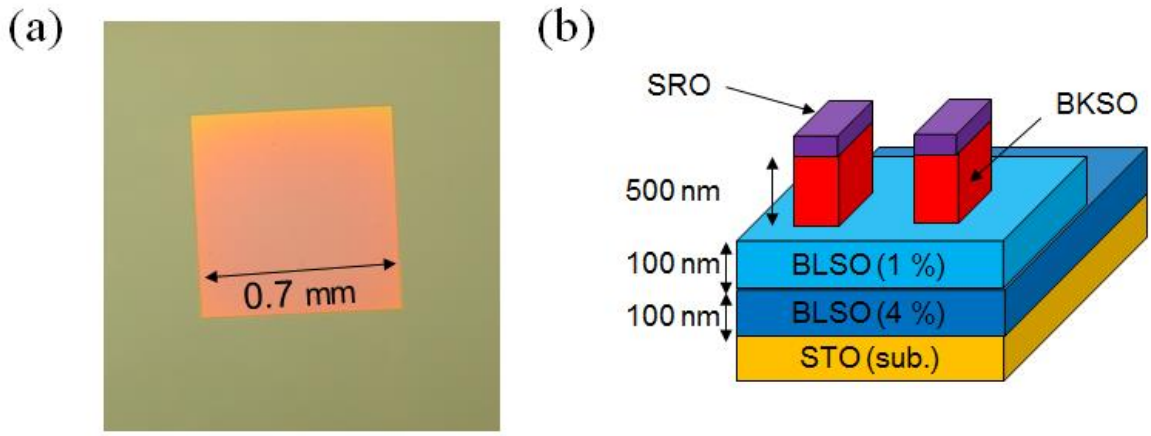

Figure 4.2. (a) The picture of cell for pn junction fabricated by using stencil mask. The area of the cell is 0.7 × 0.7 mm^2 (b) Schematics of the BKSO/BLSO pn junction. Each pn junction contains 2 cells.

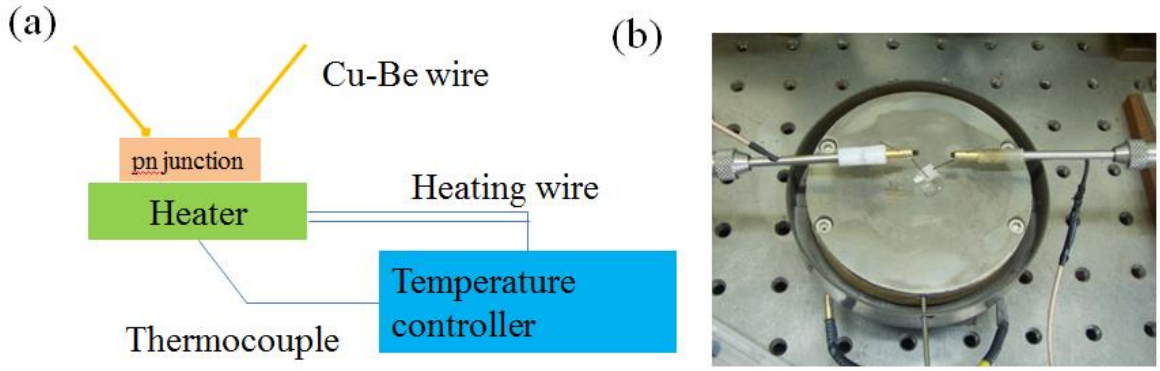

Figure 4.3. (a) The schematics of pn junction measurement system with temperature variation and (b) The picture of the pn junction measurement system.

We measure the I-V characteristics of pn junction considering the temperature change. For temperature variation measurement, we set up the temperature control system consisting of heater, thermocouple and control system. A diameter of heater is 3 inch and there exist a heating element which flow the current from the control system to raise temperature below the heating plate. The heater temperature is measured by thermocouple which put in the heating plate transferred to the control system which enable to negative feedback at a fixed temperature. Figure 4.3 (a) describe this schematics and Figure 4.3 (b) shows the picture of the heater and wire. Also, to improve contact and enlarge contact area, we use resilient 0.5 mm diameter Cu-Be wire as probe tips.

4.3 I-V characteristics of pn junction

4.3.1 The confirmation of ohmic contact

Firstly, the contact properties between the electrode and thin film and between thin films were investigated. The contact of the pn junction is very important because its rectifying behavior may originate from the Schottky-like contact between semiconductor and metal. The contact between 4 % BLSO layer and Cu-Be probe is definitely ohmic contact which resistance value is about 100 Ω because 4 % BLSO layer is degenerate semiconductor [6, 7]. Also, SRO is p-type metal [9] and 4 % BLSO and 1 % BLSO is originated from same material, between SRO-probe and 4 % BLSO-1 % BLSO is naturally ohmic contact. Therefore the most important thing to consider is the existence of the Schottky barrier at interface between SRO as p-type electrode and BKSO which carrier concentration is very low as p-type materials when we consider the contact in device.

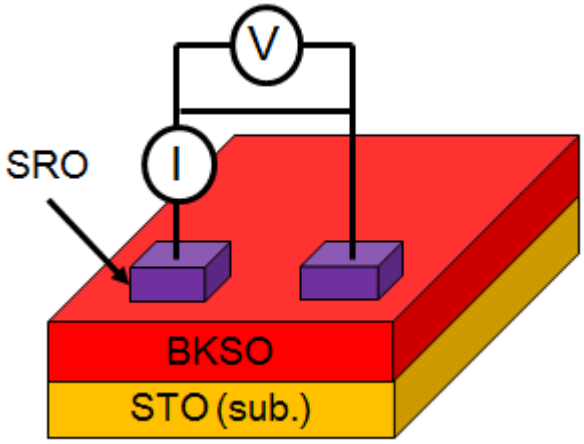

Figure 4.4. Schematics of SRO/BKSO/SRO planar junction for contact confirmation.

We confirm ohmic contact by measuring I-V characteristics of SRO/BKSO/SRO junction system at high temperature because its resistance is too high to measure at room temperature. Its schematic can be seen from Figure 4.4. I-V results in various temperatures indicated at Figure 4.5. In room temperature, the current is very low due to high resistance of BKSO thin film, shown in Figure 4.5 (a). At 100 ^{o}C measurement, the linear plot is slightly seen among the fluctuating noise because current is still very small (indicated in Figure 4.5 (b)). At 200 ^{o}C and 300 ^{o}C measurement, the contact between BKSO and SRO is definitely ohmic and their resistance is about 50 MΩ and 1 MΩ, respectively, which is quite agree with resistance of BKSO thin film discussed

at Chapter 3. We measured at 300 ^{o}C which is highest temperature for investigating junction property because the effect of the contact resistance is more dominant as temperature is increased cause of lowering the resistance of BKSO.

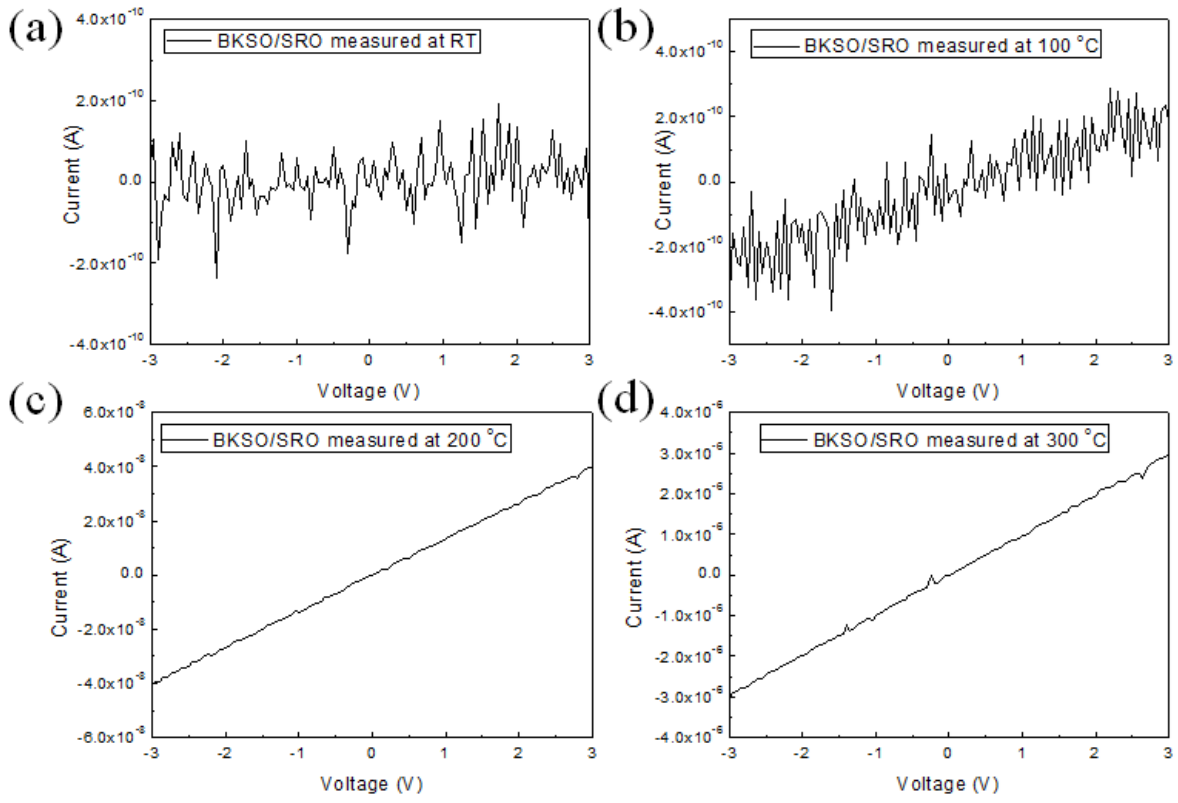

Figure 4.5. I-V characteristics of SRO /BKSO /SRO planar junction at (a) room temperature (b) 100 ^{o}C (c) 200 ^{o}C (d) 300 ^{o}C

4.3.2 I-V characteristics of pn junctions

We fabricated three kinds of pn junction with variation of thickness and carrier concentration in BKSO thin film. pn junction A composed of 11 % BKSO thin film with 500 nm thickness; pn junction B composed of 6 % BKSO thin film with 500 nm thickness; pn junction C composed of 6 % BKSO thin film with 100 nm thickness. We made those three kinds of junctions for investigating of the effect of thickness and carrier concentration of p-side. Though our pn junction is highly asymmetric and carrier concentration of n-side is very high, the n-side condition is same for all three junctions. We generally applied voltage from +3 V to -3 V. For forward bias, we sweep the voltage from 0 V to +3 V, and sweep the voltage from 0 V to -3 V for reverse bias.

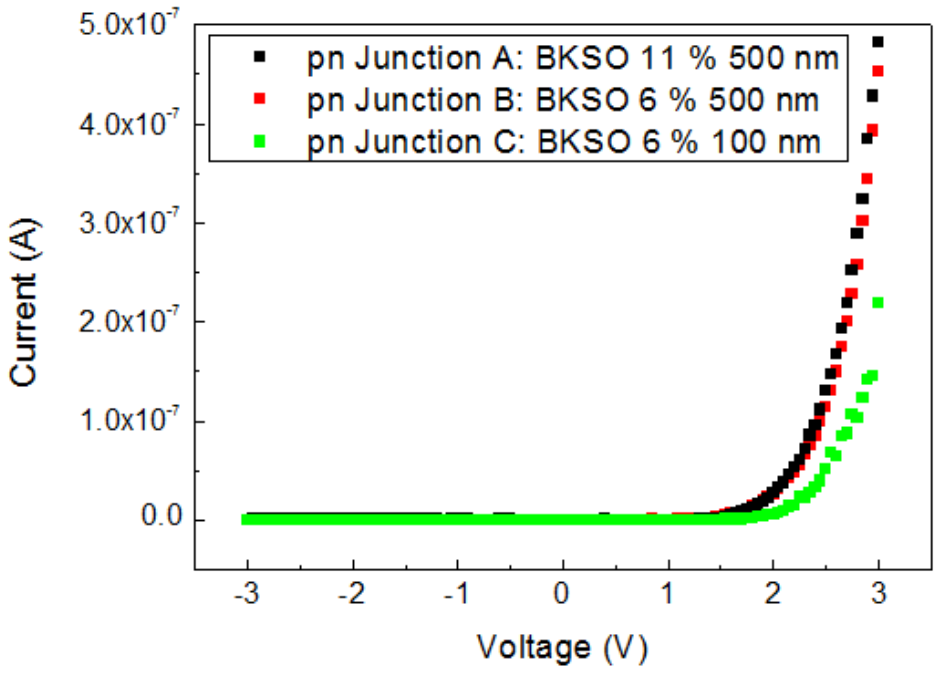

Figure 4.6. I-V characteristics of pn junction at room temperature. Junction A consists of BKSO 11 % with 500 nm; junction B consists of BKSO 6 % 500 nm; junction C consists of BKSO 6 % 100 nm for p-type. For n-type, all junction use BLSO 1 % with 100 nm thickness.

I-V characteristics for both junctions measured at room temperature are shown in Figure 4.6. Non-linear behavior is clearly observed at both junctions though current through junction is very low at room temperature. It means that these rectifying I-V characteristic in our pn junction demonstrates the diode-like behavior that is originating from the BLSO/BKSO interface. The rectification ratios (ratio between forward and reverse currents) are about 154.9, 126.8 and 46.1 at a bias of 2.0 V and 194.7, 158.7 and 101.8 at a bias of 3.0 V for junction A, B and C respectively. As you seen in Figure 4.6., the current is starting to rise after about 1 V at forward bias region for both junctions. It can be indicated that the intrinsic barrier potential is existed at pn junction because of no neutral region by high carrier asymmetry. As we will discussion below, the width of depletion region is much larger than thickness of junction itself, the current is not responded as raising voltage bias as junction seems like intrinsically charged. At reverse bias region, the current level is only 10^{-10} A order which is very low current level at room temperature and sustains even at high negative voltage region.

Although rectifying behavior is clearly observed at our pn junctions, current through junction is very low at room temperature. Because our pn junction is highly asymmetric between n-type and p-type carrier (about 10^6 ~ 10^7 order magnitude difference), the width of depletion region of p-side is larger than thickness of the p-side itself even though we use 11 % BKSO thin film. From the carrier densities of 1 % BLSO thin film for n-type and 6 % (and 11 %) BKSO thin film for p-type, we can calculate the width of depletion region of the pn junction using equation (4.9) and (4.10) with material parameters. The width of depletion region of pn junctions are even 25.1 μm for junction A and 18.5 μm for junction B (and C) at room temperature. Depletion width in the p-type

region is much larger than that of that of the n-type because the pn junction depletes further in the more lightly doped region. It means that the width of depletion region of n-type is almost negligible compared with that of p-type. In conclusion, all pn junctions show almost similar I-V characteristics in room temperature results. Moreover, we have difficulty with analyzing the experimental result with conventional pn junction formula though the rectifying behaviors of pn junctions observed.

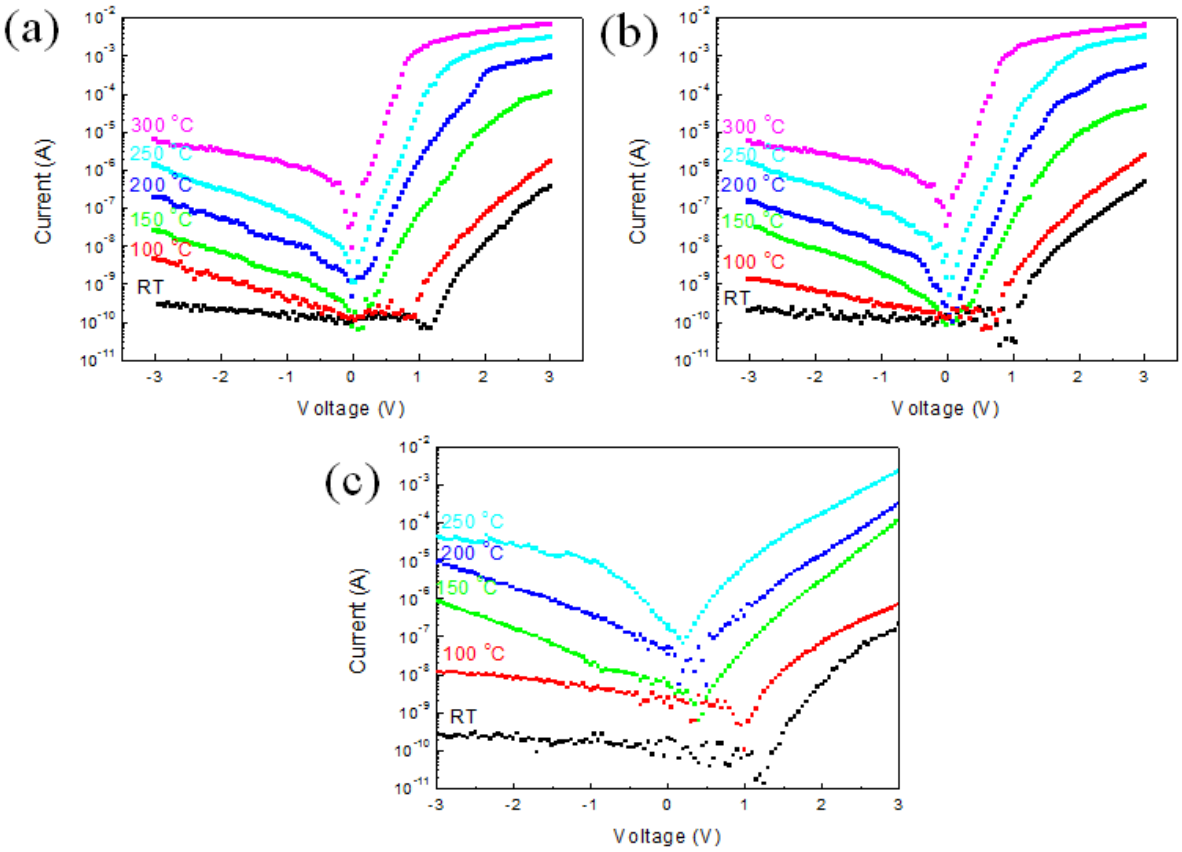

Figure 4.7. I-V characteristics of pn junction at various temperatures (a) for Junction A (b) for junction B consists (c) junction C.

Therefore, we measure the I-V characteristics of pn junctions by raising temperature [10]. We measure I-V characteristics at room temperature, 100 ^{o}C, 150 ^{o}C, 200 ^{o}C, 250 ^{o}C and 300 ^{o}C for junction A and B. We measure I-V characteristics at room temperature, 100 ^{o}C, 150 ^{o}C, 200 ^{o}C, 250 ^{o}C for junction C. Those results are exhibited in Figure 4.7. All measurement results show that non-linear behavior is clearly observed. All junctions show that the slope of the current is steeper for forward bias and the leakage current is increased as increasing temperature. Rectification ratios (ratio between forward and reverse currents) are about 31.1, 24.7 and 2.9 at a bias of 1.0 V in 150 ^{o}C for junction A, B and C respectively. Junction C has small ratio due to large leakage current by relatively thin p-side layer. Those rectification ratios are increased as increasing temperature for junction A and B; however, those values are decreased as increasing temperature for junction C.

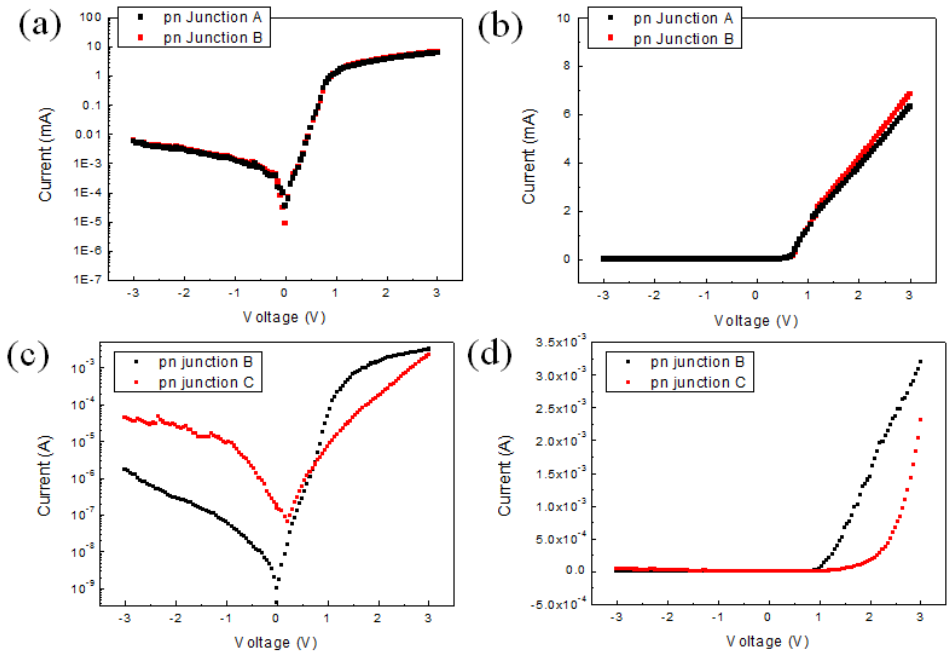

Figure 4.8. Compare I-V characteristics between junction A and B for different carrier concentration measured at 300 ^{o}C. (a) For logarithmic plot. (b) For linear plot. Compare I-V characteristics for different thickness between junction B and C measured at 250 ^{o}C. (c) For logarithmic plot. (d) For linear plot.

In order to precisely investigating the properties of pn junctions measured at high temperature, we classified I-V characteristics of pn junction for same carrier concentration with same thickness (pn junction A and B) and for thickness with same carrier concentration (pn junction B and C). The I-V characteristics of pn junction A and B measured at 300 ^{o}C are indicated in Figure 4.8 (a) for logarithmic plot and (b) for linear plot. Also, the I-V characteristics of pn junction B and C measured at 250 ^{o}C are indicated in Figure 4.8 (c) for logarithmic plot and (d) for linear plot. The result of I-V at junction A and B are almost same as shown in Figure 4.8 (a). The rectification ratios are about 1.16 x 10^{3} at a bias of 1.0 V which is higher than the values of low temperature region. And the I-V plot looks like linear plot at high forward bias region as exhibited in Figure 4.8 (b). It is originated from that the current is seems limited by series resistance of the devices for both junctions. However, the result of I-V at junction B and C are completely different as shown in Figure 4.8 (c). The rectification ratios are about 2.10 × 10^{3} at a bias of 3.0 V for junction B and 1.96 × 10^{2} at a bias of 3.0 V for junction B; which is about ten times lower than that of junction B. And the I-V result as linear plot is exhibited Figure 4.8 (d). As mentioned above, the I-V plot looks like linear plot at high forward bias region for junction B by limiting series resistance. However, I-V characteristic of junction C is still rectifying behavior at high temperature as shown in Figure 4.8 (d).

These differences are basically derived from the width of the depletion region. The carrier concentration of 6 % BKSO thin film is 1.32 × 10^{16} /cm^{3} at 250 ^{o}C and 3.48 x 10^{16} /cm^{3} at 300 ^{o}C. And for 11 % BKSO thin film, the carrier concentration is 3.03 × 10^{16} /cm^{3} at 250 ^{o}C and 7.81 × 10^{16} /cm^{3} at 300 ^{o}C. In

high temperature, the current is significantly raise by more p-type carrier is activated due to thermal activation. For n-type 1% BLSO thin film, the carrier concentration is almost same by changing temperature because it is degenerate semiconductor. From the equation (4.9) and (4.10), we calculate depletion region at various temperature using above parameters. The width of the depletion region is 6.58×10^{-5} cm at 250 ^{o}C and 4.06×10^{-5} cm at 300 ^{o}C for 6 % BKSO thin film and 4.35×10^{-5} cm at 250 ^{o}C and 2.71×10^{-5} cm at 300 ^{o}C for 11 % BKSO thin film. In conclusion, junction thickness is more significant factor for I-V characteristics of junctions than doping concentration because the depletion region is critical parameter for determining I-V characteristics in case of our pn junctions. These results are basically originated that balance of carrier is not matched between n-type and p-type carrier because of deep energy level of K in BKSO thin film. Therefore, we concluded that these pn junctions can be more useful when the dopant which has lower activation energy than K is found.

4.3.3 High-temperature stability of pn junction

The thermal stability of the device is one of the importance things to consider when device was operated especially at high temperature. We evaluated the thermal stability of our pn junction for thermal cycling which means sequentially measuring I-V characteristics at room temperature, at high temperature (300 ^{o}C) and room temperature again. As shown in Figure 4.9., both junction A and B exhibit excellent thermal stability that the I-V characteristics at room temperature are almost unchanged even after several thermal cycling. The slight change of the forward bias might come from the slight temperature difference of the device itself. It shows that our pn junction is highly stable for changing temperature and implicate that potassium in junction is not volatile even at 300 ^{o}C. Also, the interface of the junction is very unchangeable about temperature variation.

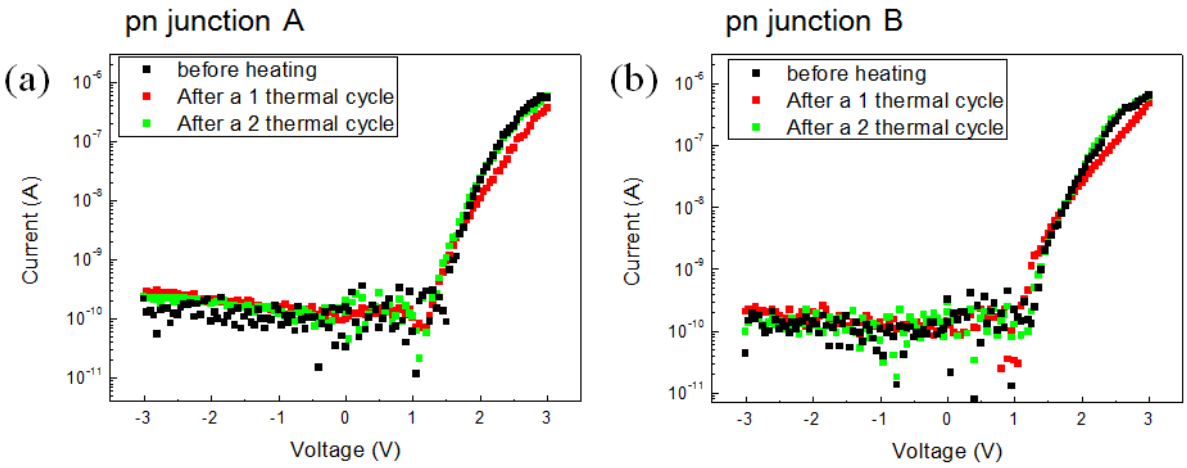

Figure 4.9. The thermal stability measurement of BLSO/BKSO pn junction. The thermal cycling is that I-V characteristics sequentially measured at room temperature, at high temperature (300 ^{o}C) and room temperature again. Repetition of I-V characteristics (a) for Junction A (b) for Junction B.

4.4 Analysis of pn junction

The observed behavior of the BLSO/BKSO pn junction device I-V characteristics is explained with a simple model of pn junction diode with a series resistance R, as shown in Figure 4.10. The measurement at different temperature changes the series resistance and junction parameter in device circuit. The current through junction at temperature T in series resistance R is given by following equation:

$$V = V_t \ln\left[\left(\frac{I}{I_s} + 1\right)\right] + IR \quad (4.17)$$

$$I_s = qAD_n n_{p0}/L_n \quad (4.18)$$

The data can be fitted with fitting variables such as I_s for reverse saturation current, V_t for thermal voltage and R for series resistance values [11-13]. The first part of equation (4.17) is originate from conventional pn junction formula, $I=I_s[\exp(V/V_t)-1]$. In equation (4.18), q is elementary charge, A is the area of junction, D_n is diffusion constant for electron, L_n is the diffusion length and n_{p0} is the electron minority carrier concentration at equilibrium. The hole part for I_s is negligible because the more lightly doped side of the pn junction will produce a larger number of minority carriers and the larger current component [14, 15].

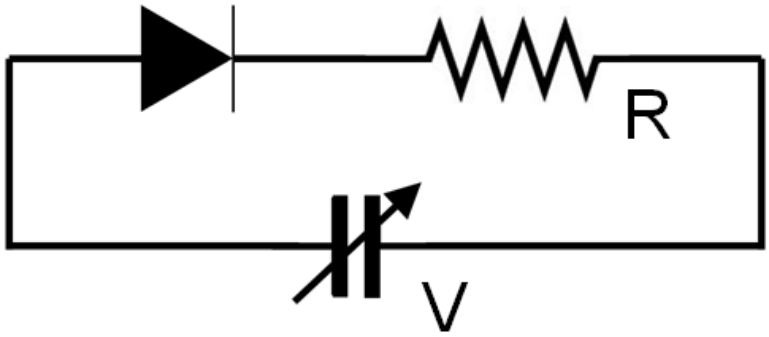

Figure. 4.10. The pn junction with series resistance model. V is the applied voltage and R is series resistance parasitic in junction diode.

The fitting analysis results for junction A are indicated in Figure 4.11 and for junction B are indicated in Figure 4.12. Firstly, we investigated junction parameter by fitting of the pn junction at 150 ^{o}C, 200 ^{o}C, 250 ^{o}C, and 300 ^{o}C. The reverse saturation current of junction A is 2.60 × 10^{-10} A at 150 ^{o}C, 6.64 ×10^{-10} A at 200 ^{o}C, 2.60 × 10^{-9} A at 250 ^{o}C and 2.28 × 10^{-8} A at 300 ^{o}C. From the results of high temperature (above at 250 ^{o}C) for junction A, the barrier height of the pn junction is about 1.16 eV for 250 ^{o}C and 1.19 eV for 300 ^{o}C. And the reverse saturation current of junction A is 8.43 × 10^{-11} A at 150 ^{o}C, 5.72 × 10^{-10} A at 200 ^{o}C, 4.62 × 10^{-9} A at 250 ^{o}C and 2.80 × 10^{-8} A at 300 ^{o}C. For estimation of the minority carrier concentration, the values of n_{p0} for junction A and B are 2.07 × 10^{8} /cm^{3} and 2.27 × 10^{8} /cm^{3} at 250 ^{o}C and 1.10 × 10^{9} /cm^{3} and 8.37 × 10^{8} /cm^{3} at 300 ^{o}C.

And we calculate the thermal voltage V_t from the fitting results. The thermal voltage for junction A is 0.142 V at 150 ^{o}C, 0.122 V at 200 ^{o}C, 0.089 V at 250 ^{o}C and 0.061 V at 300 ^{o}C. From the conventional pn junction formula, thermal voltage V_t is equal to mkT/q where k is Boltzmann constant, T is temperature and q is elementary charge and m is the ideality factor of the junction. Using above result, we can calculate ideality factors which are 3.90 at 150 ^{o}C, 3.02 at

200 ^{o}C, 2.1 at 250 ^{o}C and 1.3 at 300 ^{o}C, each. And, the thermal voltage for junction B is 0.120 V at 150 ^{o}C, 0.090 V at 200 ^{o}C, 0.076 V at 250 ^{o}C and 0.069 V at 300 ^{o}C. Their ideality factors are 3.3 at 150 ^{o}C, 2.2 at 200 ^{o}C, 1.95 at 250 ^{o}C and 1.4 at 300 ^{o}C, respectively. The ideality factor is temperature dependent and decreases consistently with increasing temperature mainly due to generally improving p-type transport with increasing temperature cause of the higher activation of acceptors at elevated temperatures [16]. Also the behavior of junction is more idealistic because the width of depletion region is decreased as increasing temperature.

Furthermore, we can obtain the series resistance values of the device circuit by analyzing the fitting of pn junctions. The series resistance for junction A is 4400 Ω at 150 ^{o}C, 1220 Ω at 200 ^{o}C, 520 Ω at 250 ^{o}C and 325 Ω at 300 ^{o}C. And the series resistance for junction A is 5800 Ω at 150 ^{o}C, 2450 Ω at 200 ^{o}C, 480 Ω at 250 ^{o}C and 350 Ω at 300 ^{o}C. We attribute that p-type transport properties generally improve with increasing temperature because of the higher activation of acceptors at elevated temperatures [16]. As mentioned above, the current through junction is limited by series resistance factor when current level is up to 10^{-3} A order. If tens of mA orders of current can be achieved, it has possibility that BKSO/BLSO homojunction exhibit luminescence behavior at the visible light or near UV region by 3 eV of BSO band gap as demonstrating GaN [17-19] and manganite [20, 21] results. The demonstration of the pn junctions based on a single transparent perovskite semiconductor (TPS) material further enhances the potential of the BSO system.

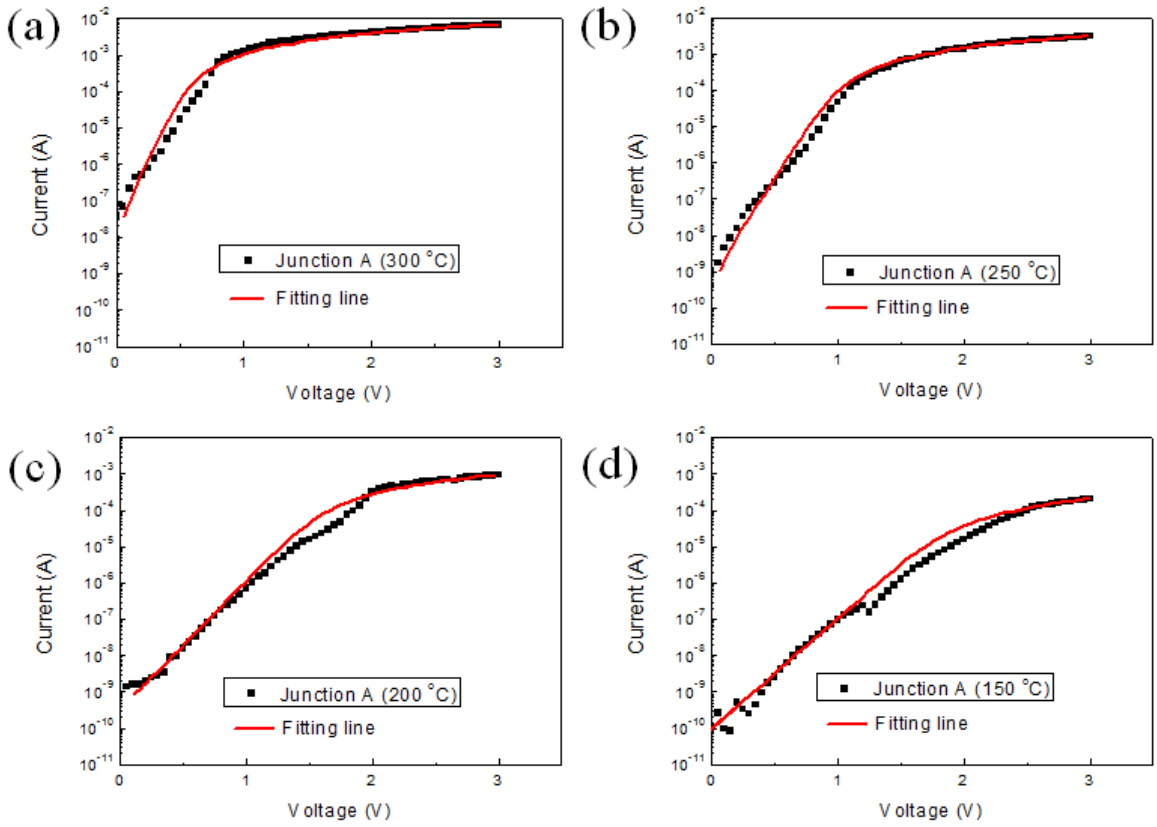

Figure. 4.11. I-V characteristics of the pn junction A with fitting lines using equations by series resistance model. Each graph is measured at (a) 300 ^{o}C (b) 250 ^{o}C (c) 200 ^{o}C (d) 150 ^{o}C.

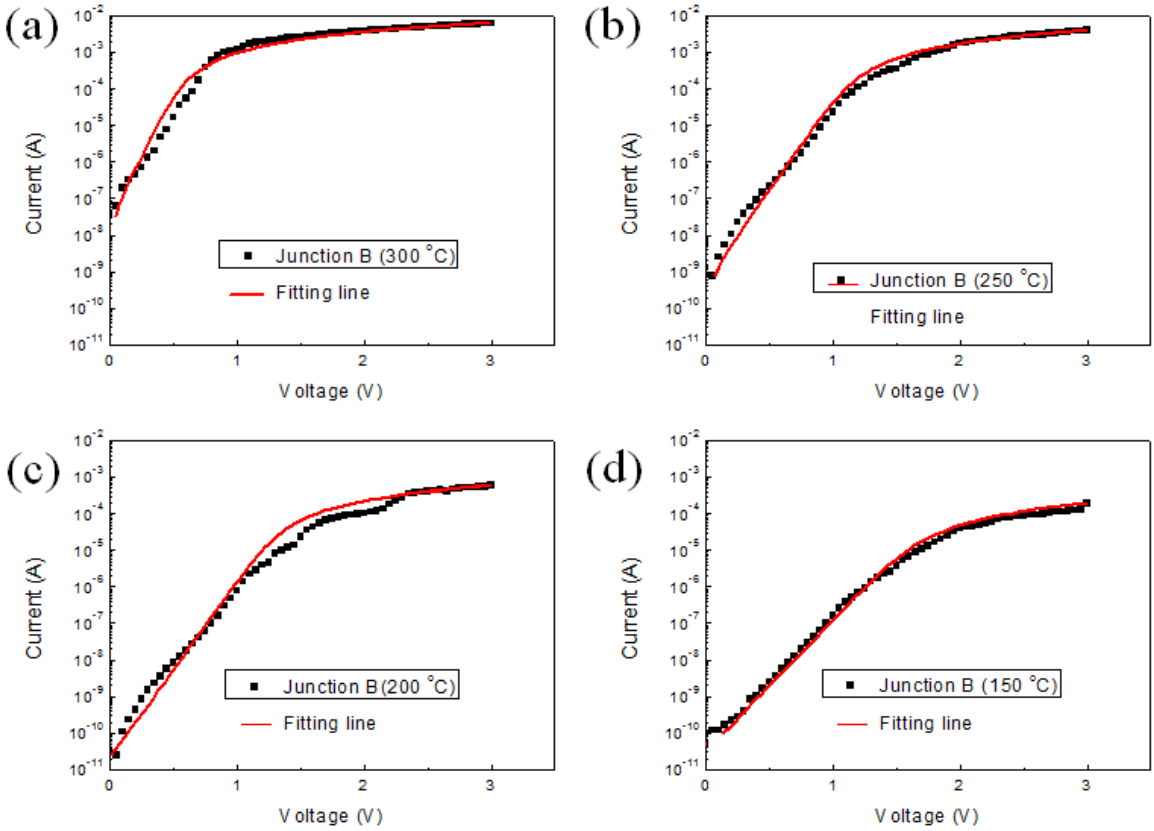

Figure. 4.12. I-V characteristics of the pn junction B with fitting lines using equations by series resistance model. Each graph is measured at (a) 300 ^{o}C (b) 250 ^{o}C (c) 200 ^{o}C (d) 150 ^{o}C.

Reference

[1] S. M. Sze, Semiconductor devices. 2nd Edition (Wiley, 2001), Chapter 4.

[2] M. Balkanski & R. F. Wallis, Semiconductor Physics and Applications. (Oxford, 2000), Chapter 12.

[3] R. F. Pierret, Semiconductor Device Fundamentals. (Addison Wesley, 1996), Chapter 5 and 6.

[4] D. J. Roulston, An introduction to the Physics of Semiconductor Devices. (Oxford, 1999) Chapter 2 and 3.

[5] J. A. J. Tejada, A. Godoy, A. Palma & J. A. L. Villanueva J. Appl. Phys. **92**, 320 (2002).

[6] H. J Kim, U. Kim, H. M. Kim, T. H. Kim, H. Mun, B. G. Jeon, K. T. Hong, W. J. Lee, C. Ju, K. H. Kim & Kookrin Char, Appl. Phys. Exp. **5**, 061102 (2012).

[7] H. Mun, U. Kim, H. M. Kim, C. Park, T. H. Kim, K. H. Kim & K. Char, Appl. Phys. Lett. **102,** 252105 (2013).

[8] M. Tapajna, P. Pisecny, R. Luptak, K. Husekova, K. Frohlich, L. Harmatha, J. C. Hooker, F. Roozeboom, & J. Jergel, Mater. Sci. Semicond. Process. **7**, 271 (2004).

[9] H. M. Christen, L. A. Boatner, J. D. Budai, M. F. Chisholm, L. A. Gea, D. P. Norton, C. Gerber & M. Urbanik Appl. Phys. Lett. **70** ,2147 (1997).

[10] J. Zhang, H. Tanaka and T. Kawai Appl. Phys. Lett. **80**, 4378 (2002).

[11] F. J. G. Sanchez, A. Ortiz-Conde & J. J. Liou, Proc. Circuits Devices

Syst. **143**, 68 (1996).

[12] H. Bayhan & A. S. Kavasoglu, Turk. J. Phys. **31**, 7 (2007).

[13] V. L. Borblik, Y. M. Shwarts, M. M. Shwarts, Semicon. Phys. Quan. Elec. & Optoelec. **12**, 339 (2009).

[14] D. O. Scanlon, Phys. Rev, B **87**, 161201 (2013).

[15] F. J. Garcia Sanchez, A. Ortiz-Conde, J.J Liou, IEE proc. Circuits Devices syst. **143**, 68 (1996).

[16] J. M. Shah, Y.L. Li, T. Gessmann & E. F. Schubert, J. Appl. Phys. **94**, 2627 (2003).

[17] E. S. M. Goh, H. Y. Yang, Z. J. Han, T. P. Chen & K. Ostrikov Appl. Phys. Lett. **101**, 263506 (2012).

[18] S. Nakamura, T. Mukai & M. Senoh Jap. J. Appl. Phys. **30**, 1998 (1991).

[19] T. Wang, H. Wu, Z. Wang, C. Chen & C. Liu, Appl. Phys. Lett. **101**, 161905 (2012).

[20] J. R. Sun, S. Y. Zhang, B. G. Shen & H. K. Wong Appl. Phys. Lett. **86**, 053503 (2005).

[21] K. Lord, D. Hunter, T. M. Williams, & A. K. Pradhan, Appl. Phys. Lett. **89**, 052116 (2006).

5. The properties of $SrSnO_3$ thin films & their pn junction

5.1 Structural properties of $SrSnO_3$ thin film

Perovskite $SrSnO_3$ (SSO) has an orthorhombic structure (space group Pbnm) with a high degree of pseudo-cubic symmetry at room temperature [1-3] indicated in figure 5.1 (b). The orthorhombic perovskite structure is elongated $\sqrt{2}$ times to the a and b axis and 2 times extended to the c axis direction from the cubic perovskite structure exhibited in Figure 5.1. The lattice parameters were reported to be a = 5.708 Å, b = 5.703 Å, and c = 8.065 Å by the least-squares refinement [3]. The octahedral tilting distortion will take place in the corner sharing octahedral network and the Sn-O-Sn bonds bend increasingly [3-5]. The first Brillouin zone (BZ) of the cubic perovskite structure is cubic; however, the first BZ of the orthorhombic perovskite is monoclinic shape, as indicated in Figure 5.2 [6]. Because of difference of the BZ, the band structures of the BSO and SSO are completely different, as shown in Figure 5.3 [7]. In Figure 5.3 (a), the band gap of the BSO is definitely indirect while band structure of SSO exhibit almost direct band gap (The values of the band gap in Figure 5.3 are underestimating. [8]). The band gap of the SSO is known to 4 eV [2, 8-9]. The investigations of direct band gap material for measuring the electrical properties and fabricating pn junction are very important because it is able to exhibit light emitting diode (LED) or photo-response behavior.

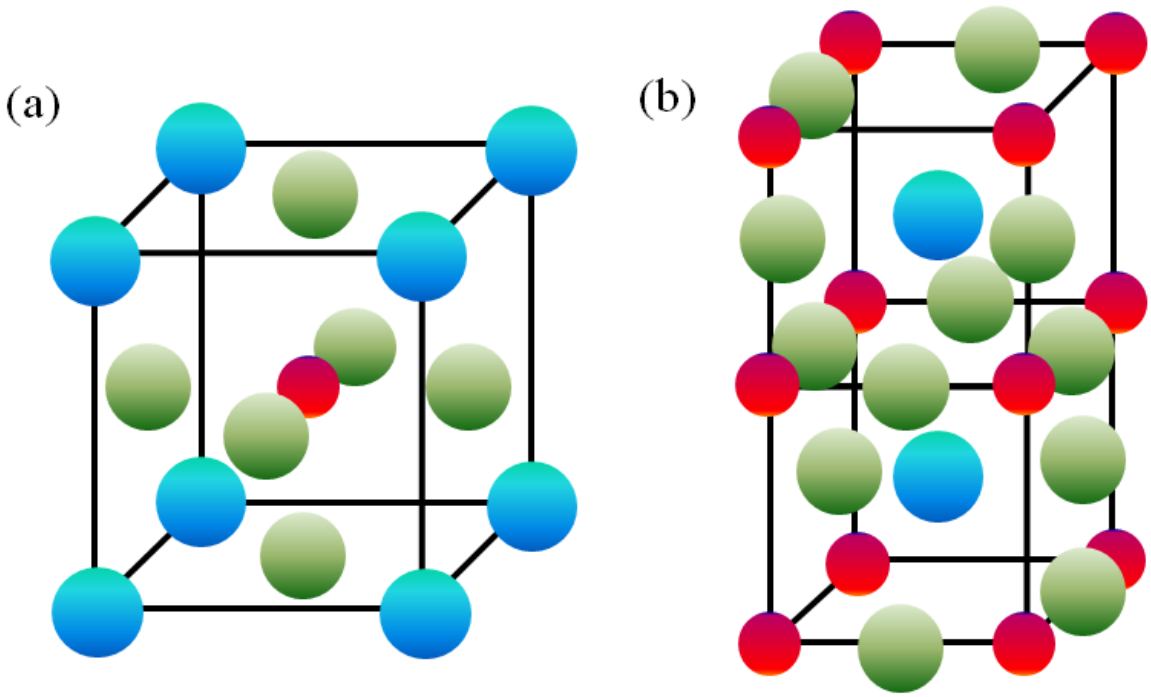

Figure 5.1. The structure of (a) cubic perovskite and (b) orthorhombic perovskite structure. The blue circle is A cation, red one is B cation and green one is oxygen. The orthorhombic perovskite is axis elongated $\sqrt{2}$ times for a and c and 2 times extended to the b axis direction from the cubic perovskite structure.

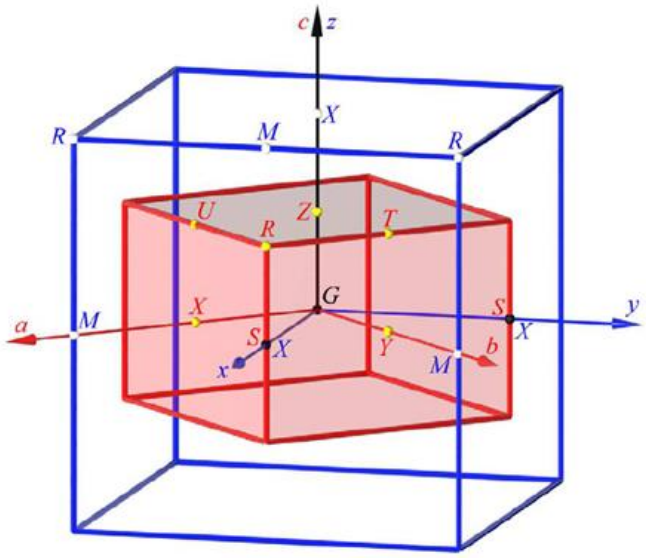

Figure 5.2. The first Brillouine zone of the cubic perovskite (blue) and orthorhombic perovskite (red) [6].

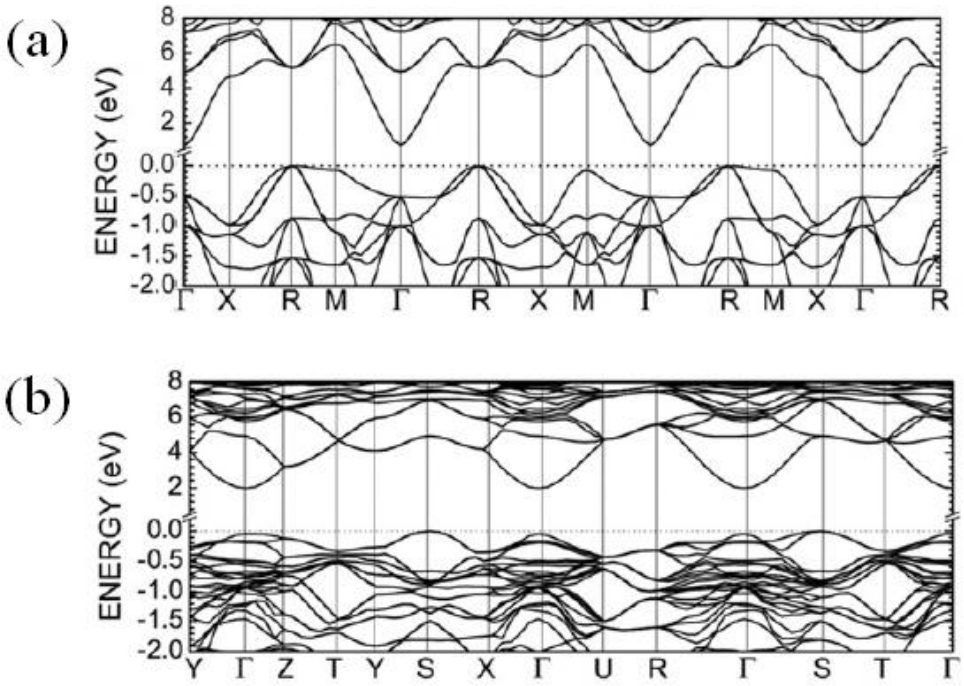

Figure 5.3. The band structure of (a) $BaSnO_3$ and (b) $SrSnO_3$ structure [7].

5.2 Properties of SSO thin films

5.2.1 SSO thin film deposition

We deposited various doped SSO thin films on 5 nm thick SSO buffer layer (deposited at 750 ^{o}C) on the $KTaO_3$ (KTO) substrate using $Sr(Sb,Sn)O_3$ (SSSO) and $SrSnO_3$ targets for SSSO thin films; $SrSnO_3$ and $La_2Sn_2O_7$ (LSO) targets are used for $(La,Sr)SnO_3$ (SLSO) thin films; and $SrSnO_3$ and $SrRuO_3$ targets are used for $Sr(Ru,Sn)O_3$ (SSRO) thin films by pulsed laser deposition system with a KrF excimer laser (λ = 248 nm) under 100 mTorr oxygen pressure with 1 ~ 1.5 J/cm^2 energy intensity. To specifically dope various dopants ions, we used a sequential deposition method which deposits thin films by sequentially alternating targets for each determined pulse shots [10]. The plume of the SSO, SSSO, LSO and SRO targets are shown in Figure 5.4 when laser is ablaze at target. We determine the doping rate is same as the nominal doping rate by measuring growth rate of each material and controlling shot ratios. Also, we assumed that dopant atoms are not volatile at high temperature.

We firstly grew the SSO thin film on STO substrate. However, because the lattice mismatch between STO and SSO is quite a big which shows in Table 5.1, the SSO thin film is still orthorhombic structure and their conductivity are not observed even at carrier doping. The SSO thin film seems to be more affected be lattice mismatch between substrate and thin film than BSO thin film because of their orthorhombic structure with tilting of SnO_6 octahedral [5, 11]. The conduction band of BSO is formed by the interaction between Sn 5s and O 2p orbitals, and thereby, the electron conduction channels pass through SnO_6 octahedral [11, 12]. Therefore, the tilting of SnO_6 octahedral may significantly affect to conduction of the SSO thin film. So we choose KTO as more suitable

substrate. KTO has cubic perovskite structure with lattice constant 3.989 Å for depositing various oxide thin films [13, 14]. The lattice mismatch between SSO and KTO shows only 1.1 % as it seen in Table 5.1, therefore, KTO is the more suitable substrate for depositing SSO thin film than STO. We etched the KTO substrate using 4 % HNO_3 for 30 minute. The surface of the KTO is almost atomically flat and their roughness is 0.107 nm as shown at figure 5.5.

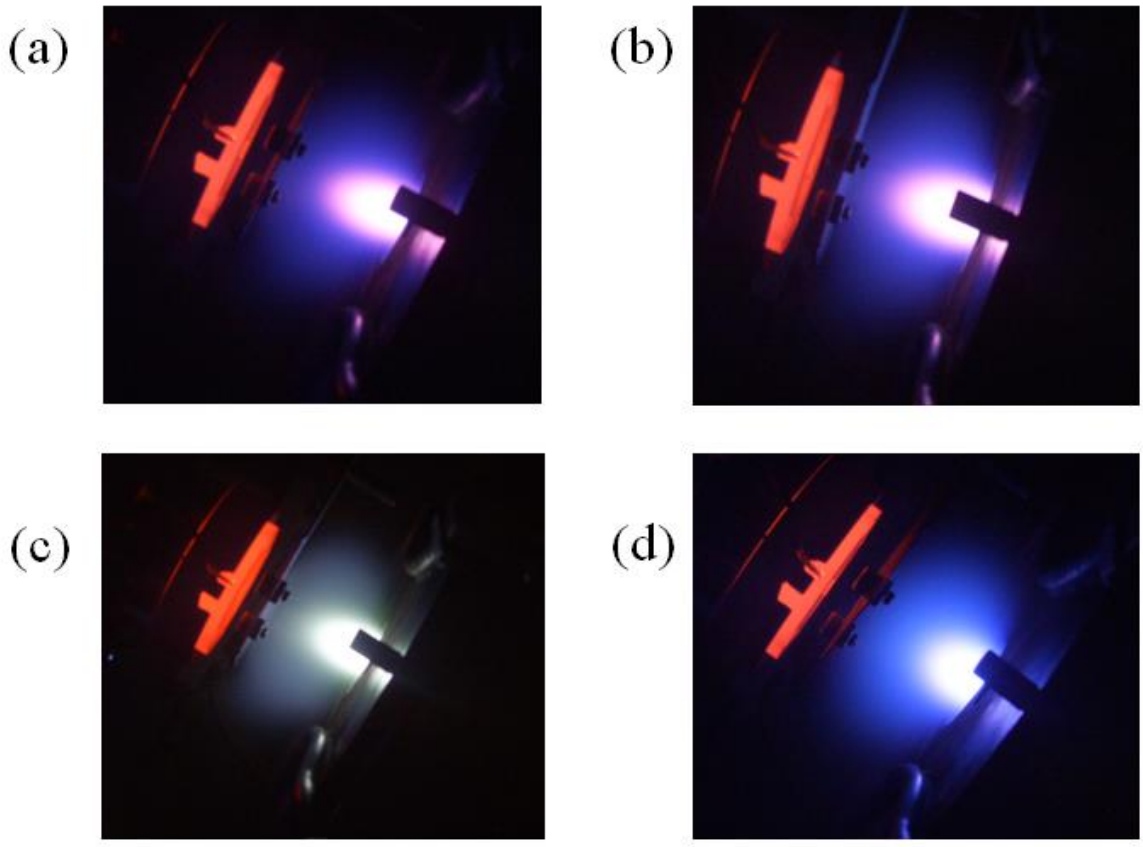

Figure 5.4. Shape of the plumes for laser ablation (a) plume of SSO (b) plume of SSSO (c) plume of LSO (d) plume of SRO.

	Cell plane(Å^2)	Lattice mismatch (%)
$SrSnO_3$	16.322	0
$SrTiO_3$	15.249	-3.45
$KTaO_3$	15.984	-1.11

Table 5.1. The cell plane area and their lattice mismatch with $SrSnO_3$.

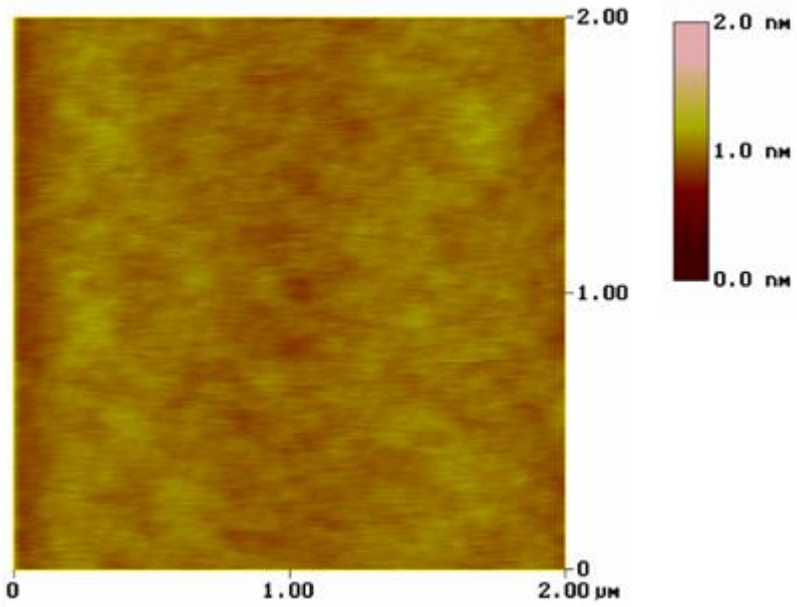

Figure 5.5. AFM image of HNO_3 etched KTO substrate. Its roughness value is 0.107 nm.

5.2.2 Structure and dislocations in SSO thin film

For proof of the epitaxiality of the SSO thin film, as already shown in BSO [15], we obtained the structural information of SSO thin film by the X-ray diffraction method, represented in Figure 5.6. The θ-2θ scan confirms that the epitaxial film was deposited along the direction of KTO substrate. The 2θ angle of the SSO (200) peak is 44.75^{o}. From this value, we can calculate the lattice constant of the SSO tin film for c axis direction that shows 4.050 Å. The values of full width at half maximum (FWHM) of the ω-scan at the SSO (002) peak is 0.09^{o} as indicated at inset of Figure 5.6 which shows that SSO film have highly crystalline and well oriented structure. In order to investigate the in-plane lattice constant and strain state of this film, we use reciprocal space mapping (RSM) method which peaks close to the (103) reflection of the SSSO thin films grown on KTO (001) substrates was measured and shown in Figure 5.7. It is seen that, due to a small lattice mismatch of 1.1 % between the SSO films and the KTO substrates, the film is strained elongated to the c axis. However, on the STO substrate, BSO films [12, 15-16] and SSO films [17, 18] are almost strain relaxed mainly due to the large lattice mismatch between thin film and substrate. It is calculated that the SSO film on KTO has quite a different in-plane and out-of-plane lattice constants of 3.992 Å and 4.049 Å, respectively. RSM method shows that the in-plane direction SSO films have large compressive strain, while they are slightly elongated along the out-of-plane direction. The circle-like shape (103) reflection of the films might mean low density of defects exists in thin film. To confirm the surface homogeneity of the SSO film, we use the AFM image as shown in Figure 5.8. Through the AFM image, we found the surface of the SSO films to be almost atomically flat and it has a very low roughness value which is 0.194 nm.

To proof the dislocation-free of the SSO thin film on KTO substrate, we investigated threading dislocations using TEM and AFM as shown at Figure 5.9. Contrary to TEM image of BSO case as shown in Figure 2.1, there are almost no dislocations at TEM image exhibited in Figure 5.9 (a). It is definitely confirmed that SSO thin film on KTO substrate has few dislocations. Also, we checked the dislocations in HNO_3 etched SSO thin film by using AFM image. The etching creates depressed holes near the dislocations core due to slightly faster etching of the defective atomic structure [18]. The AFM image shows very flat surface even after HNO_3 etching means that there are almost no dislocations in SSO thin film on KTO substrate shown at Figure 5.9 (b).

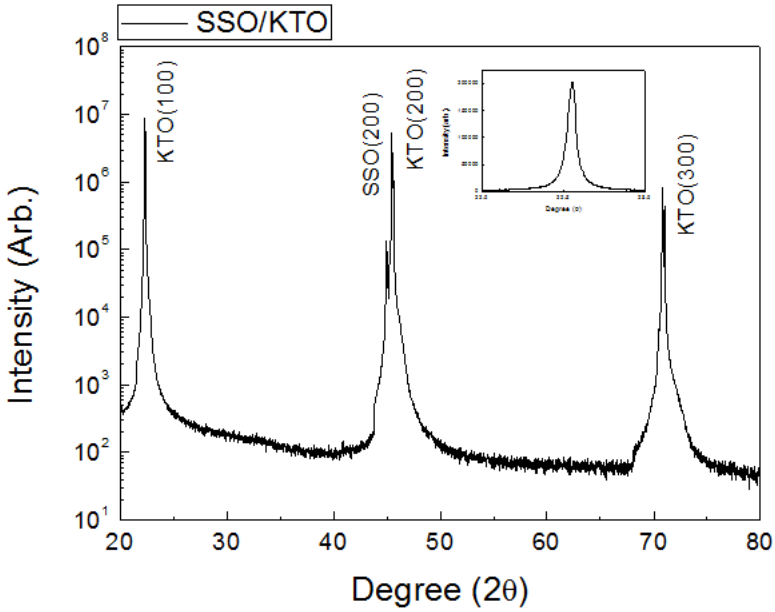

Figure 5.6. θ - 2θ scan of the $SrSnO_3$ thin film on $KTaO_3$ substrate. Inset: rocking curve of the SSO (200) peaks. The Full Width Half Maximum (HWFM) is 0.09^o.

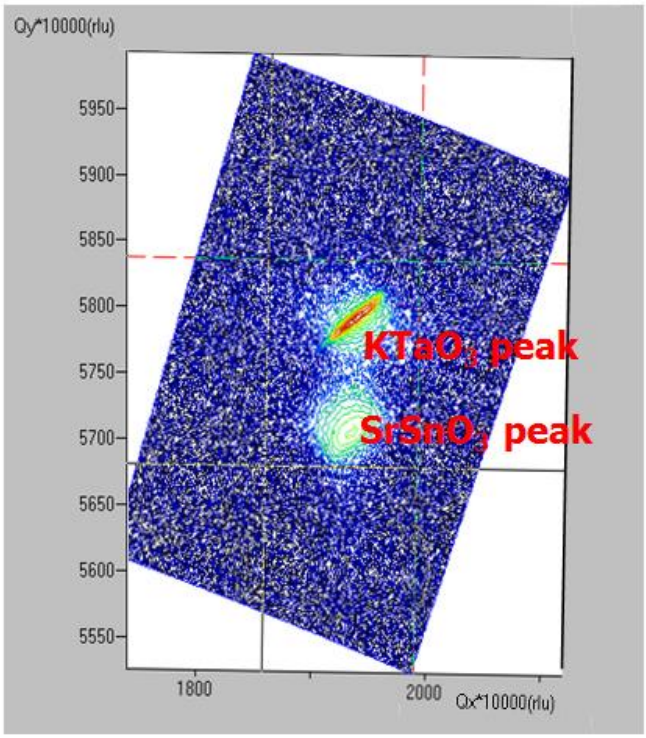

Figure 5.7. Reciprocal space mapping (RSM) of the SSO thin film on KTO substrate.

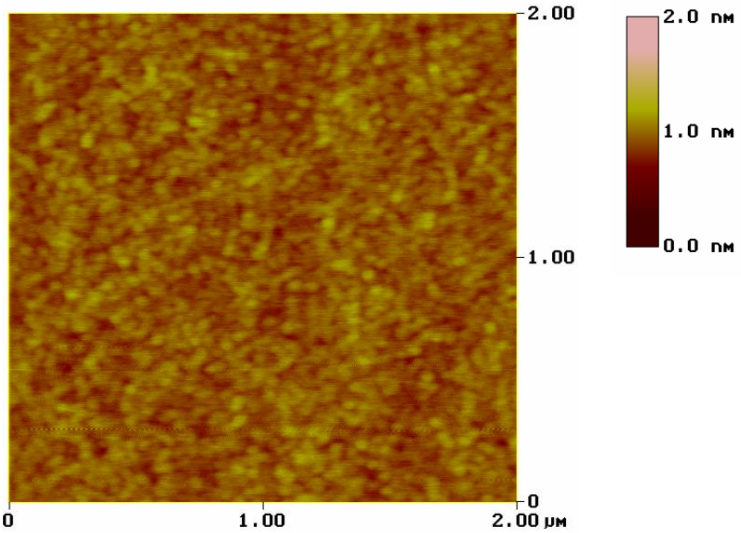

Figure 5.8. AFM image of SSO thin film on KTO with roughness value 0.194 nm.

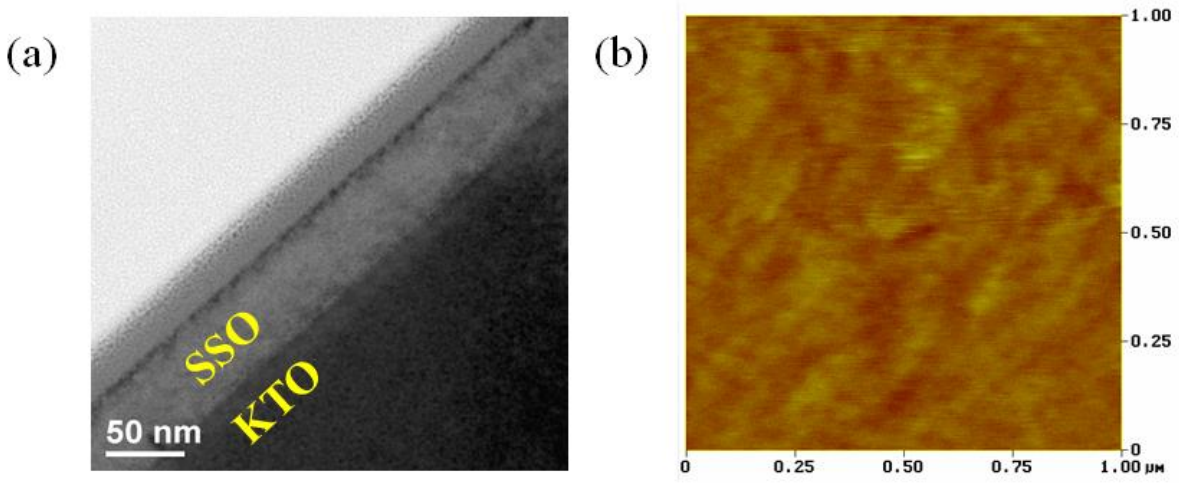

Figure 5.9. (a) TEM image of the SSO /KTO thin film. (b) AFM image of the SSO /KTO thin film. Results of (a) and (b) indicate that SSO thin film on KTO substrate has almost no threading dislocations. AFM imaged measured after 0.4 % HNO_3 etching for 30 s.

5.2 Electrical properties of SSO thin films

5.2.1 Sb-doped SSO (SSSO) thin films

We deposited various Sb doped SSO thin films and measured their resistivity, mobility and carrier concentrations by Hall measurement system. We analyzed resistivity, mobility and carrier concentrations by Sb doping rate as shown in Figure 5.10. Surprisingly, the 4 % Sb doped SSSO thin film shows lowest resistivity, (0.231 Ω·cm), highest mobility (0.516 $cm^2/V \cdot s$) and highest carrier concentration (5.24×10^{19} $/cm^3$). Although we dope Sb ions more than 4 %, these films show higher resistivity and lower mobility and carrier concentration than 4 % SSSO. We suggested that this phenomenon is mainly related with Sb ions because almost same behavior is observed in BSO case [12]. We suggested that the reasons for this phenomenon come from existing multi valence of Sb ions or some kind of charge density wave.

The plot of resistivity and mobility by their carrier concentration is exhibited in Figure 5.11. As shown in Figure 5.11, the mobility is decreased when carrier concentration is increased, as same as BSO [12, 19]. In BSO case, this behavior is explained as scattering at threading dislocations or grain boundaries. However, we need another explanation in case of SSO thin films because there are almost no dislocations in SSO thin films on KTO substrate. We suggested that the SnO_6 octahedral tilting in SSO structure as scattering center is the dominant factor to deteriorate the transport properties in SSSO thin films.

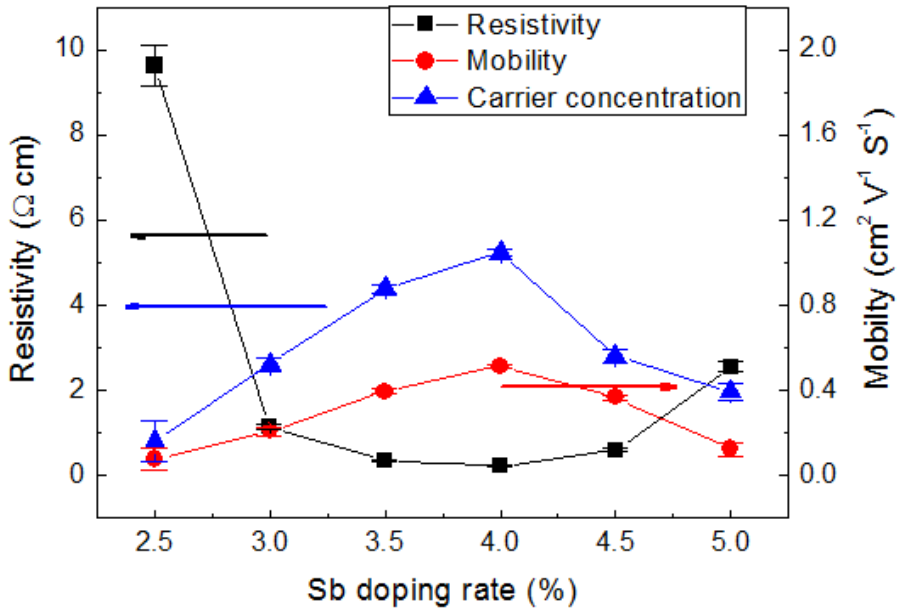

Figure 5.10. (a) Resistivity, mobility and carrier concentration about Sb doping rate of SSSO thin films on KTO substrate.

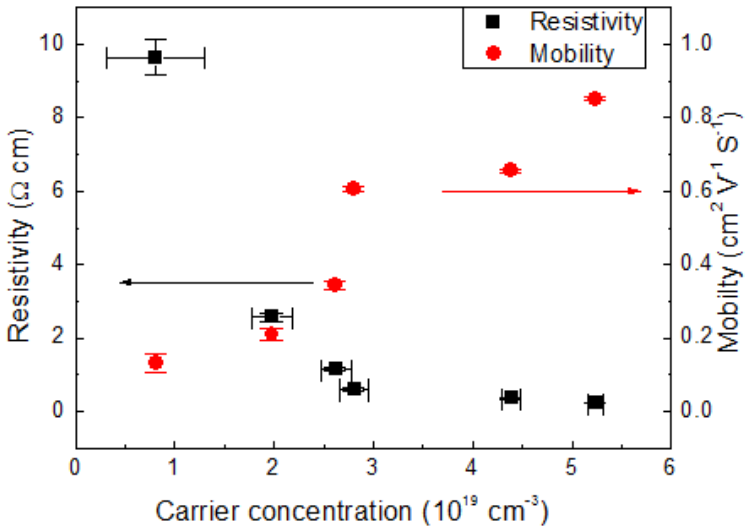

Figure 5.11. Resistivity and mobility as function of the carrier concentration of the SSSO thin film on KTO substrate. Error bar of carrier concentration is indicated at points of resistivity.

5.2.2 La-doped SSO (SLSO) thin films

We deposited various La doped thin films and measured their resistivity, mobility and carrier concentrations by Hall measurement system as same as SSSO case. We analyzed resistivity and mobility by their carrier concentration as shown in Figure 5.12. The SLSO thin film shows no distinctive variation and special tendency of resistivity or mobility as variation of carrier concentration. The range of resistivity (1.36 to 5.82 $cm^2/V \cdot s$) and carrier concentration (1.86×10^{19} to 3.86×10^{19} $/cm^3$) is small for various doped thin films. Although mobility and resistivity are slightly higher than that of Sb doped case, it needs more investigation about exact doping rate and their electrical conduction mechanism. And interestingly, the difference of the mobility and resistivity in SSO system between Sb- and La- doped thin film is very different to those of BSO system [12, 15]. In BSO system, mobility of the La-doped thin film is about ten times higher than that of Sb-doped thin film. We explained this phenomenon from large enhancement of scattering by the threading dislocations in Sb-doped $BaSnO_3$ films and the Sb impurities around the threading dislocation [12]. It is indicated that there are other mechanism for the restriction of electrical conduction of the SSO system such as SnO_6 octahedral tilting. The lanthanum oxides may form a kind of segregation when thin films deposit using sequential deposition method by pulsed laser deposition system using SSO and LSO targets.

5.2.3 Ru-doped SSO (SSRO) thin films

Ru is doped for various thin film oxides for enhance ferromagnetism [20, 21] and sensor response [22]. Among them, SRO is widely used as conducting electrode due to its low resistivity. Moreover, SRO is originally known at p-type metal even alloying with SSO [23]. In SRO, the t_{2g} orbital of Ru lay over the Fermi level. The electrical properties mainly originated from the very strongly hybridized Ru 4d with O 2p orbital extending from -8 to 14 eV relative to the Fermi energy [24]. We deposited various Ru doped SSRO thin films and measured their resistivity, mobility and carrier concentrations by Hall measurement system. We analyzed resistivity and mobility by their carrier as shown in Figure 5.13. All SRSO thin films have p-type carrier with large concentration and relatively low mobility. The Ru dominant region is almost metallic which have high carrier concentration (~10^{22} /cm^3) and low mobility (below 0.1 cm^2/V·s). The lowering the Ru doping, the more semiconducting behavior is appeared that show low carrier concentration and relatively high mobility. The possibility of forming the half-metal state or dilute magnetic semiconductor state is existed because the SSRO is the semiconductor system between SRO as the metallic state and SSO as the wide gap semiconductor. Ru is reported that it is quite volatile [25], it needs more investigation about variation of low doping Ru concentration region and growth temperature for depositing thin films.

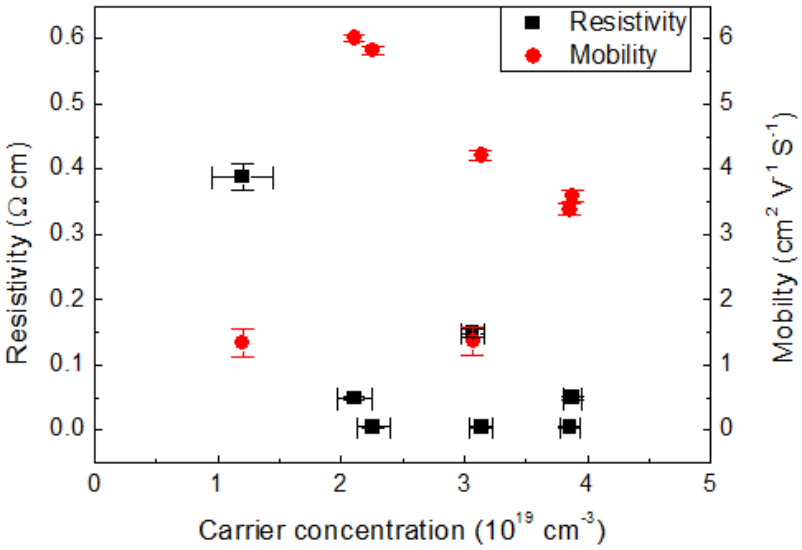

Figure 5.12. Resistivity and mobility as function of the carrier concentration of the SLSO thin film on KTO substrate. Error bar of carrier concentration is indicated at points of resistivity.

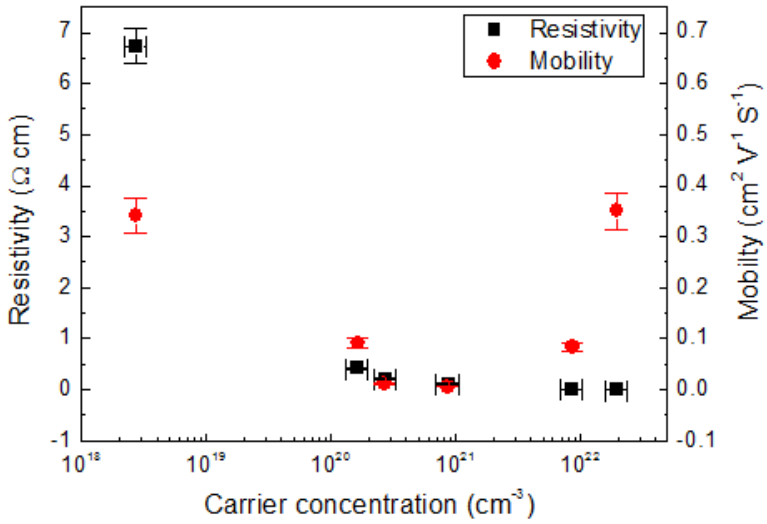

Figure 5.13. Resistivity and mobility as function of the carrier concentration of the SSRO thin film on KTO substrate. Error bar of carrier concentration is indicated at points of resistivity.

5.3 pn junctions fabricated with SSSO and SSRO

5.3.1 Fabrication of pn junction

We fabricate the SSSO/SSRO pn junction which consists of 2.5 % of SSSO for the n-type and SSRO which has lowest carrier concentration exhibited in Figure 5.13 for the p-type. Firstly, 4 % SSSO layer was deposited on the KTO (001) substrate for conduction path. The resistivity of 4 % SSSO layer is about 0.231 Ω·cm, the resistance through this conducting layer is about 13 kΩ including contact resistances. Then we deposited 2.5 % SSSO film with 100 nm thickness using Si stencil mask. The resistivity, mobility and carrier concentration of 2.5 % SSSO film which is used for n-type were 9.63 Ω·cm, 0.079 $cm^2/V{\cdot}s$ and 8.1×10^{18} cm^3, respectively. And SSRO film was deposited at 0.7×0.7 mm^2 patterned cell by using another Si stencil mask. The picture of the cell is shown in Figure 5.14 (a). And then, about 5 nm thick metallic SRO layer was deposited on SSRO thin film to improve the contact between junction and probe. The whole schematic of pn junction structure is illustrated in Figure 5.14 (b). I-V measurement system used same as for BSO based pn junction system which indicated at Figure 4.3.

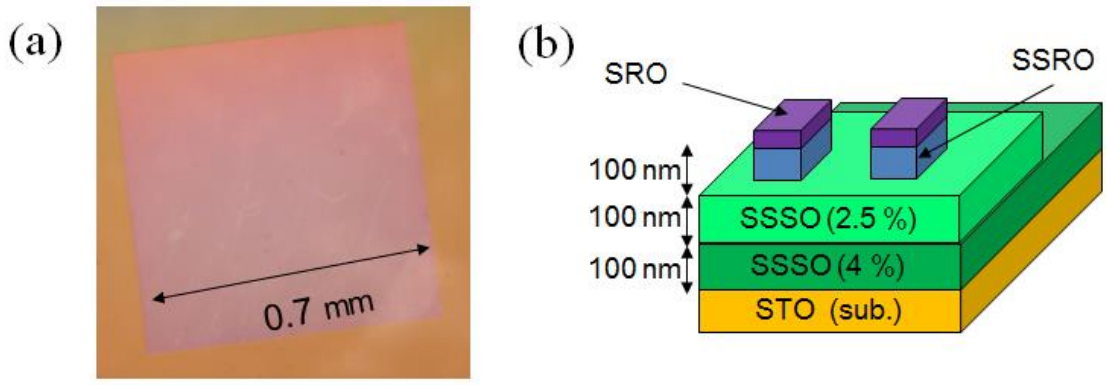

Figure 5.14. (a) The picture of cell for pn junction fabricated by using stencil mask. The area of the cell is 0.7 × 0.7 mm^2. (b) Schematics of the SSSO /SSRO pn junction. Each pn junction contains 2 cells.

5.3.2 I-V characteristics of pn junction

We applied voltage from +3 V to -3 V for measuring I-V characteristics. For forward bias, we sweep the voltage from 0 V to +3 V, and sweep the voltage from 0 V to -3 V for reverse bias. I-V characteristics measured at room temperature are shown in Figure 5.15. Rectifying behavior is clearly observed at junctions with relatively large current through junction about tens μA scales. It means that these rectifying I-V characteristic in our pn junction demonstrates the diode-like behavior originating from the SSSO/SSRO interface. The rectification ratio (ratio between forward and reverse currents) is about 6.46 at a bias of 2.0 V and 2.28 at a bias of 3.0 V. These values are much lower than those of BSO based pn junction, discussed at Chapter 4. This means that SSO-based pn junction has large leakage current at reverse bias region. At reverse bias region, the current level is up to 10^{-4} A order which is very large current level at

high voltage region. As you seen at Figure 5.15 (b), the current is starting to rise just after about 0 V which means that there might have neutral region by relatively more carrier matching than BSO-based pn junction.

As you seen at Figure 5.15 (a), it is originated from that the current is seems limited by series resistance of the devices for both junctions. The estimated value of the series resistance of the pn junction is about 15.8 kΩ. It is mainly originated from the line resistance of the conducting path layer (SSSO 4 %) which has very large resistance as using conducting path. Although the pn junction based SSO system shows large junction current forward bias region, there are many drawbacks such as large leakage current at reverse bias region and no excellent epitaxial film for conducting path. And, there are reported that SSO system exhibit linear band gap variation with BSO system [7, 8]. By the band gap engineering with BSO system, it can be possible to make the direct band gap with low leakage current pn junction attaching low resistivity conduction line with carrier matching.

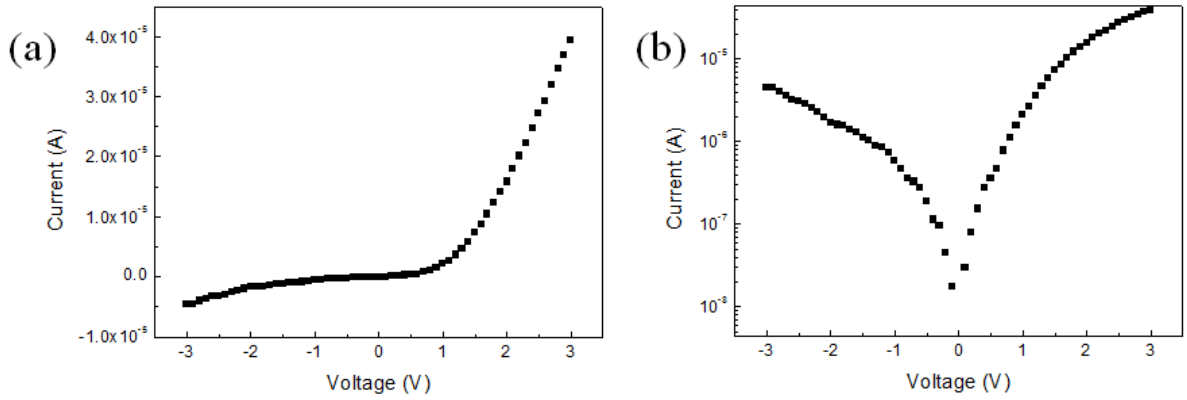

Figure 5.15. I-V characteristics of SSRO /SSSO pn junction at room temperature. (a) Linear plot. (b) Logarithmic plot.

Reference

[1] W. Zhanga, J. Tanga & J. Yea, J. Mater. Res. **22**, 1859 (2007).

[2] L. Shi, Y. F. Duan, X. Q Yang & L. X. Qin ,Chin. Phys. Lett. **27**, 096201 (2010).

[3] P. S. Beurmann, V. Thangadurai & W. Weppner, J. Solid State Chem. **174**, 392 (2003).

[4] E. Moreira, J. M. Henriques, D. L. Azevedo, E. W. S. Caetano, V. N. Freire & E. L. Albuquerque., J. Sol. Stat. Chem. **184**, 921 (2011).

[5] E. H. Mountstevents & S. A. T. Redfern, Phys. Rev. B **71**, 220102 (2005).

[6] E. Pavarini, A. Yamasaki, J. Nuss & O. K. Andersen, New J. Phys. **7**, 188 (2005).

[7] E. Moreira, J. M. Henriques, D. L. Azevedo, E. W. S. Caetano, V. N. Freire & E. L. Albuquerque, J. Sol. Stat. Chem. **187**, 186 (2012).

[8] Q. Liu, B. Li, J. Liu, H. Li, Z. Liu, K. Dai, G. Zhu, P. Zhang, F. Chen and J. Dai, Euro. Phys. Lett. **98**, 47010 (2012).

[9] W. F. Zhang, J.Tang & J. Ye, Chem. Phys. Lett. **418**, 174 (2006).

[10] L. Mieville, T. H. Gaballe, L. Antagnazza, and K. Char, Appl. Phys. Lett. **70**, 126 (1997).

[11] H. Mizoguchi, H. W. Eng and P. M. Woodward, Inorg. Chem. **43**, 1667 (2004).

[12] U. Kim, C. Park, T. Ha, R. Kim, H. Mun, H. M. Kim, H. J. Kim, T. H. Kim, N. Kim, J. Yu, K. H. Kim, J. H. Kim & K. Char APL materials

submitted.

[13] M. Naito *et al.,* Supercond. Sci. Technol. **15**, 1663 (2002).

[14] S. Inoue, M. Kawai, Y. Shimakawa, M. Mizumaki, N. Kawamura, T.Watanabe, Y. Tsujimoto, H. Kageyama, & K. YoshimuraAppl. Phys. Lett. **92**, 161911 (2008).

[15] H. J Kim, U. Kim, H. M. Kim, T. H. Kim, H. Mun, B. G. Jeon, K. T. Hong, W. J. Lee, C. Ju, K. H. Kim & Kookrin Char, Appl. Phys. Exp. **5**, 061102 (2012).

[16] H. Mun, U. Kim, H. M. Kim, C. Park, T. H. Kim, K. H. Kim & K. Char, Appl. Phys. Lett. **102,** 252105 (2013).

[17] Q. Z. Liu, H. F. Wang, F. Chen, & W. Wu, J. Appl. Phys. **103**, 093709 (2008).

[18] Q. Liu, J. Dai, X. Zhang, G. Zhu, Z. Liu & G. Ding, Thin Solid Films **519**, 6059 (2011).

[19] H. J. Kim, U. Kim, T. H. Kim, J. Kim, H. M. Kim, B. G. Jeon, W. J. Lee, H. S. Mun, K. T. Hong, J. Yu, K. Char & K. H. Kim, Phys. Rev. B 86, 165205 (2012).

[20] F. Yan, M. O. Lai, L. Lu & T.Jun, J. Phys. Chem. C **114**, 6994 (2010).

[21] H. Yamada, M. Kawasaki & Y. Tokura Appl. Phys. Lett. **86**, 192505 (2005).

[22] N. S. Ramgir, I. S. Mulla & K. P. Vijayamohanan, Sensors and Actuators B **107**, 708 (2005).

[23] H. M. Christen, L. A. Boatner, J. D. Budai, M. F. Chisholm, L. A. Gea, D. P. Norton, C. Gerber & M. Urbanik Appl. Phys. Lett. **70** ,2147 (1997).

[24] David J. Singh, Appl. Phys. Lett. **79**, 4818 (1996)

[25] P. Pohl & W. Zyrnicki, J. Anal. At. Spectrom **17**, 746 (2002).

6. Summary

In this work, we are attempting to find a suitable substrate that is more suitable than $SrTiO_3$ (STO) for improving the electrical properties of the BLSO thin films. However, BLSO thin films on r-sapphire, $MgAl_2O_4$ spinel and MgO substrates show a poorer mobility than those on STO. The small amount of La-doped BSO thin film acts like a p-type semiconductor due to the effect of threading dislocations even though dopant is an n-type. The high asymmetry of the pn junction carrier partially originates from this phenomenon.

We deposited BKSO thin films on BSO buffer layer using a STO-(100) substrate and investigated the structure, surface properties, and electrical characteristics. The resistances of the BKSO thin films generally followed the Arrhenius formula, and the activation energy of K in the BKSO films was estimated as 0.49 eV. The p-type semiconductor behavior was manifested in the increasing that resistance when the background gas changed from O_2 to Ar.

Using the BKSO and BLSO films p- and n-type semiconductors, we successfully fabricated a pn junction based on single TPS. Although the BKSO/BLSO junction is highly asymmetrically doped, it exhibits typical rectifying behavior. An analysis and fit of the measurement conducted at 300 ^oC, revealed the possibility of using this pn junction for a wide semiconductor LED. If a dopant with activation energy lower than K can be found, the BSO based pn junction will be more useful. These demonstrations of a p-type BKSO thin film and a pn junction based on a TPS material further enhances the potential of the BSO system.

We have also successfully deposited dislocation free SSO thin films on KTO substrates, as confirmed by TEM and AFM images. The electrical properties of

this n-type SSO thin film are not as good as those of the BSO system. Ru-doped SSO thin film show distinctive p-type behavior even at room temperature. A pn junction consisting of Sb-doped SSO (n-type) and Ru-doped SSO (p-type) also showed rectifying behavior. The current of this junction was even larger than that of BKSO-BLSO pn junction; however, the leakage current was very high and an epitaxial layer with a higher conductivity is needed. Combining the BSO and SSO systems will allow us to modulate the band gap in a linear manner.

국문초록

투명 산화물 반도체는 가시광선 및 자외선 영역에서 광학적으로 투명하고 그 전기전도도를 조정할 수 있는 특징이 있어 투명 전극으로 널리 이용되어 왔다. 하지만 이러한 투명 산화물 반도체의 응용은 p형 투명 산화물 반도체가 부재하기 때문에 투명 전극과 화면 패널로 제한되어 왔다. Cu를 기반으로한 p형 투명 산화물 반도체가 발견됨으로써 투명 산화물 반도체를 이용한 pn 접합 또는 전계효과 트랜지스터의 제작이 가능하게 되었다. 하지만 한 투명 산화물 반도체 물질로서 동시에 p형 그리고 n형을 구현한 경우는 거의 보고되지 않고 있다.

최근에 La을 도핑한 $BaSnO_3$ (BSO)가 높은 산소의 안정성과 뛰어난 전기전도도를 가짐이 보고된 바 있었다. 하지만 $BaSnO_3$ 박막이 기판에 대한 뛰어난 결맞음을 지니기는 하지만 박막에 수많은 결정립계 (grain boundaries)와 전위 (dislocations)가 존재하여 이들이 전하를 속박하거나 산란의 요인이 되는 단점이 있었다. 우리는 La을 도핑한 BSO 박막의 전기적인 성질을 증가시키기 위하여 널리 쓰이는 $SrTiO_3$ (STO) 기판 이외에 좀 더 BSO 에 걸맞은 기판을 찾아보았지만 이들 기판은 모두 STO 기판에 비하여 낮은 전기전도도를 나타내었다. 또한, 아주 적은 양의 La만을 도핑 하였을 경우에는 La을 도핑한 BSO 박막이 박막 내의 전위의 영향에 의하여 n형 전하를 도핑 하였음에도 p형 반도체와 같이 행동함을 알 수 있었다.

d-orbital이 Sn과 O사이의 결합에 관계하지 않으므로, BSO 는 다른 페로브스카이트 물질에 비하여 Sn과 O사이의 결합이 강하고 이는 곧 BSO 에 p형 전하를 도핑할 수 있는 가능성을 보임을 의미한다. 우리는 p형 전하를 도핑하기 위해 BSO 에 K을 펄스 레이저 증착법 (Pulsed Laser Deposition: PLD)를 이용하여 도핑하였다. K을 도핑한 BSO 가 상온에서는 상당히 높은 저항을 보이지만 고온으로 올라갈수록 그 저항이 급격하게 감소하였다. 도핑된 K의 활성화 에너지는 약 0.5 eV로 계산되었다. 더욱이 고온에서 박막의 산소를 약간만 제거시켜도 전도도가 눈에 띄게 떨어짐으로써 이 물질이 p형 산화물과 같은

행동을 보임을 관측하였다. K이외에 Ga과 Cu를 도핑한 결과 역시 비슷한 양상을 보였다.

우리는 K를 도핑한 BSO를 p형으로, La을 도핑한 BSO를 n형으로 하여 pn 접합을 제작하였다. 이 소자의 전류-전압 특성을 측정한 결과 pn접합의 전형적인 정류 현상을 보였다. 고온에서 이 pn 접합은 1에서 2사이의 이상계수 (ideality factor)를 보이는 데 이는 고온에서의 BSO의 높은 신뢰성 때문이라 생각한다. 더욱이 이 접합은 높은 인가 전압과 고온에서의 반복 측정에도 아주 안정적인 특성을 나타내었다. 한 페로브스카이트 물질인 BSO를 이용한 pn junction의 구현은 높은 전하 이동도와 산소의 안정성을 갖는 투명 페로브스카이트 반도체로서의 BSO의 가능성을 더욱 높이게 되었다.

그리고 약 4 eV의 직접 밴드 갭 (direct band gap)을 갖는 $SrSnO_3$ (SSO) 시스템에 대하여도 같은 방법을 이용하여 연구하였다. SSO박막은 STO에 비하여 SSO와 더욱 격자상수가 맞는 $KTaO_3$ (KTO) 기판을 이용하였다. 투과 전자 현미경(Transmission electron microscope)과 원자간 힘 현미경 (Atomic Force Microscope)를 이용하여 측정한 결과, KTO기판위의 SSO박막은 전위가 거의 없음을 확인할 수 있었다. SSO박막의 전기적인 성질을 조사하기 위하여 Sb, La, Ru을 도핑하였는데 이들 물질은 SnO_6 팔면체의 기울어짐 때문에 BSO의 경우보다 대체적으로 전하 이동도가 낮았다. 이들 가운데 Ru을 도핑한 SSO는 상온에서도 p형 반도체의 특징이 잘 관측되었기 때문에 Sb를 도핑한 SSO를 n형으로, Ru을 도핑한 SSO를 p형으로 하여 pn 접합을 제작하였다. SSO를 기반으로 한 pn 접합은 BSO 기반 접합에 비하여 전류가 크게 증가하였지만 큰 누설전류와 큰 기생저항 등의 문제가 발견되었다. BSO와 SSO를 결합한 시스템을 이용한다면 직접 밴드 갭을 가지면서도 누설전류와 기생저항이 적은 소자의 제작이 가능하여 향후 발광 다이오드 (LED)등의 응용 등에 큰 가능성이 있다.

Keywords: 투명 산화물 반도체, $BaSnO_3$, K을 도핑한 p형 산화물, 한 페로브스카이트를 이용한 pn 동형 접합, $SrSnO_3$, Ru을 도핑한 p형 산화물

Student number: 2007-20416

감사의 글

학위 심사를 준비 하고 논문을 작성하면서 감사의 글을 쓰는 지금 그 동안 마치 멀게만 느껴졌던 졸업이 새삼 다가옴을 알 수 있었습니다. 이제 학교를 졸업하고 사회로 나아간다고 생각을 하니 두려운 마음과 함께 아쉬움이 교차합니다. 그 동안 많은 분들에게 도움을 받았는데 드디어 이 자리를 빌어서 지난 시간 동안 제가 느낀 고마움을 전할 수 있게 되었습니다.

우선 박사과정 기간 동안 많이 부족하였던 저를 가르쳐주시고 지도해 주신 차국린 교수님께 감사하다는 말씀을 드립니다. 연구에 수행함에 있어서 올바른 방법과 방향을 제시해 주셨으며 연구 외적인 측면으로도 많을 것을 배울 수 있었습니다. 자율적인 연구실 분위기에서 교수님의 지도 하에 많은 연구를 하며 배움을 얻을 수 있었습니다. 믿고 기대해 주신 것에 제가 한참 모자라고 부족한 모습을 보여 항상 죄송스럽지만 지금까지 배운 것을 잊지 않고 앞으로도 부끄럽지 않은 제자로 살아갈 수 있도록 하겠습니다. 그리고 심사 기간 동안 연구 방향과 자세에 대하여 많은 조언을 해 주신 국 양 교수님, 같은 분야의 연구를 진행하면서 항상 염려하여 주신 김 기훈 교수님, 저에게 자신감을 갖도록 격려해 주신 박 제근 교수님, 그리고 몸소 서울까지 오셔서 심사에 참여해 주신 방 윤규 교수님께 감사 드립니다. 심사 때 해주신 소중한 충고와 조언들을 깊이 새겨 앞으로 더욱 노력하겠습니다. 그리고 제가 미국의 Rutgers 대학에서 연구 경험을 쌓을 수 있도록 허락해 주신 정 상욱 교수님께도 감사를 표합니다.

오랜 실험실 생활을 하면서 많은 사람들과의 인연과 도움으로 제가 더욱 배우고 성장할 수 있었습니다. 함께 수 많은 밤을 지새며 저에게 STM을 가르쳐 주시고 연구하는 방법과 자세에 있어 모범이 되셨던 제욱이형, 실험실 생활을 비롯한 많은 것을 가르쳐 주신 진오형, 저의 반도체 연구의 기반을 다져주신 태수형, 그리고 PLD 및 연구 진행 및 프로세스를 가르쳐 주신 승란 누나에게 감사 드립니다. 또한 오랜 기간 동안 같이 있으면서 함께 많은 일을 하였던 찬종, 많은 일을 맡아 하면서 항상 의지할 수 있는 효식, 저희를 항상 배려해 주시고

같이 어울려 주신 동호 형, 연구와 지식에 대한 열정이 넘치는 우성, 모든 일에 집중력을 발휘하는 혁우, 앞장서서 실험을 하며 연구실의 분위기를 책임지는 철권, 끈기를 가지고 항상 최선을 다하는 지성, 그리고 앞으로 연구실의 미래를 이끌어 갈 주연이와 영모에 이르기 까지 많은 이들이 도움이 없었다면 제가 앞으로 나아가는 일은 불가능하였을 것입니다.

대학원 과정에서 졸업하기까지 여러 연구를 하면서 수많은 사람들에게 도움을 받았습니다. 미국 Rutgers 대학에 있을 때 많은 배려를 봐주시고 도움을 주신 채 승철 박사님, 최 영재 박사님, 이 나라 박사님에게 감사 드립니다. 그리고 같은 주제에 대하여 연구를 하면서 많은 도움을 주시고 discussion을 같이 하였던 형준이 형, 태훈이 형, 웅재씨에게 감사를 드립니다. 연구실 이동 시 많은 도움을 주셨던 강 진홍 사장님과 따뜻한 관심을 가져주신 김 융기 상무님, 그리고 김 명옥씨에게도 감사 인사를 드리고 싶습니다. 맛있는 커피와 함께 많은 이야기를 나누었던 봉수 형, 도움이 필요할 때 많은 의지가 되었던 성민 형에게도 감사를 표합니다. 그리고 스터디와 모임을 같이 하며 견문을 넓히고 많은 이야기를 나눌 수 있었던 승훈, 성민, 범용, 예리도 각자의 길에서 모두 잘 되기를 바랍니다.

이제 박사 후 연구원 과정을 통해 독일로 가게 될 승현, 역시 미국에서 박사 후 연구원으로 있는 성모와 태경, 곧 여기서의 일을 마무리 짓고 더 넓은 곳으로 나가게 될 성준에게 좋은 결과 있기를, 열심히 연구에 매진하고 있는 록연도 좋은 결과를 내고 빨리 졸업하기를 바랍니다. 주완, 광원, 예령, 소진, 희태, 영한도 각자의 자리에서 많은 것을 이루며 뛰어난 성과를 내고 있으리라 생각합니다. 외국에서 유학 생활을 하는 상윤, 연정, 형빈이도 건강하고 잘 지내기를 바랍니다. 그리고 고등학교 때부터 알고 지낸 진호, 성학, 성훈, 명진, 동협이도 더 자주 보았어야 한다는 아쉬움과 함께 앞으로도 변치 않는 우정을 이어가자는 말을 전하고 싶습니다.

그리고 오랜 시간 동안 같이 생활하면서 연구에 정진할 수 있도록 배려와 지원을 아끼지 않고 인생과 진로에 대해 아낌없는 조언을 해 준 형, 새로이

가족이 되어 많은 도움을 주시고 부족한 저를 따뜻함으로 대해 주신 형수님, 무엇보다도 저의 긴 대학원 생활 동안 부족한 저를 항상 믿어주시고 지원과 격려, 그리고 사랑을 아끼지 않으신 부모님에게 감사를 표합니다. 주신 사랑에 비하면 보잘것없지만 그래도 박사 과정을 마치어 아들 이름이 적힌 학위 논문이나마 드릴 수 있어서 다행입니다. 지금보다 더 큰 사람이 되어 앞으로 사회에서 열심히 활동하여 도와주신 모든 분들께 보답할 수 있는 사람이 될 수 있도록 하겠습니다. 이 논문을 나를 걱정해 주시고 사랑해 주신 모든 분들에게 바칩니다. 감사합니다.